Tunable Microwave Filters based on Dielectric Split Ring Resonators

by

Ahmed Sabah Noori

A thesis submitted to the University of Birmingham for the degree of Doctor of Philosophy

College of Engineering and Physical Sciences
The University of Birmingham
February 2018

Abstract

This thesis investigates a new type of microwave tunable filter; the filter is designed based on a new type of resonator called Dielectric Split Ring Resonator (Dielectric-SRR). The new tunable filter is utilised to tune the filter bandwidth at about 2.3 GHz. This bandwidth tuning is achieved by rotating the filter resonators and without adding tuning elements such as screws or varactor diodes. In the measurement the filter resonators are rotated by hand. This thesis also investigates the new Dielectric-SRRs in term of their losses and unloaded quality factor. These new microwave resonators are designed with a configuration similar to the conventional metal Split Ring Resonators (Metal-SRR), but made from dielectric material of high dielectric constant. The new Dielectric-SRR achieved unloaded quality factor Q_u 3 times higher than the Q_u value of the conventional Metal-SRR.

Besides the new tunable filter, a new class of non-tunable filter with two different configurations is investigated. The two filters are designed based on the new Dielectric-SRRs, the first design is 3rd order Chebyshev filter, and the second is a 4th order filter with two symmetric transmission zeros. The non-tunable filters achieved excellent measured performance, and good agreement between measurements and simulations.

Acknowledgement

I am extremely grateful for the patient guidance of my supervisor Professor Michael Lancaster during my PhD study in the University of Birmingham; I have benefited much from his constant support and instructive ideas. I would also like to express my deepest gratitude to my previous supervisor Dr. Paul Smith for his valuable advice and discussions. My thanks also go to the colleagues in the Emerging Device Technology Research Group at the University of Birmingham for their support through my research.

I also appreciate and thank the Iraqi Ministry of Higher Education and Scientific Research and Wasit University for financing my PhD study at the University of Birmingham.

Finally, my sincere gratitude goes to my parents, and wife.

Table of Contents

Chapter 1 Introduction

1.1 Motivation

Microwave tunable filters with stringent requirements on insertion loss are in demand for wireless and satellite applications in recent years. This due to the rapid development in the wireless communication systems, where every few years there is a new generation of wireless systems present for customers, for example the 3rd generation of cellular network is introduced in 2003 then followed by the 4th generation in 2013. The tunable filters are required to provide solutions for coexist wireless networks of multiple standards and requirements [1-2].

In addition, tunable filters can be tuned remotely; this can support the wireless stations which can be located on very high towers or in the remote rural areas [1]. The tunable filters can be beneficial for satellite applications due to the difficulty to changing or adding equipment for satellites in the space. The satellite applications also can use a tunable filter instead of the large filters bank, and this will significantly reduce on the satellite mass, size and cost [1-3].

Non-tunable filters with very high performance are using currently in wireless systems like cellular base stations and satellites, these filters employ 3-D resonators such as coaxial, dielectric and cavity resonator [6-8]. These resonators can present insertion losses lower than the planar resonators (e.g. microstrip resonator) as shown in Figure 1.1 [9]. For this reason tunable filters should use such 3-D resonators to maintain the same high performance [1].

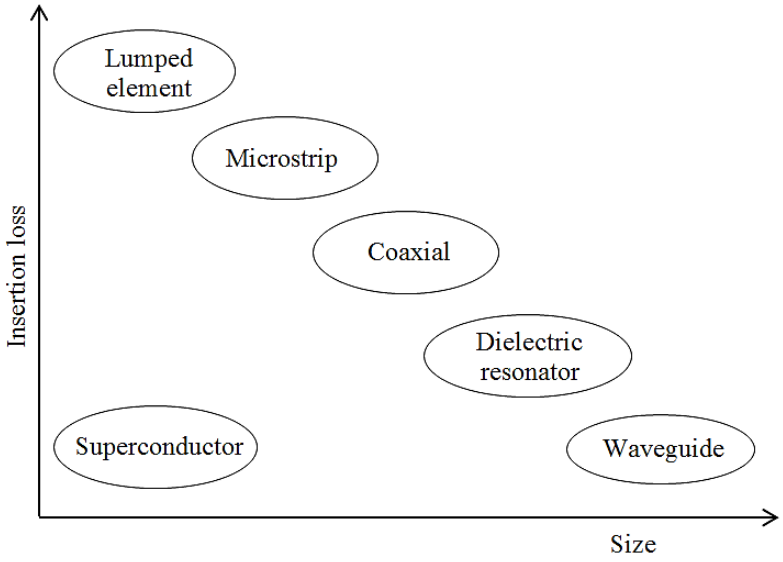

Figure 1.1 Relative size and insertion loss of the common resonators from [9]

However, the current tunable filters reported high insertion loss even when using 3-D resonators like coaxial and dielectric resonators [10-16], and this is due to use of high loss tuning elements such as MEMS, piezoelectric, varactor diode and disks [1-5].

In this thesis a new tunable filter is presented to tune the filter bandwidth (BW) at a particular centre frequency. The filter BW is tuned based on rotating the filter resonators only and without adding tuning elements. The Split Ring Resonators are chosen to design this tunable filter. In general SRRs have two different configurations, that is planar or microstrip SRRs [17] or 3-D SRRs [18]. In this research we used only the 3-D SRRs to achieve the lower insertion loss. The 3-D SRR is metal resonator and has unloaded quality factor Q_u of about 5000 at S band, similar to coaxial resonator [19, 20], these 3-D SRRs are rarely used in microwave filters [18-20], but commonly used with the microwave sensors [21, 22].

In this thesis the 3-D SRRs are made from a dielectric material of high dielectric constant instead of metal material (as the conventional Metal-SRRs) to achieve resonators with higher unloaded quality factor Q_u. This represents a new type of resonator which has the shape of conventional Metal-SRR but uses materials similar to the conventional dielectric resonator and we call it the Dielectric-SRR.

A new class of fixed or non-tunable filters, with two different configurations and based on the new Dielectric-SRRs are presented in this thesis in addition to the tunable filters. These new fixed filters are designed to validate the new Dielectric-SRRs concept, and to achieve filter response with low insertion loss which is suitable for wireless applications with stringent requirements. The novelties presented in this thesis can be grouped into two categories: (i) Dielectric-SRRs with high Q_u; (ii) tunable and non-tunable filters with low insertion loss combined with the use of Dielectric-SRRs.

1.2 Thesis overview

The thesis motivation and objectives are given in the previous section. Chapter 2 presents brief description for the fundamental filter theory. This includes overview of microwave filters, lowpass prototype filters and $n \times n$ coupling matrix representation. Chapter 3 introduces the new type of microwave resonators we called Dielectric-SRR; the new resonator is simulated and measured. The Q_u of Dielectric-SRR is compared to that of Metal-SRR. Chapter 4 presents a new class of microwave fixed filters with two different configurations. These filters are designed using the new Dielectric-SRRs. This chapter also shows the method of extracting the physical dimensions of microwave filters by using an EM simulator. Chapter 5 introduces a new type of tunable filters

designed to tune the filter bandwidth based on rotating the filter resonators and without adding tuning elements. Chapter 6 presents a summary for the thesis chapters. Also some recommendations are given for future research.

References:

[1] R. R. Mansour, F. Huang, S. Fouladi, W. D. Yan and M. Nasr, "High-Q Tunable Filters: Challenges and Potential," *IEEE Microw. Mag.*, vol. 15, no. 5, pp. 70-82, July-Aug. 2014.

[2] R. R. Mansour, "High-Q tunable dielectric resonator filters," *IEEE Microw. Mag.*, vol. 10, no. 6, pp. 84-98, Oct. 2009.

[3] P. W. Wong and I. Hunter, "Electronically Tunable Filters," *IEEE Microw. Mag.*, vol. 10, no. 6, pp. 46-54, Oct. 2009.

[4] R. Gomez-Garcia, M. A. Sanchez-Soriano, K. W. Tam and Q. Xue, "Flexible Filters: Reconfigurable-Bandwidth Bandpass Planar Filters with Ultralarge Tuning Ratio," *IEEE Microw. Mag.*, vol. 15, no. 5, pp. 43-54, July-Aug. 2014.

[5] B. Yassini, M. Yu and B. Keats, "A Ka-Band Fully Tunable Cavity Filter," *IEEE Trans. Microw. Theory and Tech.*, vol. 60, no. 12, pp. 4002-4012, Dec. 2012.

[6] R. R. Mansour, "Filter technologies for wireless base stations," *IEEE Microw. Mag.*, vol. 5, no. 1, pp. 68-74, Mar 2004.

[7] C. Wang and K. A. Zaki, "Dielectric resonators and filters," *IEEE Microw. Mag.*, vol. 8, no. 5, pp. 115-127, Oct. 2007.

[8] Chi Wang, K. A. Zaki, A. E. Atia and T. G. Dolan, "Dielectric combline resonators and filters," *IEEE Trans. Microw. Theory and Tech.*, vol. 46, no. 12, pp. 2501-2506, Dec 1998.

[9] R. J. Cameron, R. Mansour, and C. M. Kudsia, *Microwave Filters for Communication Systems: Fundamentals, Design and Applications*. Hoboken, NJ, USA: Wiley, 2007.

[10] S. Fouladi, F. Huang, W. D. Yan and R. R. Mansour, "High-Q Narrowband Tunable Combline Bandpass Filters Using MEMS Capacitor Banks and Piezomotors," *IEEE Trans. Microw. Theory and Tech.*, vol. 61, no. 1, pp. 393-402, Jan. 2013.

[11] P. W. Wong and I. C. Hunter, "A New Class of Low-Loss High-Linearity Electronically Reconfigurable Microwave Filter," *IEEE Trans. Microw. Theory and Tech.*, vol. 56, no. 8, pp. 1945-1953, Aug. 2008.

[12] A. I. Abunjaileh and I. C. Hunter, "Tunable Bandpass and Bandstop Filters Based on Dual-Band Combline Structures," *IEEE Trans. Microw. Theory and Tech.*, vol. 58, no. 12, pp. 3710-3719, Dec. 2010.

[13] G. M. Rebeiz, K. Entesari, I. C. Reines, *et al*, “Tuning in to RF MEMS,” *IEEE Microw. Mag*., vol. 10, no. 5, pp. 55–72, Oct. 2009.

[14] X. G. Wang, Y. H. Cho and S. W. Yun, "A Tunable Combline Bandpass Filter Loaded With Series Resonator," *IEEE Trans. Microw. Theory and Tech.*, vol. 60, no. 6, pp. 1569-1576, June 2012.

[15] B. Yassini, M. Yu, D. Smith and S. Kellett, "A Ku-Band High-Q Tunable Filter with Stable Tuning Response," *IEEE Trans. Microw. Theory and Tech.*, vol. 57, no. 12, pp. 2948-2957, Dec. 2009.

[16] S. Kurudere and V. B. Erturk, "Novel Microstrip Fed Mechanically Tunable Combline Cavity Filter," *IEEE Microw. and Wireless Compon. Lett.*, vol. 23, no. 11, pp. 578-580, Nov. 2013.

[17] J.-S. G. Hong and M. J. Lancaster, *Microstrip Filters for RF/Microwave Applications*. New York, NY, USA: Wiley, 2011.

[18] M. Mehdizadeh, T. K. Ishii, J. S. Hyde and W. Froncisz, "Loop-Gap Resonator: A Lumped Mode Microwave Resonant Structure," *IEEE Trans. Microw. Theory and Tech.*, vol. 31, no. 12, pp. 1059-1064, Dec. 1983.

[19] R. F. Mostafavi, D. Mirshekar-Syahkal and Y. C. M. Lim, "Small filters based on slotted cylindrical-ring resonators," *IEEE Trans. Microw. Theory and Tech.*, vol. 49, no. 12, pp. 2369-2375, Dec. 2001.

[20] H. Salehi, R. R. Mansour, and V. Dokas, “Lumped-element conductorloaded cavity resonators,” *IEEE MTT-S Int. Microw. Symp. Dig*., vol. 3, Seattle, WA, Jun. 2002, pp. 1601–1604.

[21] H. Choi, J. Naylon. S. Luzio, *et al*, “Design and In Vitro Interference Test of Microwave Noninvasive Blood Glucose Monitoring Sensor," *IEEE Trans. Microw. Theory and Tech.*, vol. 63, no. 10, pp. 3016-3025, Oct. 2015.

[22] D. J. Rowe, S. al-Malki, A. A. Abduljabar, A. Porch, D. A. Barrow and C. J. Allender, "Improved Split-Ring Resonator for Microfluidic Sensing," *IEEE Trans. Microw. Theory and Tech.*, vol. 62, no. 3, pp. 689-699, Mar. 2014.

Chapter 2 Fundamental Filter Theory

2.1 Overview of Microwave Filters

A filter is a two-port signal selective device used in the communication systems to select the wanted signals and reject the unwanted signals [1]. There are four types of filter based on the attenuation characteristics. These types are low-pass, high-pass, bandpass and band-stop as shown in Figure 2.1 [2].

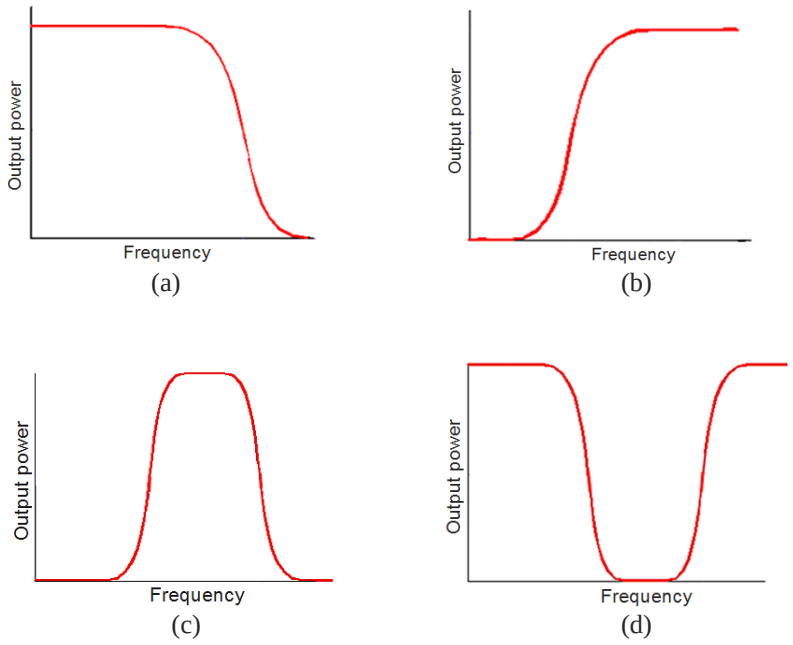

Figure 2.1 Categories of filter responses, (a) low-pass response, (b) high-pass response, (c) bandpass response and (d) bandstop response

Most two-port microwave filters (or other circuit) can be represented by a typical network as shown in Figure 2.2, where V_1 and V_2 are the voltage variables, I_1 and I_2 are the current variables, for both network ports, Z_{01} and Z_{02} are the terminal impedances, and e_s is the source voltage [1].

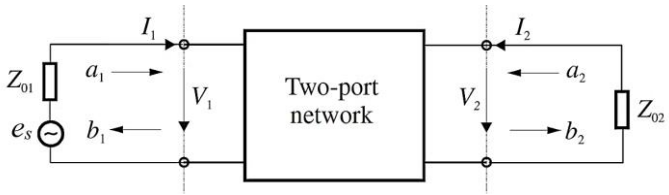

Figure 2.2 Two-port network filter representation and its variables [1]

a_1, b_1 and a_2, b_2 as shown in Figure 2.2 are wave variables. These variables are used due to the difficulty in measuring the voltage and current at RF/microwave frequencies. *a* variable represents the incident waves and *b* variable represents reflected waves. The relationships between these variables (*a* and *b*) and the voltage and current variables are [1],

$$a_n = \frac{1}{2}\left(\frac{V_n}{\sqrt{Z_{0n}}} + \sqrt{Z_{0n}} I_n\right)$$
$$b_n = \frac{1}{2}\left(\frac{V_n}{\sqrt{Z_{0n}}} - \sqrt{Z_{0n}} I_n\right) \qquad n=1 \text{ and } 2 \qquad (2\text{-}1)$$

The above waves variables (*a* and *b*) are represented by coefficients called scattering parameters (S-parameters) [1],

$$S_{11} = \left.\frac{b_1}{a_1}\right|_{a_2=0} \qquad S_{12} = \left.\frac{b_1}{a_2}\right|_{a_1=0}$$
$$S_{21} = \left.\frac{b_2}{a_1}\right|_{a_2=0} \qquad S_{22} = \left.\frac{b_2}{a_2}\right|_{a_1=0} \qquad (2\text{-}2)$$

when the incident waves (a_n) equal to zero this presents a perfect impedance match at ports. The parameters S_{11} and S_{22} represent the reflection coefficients of the two-ports network, whereas the S_{12} and S_{21} represent the insertion transmission coefficients. In

case of the microwave filter which is generally reciprocal and symmetric, the reflection coefficients and insertion transmission coefficients are equal (S_{11} = S_{22}, S_{12} = S_{21}). These parameters are directly measurable at microwave frequencies [1]. The S-parameters are complex and introduced in terms of amplitudes and phases. The S-parameters amplitudes are determined as [1],

$$L_A = -20\log_{10}\left(|S_{21}|\right) \text{ dB}$$
$$L_R = -20\log_{10}\left(|S_{11}|\right) \text{ dB} \quad (2\text{-}3)$$

The logarithm operations of both equations are base 10, where L_A indicates the insertion loss and L_R indicates the return loss.

2.2 Microwave Filter Theory

This section describes briefly the important fundamental theory for designing a general microwave filter.

2.2.1 Transfer function

The transfer function is a mathematical expression of the insertion transmission coefficient (S_{21}) for a two-port filter [1].

2.2.1.1 All-pole Chebyshev filters

The filter of Chebyshev response gives an equal-ripple signal in the passband and a roll off from ω = 1 as shown in Figure 2.3 [1]. The amplitude-squared transfer function for a two-port filter with Chebyshev response is defined as [3]

$$\left|S_{21}(s)\right|^2 = \frac{1}{1+\varepsilon^2\left|D(s)\right|^2} \tag{2-4}$$

where ε is the ripple constant and s is a complex variable, the ripple constant (ε) can be obtained from the passband ripple L_{Ar} (in dB) as [1]

$$\varepsilon = \sqrt{10^{\frac{L_{Ar}}{10}} - 1} \tag{2-5}$$

$D(s)$ represents a characteristic function; it can be defined as a ratio of two polynomials [3]

$$D(s) = \frac{F(s)}{P(s)} \tag{2-6}$$

For the two-port network the transfer function can be defined in term of a rational function as [3]

$$S_{11}(s) = \frac{F(s)}{E(s)} \quad S_{21}(s) = \frac{P(s)}{\varepsilon E(s)} \tag{2-7}$$

$E(s)$ and $F(s)$ are characteristic polynomials with N^{th} degree and highest-power coefficients equal to one. The degree of $E(s)$ and $F(s)$ refers to the filter order, while the degree of polynomial $P(s)$ represents the number of transmission zeros at finite frequencies. More details about the characteristic polynomials $F(s)$ $P(s)$ and $E(s)$ can be found in [3].

The polynomials of Chebyshev transfer function can be expressed as [4]

$$\begin{aligned} P(s) &= 1 \\ F(s) &= \cosh\left[\sum_{n=1}^{N} \cosh^{-1}(s)\right] \end{aligned} \tag{2-8}$$

The Chebyshev filter achieve all pole response because its transmission zeros are located at infinity, the stopband of all pole response attenuates smoothly [3].

The typical amplitude response of a Chebyshev filter is shown in Figure 2.3. This response is for a 6th order filter and normalised to achieve a unit cut-off frequency. The passband ripple L_{Ar} is 0.043 dB as shown in Figure 2.3b, by using equation (2-3). The return loss is better than 20 dB.

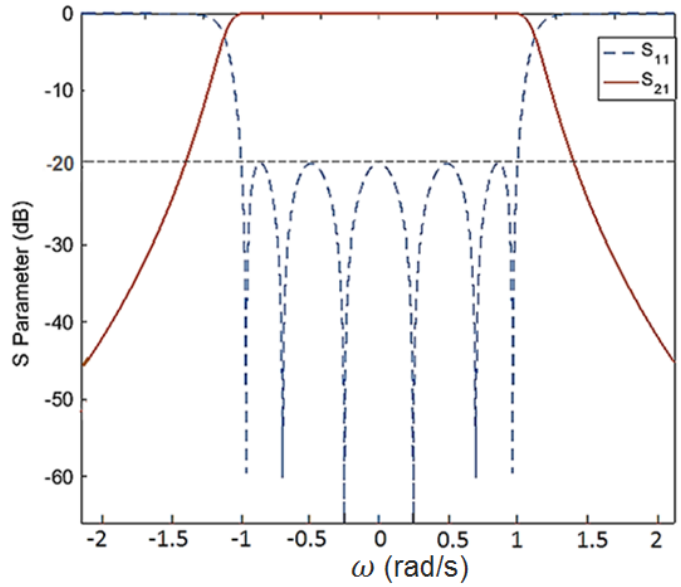

(a)

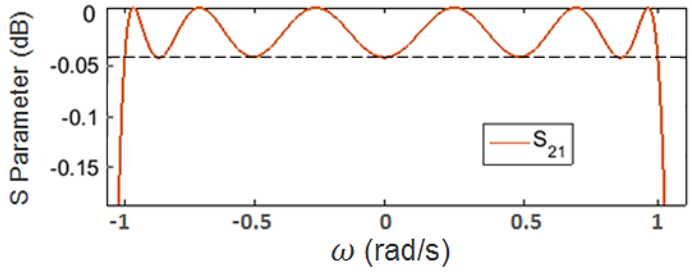

(b)

Figure 2.3 Chebyshev Lowpass responses, (a) S_{11} and S_{21} magnitude in dB, and (b) S_{21} passband ripple

2.2.1.2 Filters with Finite Transmission Zeros

In order to add transmission zeros (TZs) to the filter response, the order of the polynomial *P(s)* in equation (2-7) should be equal to the required number of transmission zeros at finite frequencies. All polynomials *F(s)*, *P(s)* and *E(s)* are normalized to the highest-power coefficients and assumed equal to one [3].

The addition of transmission zeros to the filter transfer function leads to increase the selectivity of the filter. Figure 2.4a shows the sixth order Chebyshev filter responses with same specifications of the example (in Figure 2.3) except adding two symmetrical transmission zeros located at ±1.5. The filter response with TZs achieved higher selectivity than the all pole response as shown in Figure 2.4.

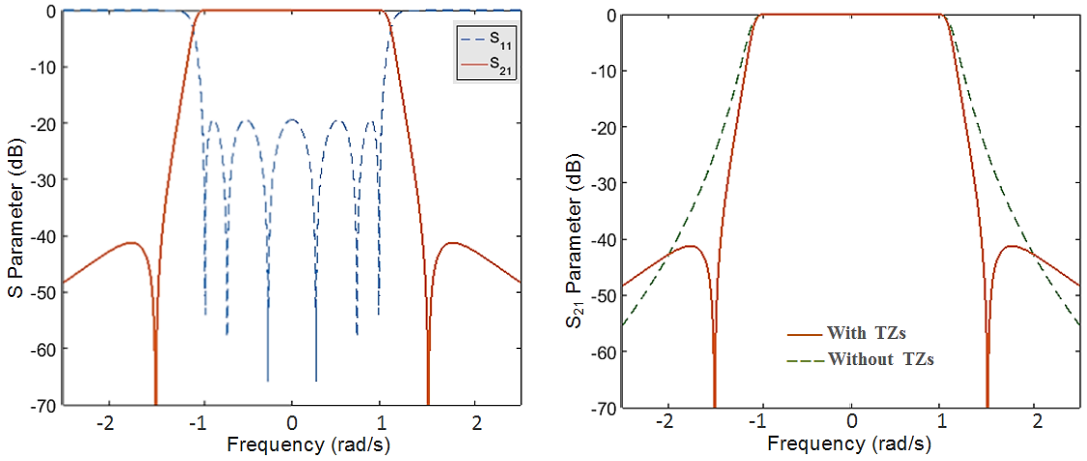

(a) (b)

Figure 2.4 (a) Lowpass responses with 2 symmetric transmission zeros, and (b) Comparison between S21 responses with TZs and without TZs

2.2.2 Lowpass Prototype Filter

The lowpass prototype filter is a lumped element circuit used to realise the transfer function. This prototype is the same as a general lowpass filter in terms of response and

circuit elements, except that elements values of the lowpass prototype filter are normalized to make the source resistance/conductance (g_0) and the cut-off angular frequency (Ω_c) equal to one [1].

There are two possible forms of n^{th} order lowpass prototype filters as shown in Figure 2.5. Both these prototype forms present the same response, and can be used to realise an all-pole filter response such as a Chebyshev filter. n in Figure 2.5 represents the number of reactive elements, g_{n+1} is the conductance/resistance of the load, and g_i for i=1 to n, represents the capacitance of the parallel capacitors or the inductance of the series inductors. The lowpass prototype filter in general can be utilised to design practical filters with frequency and element transformation given below [1].

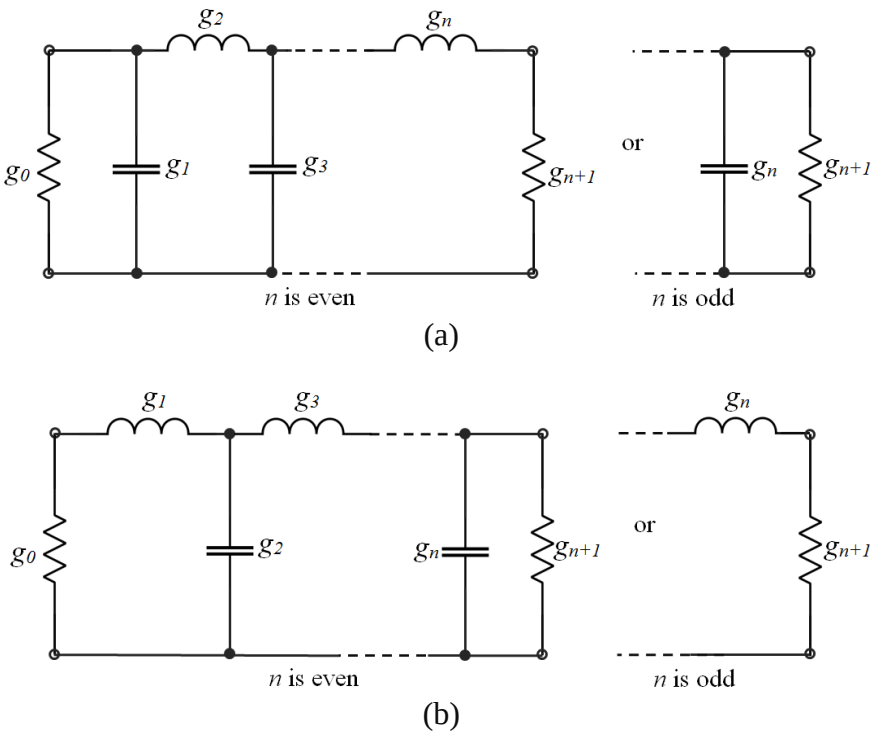

Figure 2.5 Lowpass prototype filters for all-pole responses, (a) ladder filter circuit, and (b) its dual

2.2.3 Low-pass to Band-pass Transformation

The lowpass prototype filter with normalised values g_n and Ω_c can be employed to design practical bandpass filters by applying frequency and element transformation. For frequency transformation, assuming the desired bandpass response having pass-edges angular frequency ω_1 and ω_2, the desired frequency transformation is given as [1]

$$\Omega = \frac{\Omega_c}{FBW}\left(\frac{\omega}{\omega_0} - \frac{\omega_0}{\omega}\right) \tag{2-9}$$

$$FBW = \frac{\omega_2 - \omega_1}{\omega_0}$$
$$\omega_0 = \sqrt{\omega_1 \omega_2} \tag{2-10}$$

where Ω_c is the lowpass prototype cut-off frequency, ω is the frequency variable, ω_0 represents the centre angular frequency and FBW is the fractional bandwidth. This frequency transformation if applied to the lowpass prototype filter in Figure 2.5 of parallel capacitors and series inductors is given as [1]

$$j\Omega g \rightarrow j\omega \frac{\Omega_c g}{FBW\,\omega_0} + \frac{1}{j\omega}\frac{\Omega_c \omega_0 g}{FBW} \tag{2-11}$$

This leads to transform a series inductor or parallel capacitor in lowpass prototype filter to series or parallel *LC* resonant circuit in the bandpass filter [1]. The elements transformation from lowpass prototype filters to practical bandpass filters is shown in Figure 2.6.

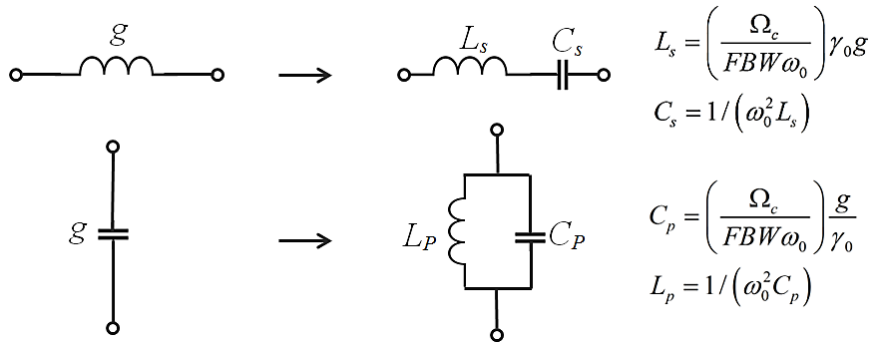

Figure 2.6 Elements transformation from lowpass prototype filter to bandpass filter

Figure 2.7 shows a practical equivalent circuit of a 3rd order bandpass Chebyshev filter obtained from the element transformation of a 3rd order Chebyshev lowpass prototype [1].

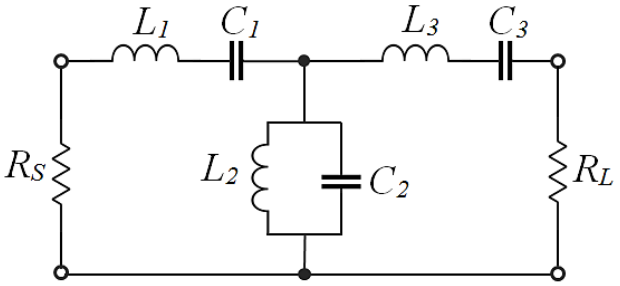

Figure 2.7 Practical equivalent circuit of 3rd order bandpass Chebyshev filter

2.2.4 Microwave Resonator and Unloaded Quality Factor

A microwave resonator is any structure that has one or more oscillating electromagnetic fields [1]. This device employed in microwave filters usually work in the microwave frequency range from 30 MHz to 300 GHz [5]. Examples for the microwave resonators are microstrip resonator, combline resonator, dielectric resonator and cavity resonator [2]. The microwave resonator can be represented by a lumped-element or an *LC* circuit. However, lumped elements are very difficult to manufacture at microwave frequencies

[5]. The lumped element circuit representation assists in the understanding and design showing the common and the basic characteristics of microwave filters such as the filter responses, losses and coupling matrix [2].

The *LC* resonant equivalent circuit can be in series or in parallel as shown in Figure 2.8a and 2.7b. In practice, the microwave resonators losses are present and these losses can be represented by adding resistors to the *LC* resonant circuit as shown in Figure 2.8c and 2.7d [1].

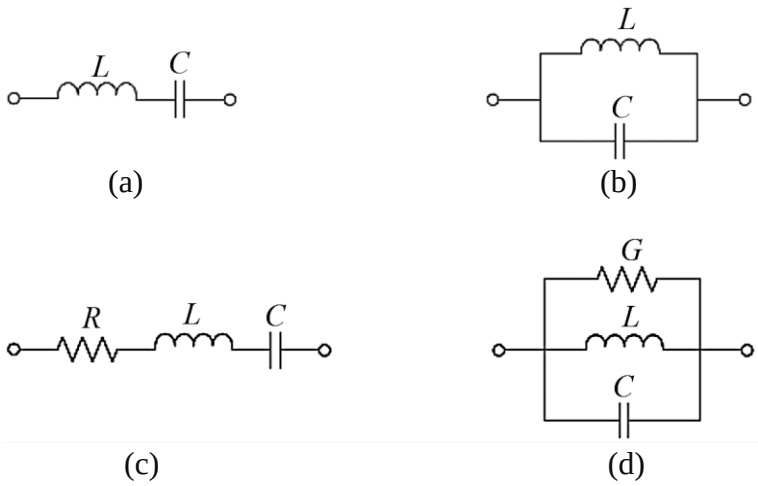

Figure 2.8 Lumped-element resonant circuits (a) Series *LC* resonant circuit, (b) Parallel *LC* resonant circuit. (c) Series *RLC* resonant circuit, and (d) Parallel *RLC* resonant circuit

The losses of the *RLC* resonant circuit can be determined by a parameter called unloaded quality factor (Q_u), where a resonator with higher loss implies a lower Q_u [2]. In general the unloaded quality factor Q_u of microwave resonator is defined by

$$Q_u = \omega_0 \frac{\text{Time-average energy stored in resonator}}{\text{Averange power lost in resonator}} \tag{2-12}$$

The Q_u of the series *RLC* resonance circuits can be determined by [2]

$$Q_u = \frac{\omega_0 L}{R} = \frac{1}{\omega_0 RC} \tag{2-13}$$

For parallel *RLC* resonance circuits the Q_u can be determined by [2]

$$Q_u = \frac{R}{\omega_0 L} = \omega_0 RC \tag{2-14}$$

The microwave resonator losses may be from conductor, dielectric, or radiation. The total Q_u of a microwave resonator with these losses is given as [2]

$$\frac{1}{Q_u} = \frac{1}{Q_c} + \frac{1}{Q_d} + \frac{1}{Q_r} \tag{2-15}$$

The *Q*-factors in the equation are conductor quality factor Q_c, dielectric quality factor Q_d and radiation quality factor Q_r.

The *Q*-factors (Q_u, Q_c, Q_d, and Q_r) of the microwave resonator can all be determined by using an EM simulator. The Q_u can also be measured directly by coupling the resonator to external ports (source and load) and then measured with a vector network analyser (VNA). The microwave resonator simulation and measurement are described in Chapter 3.

2.3 *n* × *n* Coupling Matrix Representation of n^{th} order filter

The coupling matrix is a concept used to represent the filter topologies based on lumped element circuit [1]. The coupling matrix representation was introduced for the first time

by Atia and Williams in 1970 [6-8]. It was an $n \times n$ coupling matrix, where n is the filter order. Later the coupling matrix developed and extended to be a $n + 2$ matrix [9]. This section discusses only the $n \times n$ coupling matrix, as this type will be needed in the filter design later.

Figure 2.9a shows n^{th} order equivalent circuit with magnetic coupled resonators, and Figure 2.9b shows n^{th} order equivalent circuit with electric coupled resonators. The Kirchhoff's voltage law can be used for analysing the equivalent circuit of the magnetic coupled resonators as given in Figure 2.9a, and Kirchhoff's current law can be used for analysing the equivalent circuit of the electric coupled resonators as given in Figure 2.9b. The resistance, inductance, and capacitance of the circuit are denoted by R, L and C respectively, i denote the loop current, G is the conductance and e_s is the voltage source [1].

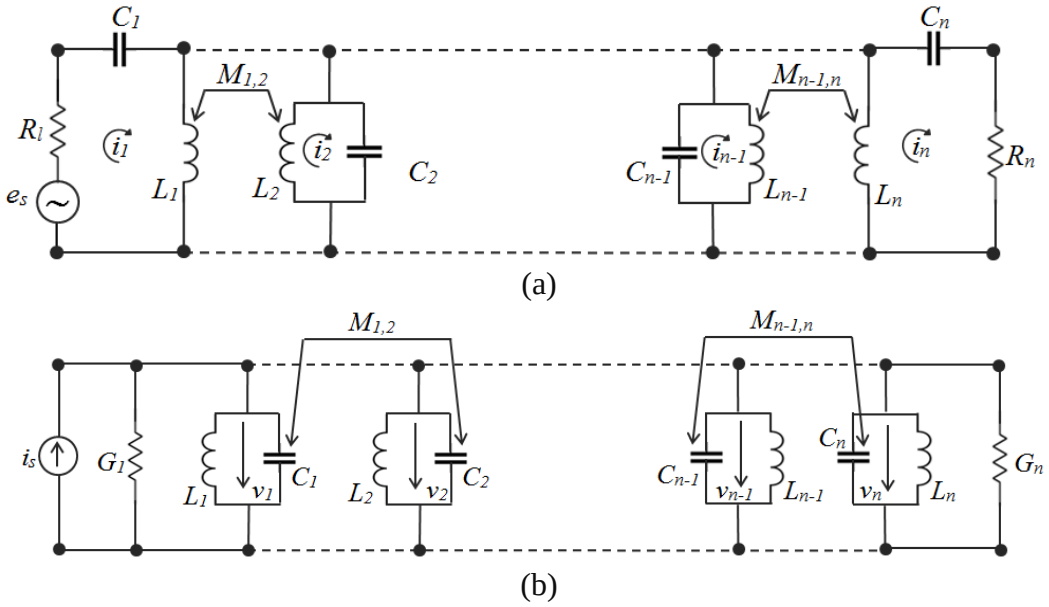

Figure 2.9 Equivalent circuits of n^{th} coupled resonators. (a) Magnetic coupled resonators (Kirchhoff's voltage law) and (b) electric coupled resonators (Kirchhoff's current law) [1]

The circuit of magnetic coupled resonators is analysed by the Kirchhoff's loop equations as given in [1]

$$\begin{aligned}
&\left(R_1 + j\omega L_1 + \frac{1}{j\omega C_1}\right)\cdot i_1 - j\omega L_{1,2}\cdot i_2 \;\cdots\; - j\omega L_{1,n}\cdot i_n = e_s \\
&\quad - j\omega L_{2,1}\cdot i_1 - \left(j\omega L_2 + \frac{1}{j\omega C_2}\right)\cdot i_2 \;\cdots\; - j\omega L_{2,n}\cdot i_n = 0 \\
&\qquad\qquad\qquad\qquad\qquad\qquad\qquad\qquad\qquad\qquad\qquad\qquad \vdots \\
&-j\omega L_{n,1}\cdot i_1 - j\omega L_{n,2}\cdot i_2 \;\cdots\; + \left(R_n + j\omega L_n + \frac{1}{j\omega C_n}\right)\cdot i_n = 0
\end{aligned} \tag{2-16}$$

where $L_{ij}=L_{ji}$ are the mutual inductance between resonators i^{th} and j^{th}, and as shown in Figure 2.9a. The loop currents are assumed to be at same direction. These Kirchhoff's voltage equations (2-16) are given in matrix form as [1]

$$\begin{bmatrix}
R_1 + j\omega L_1 + \frac{1}{j\omega C_1} & -j\omega L_{1,2} & \cdots & -j\omega L_{1,n} \\
-j\omega L_{2,1} & j\omega L_2 + \frac{1}{j\omega C_2} & \cdots & -j\omega L_{2,n} \\
\vdots & \vdots & \vdots & \vdots \\
-j\omega L_{n,1} & -j\omega L_{n,2} & \cdots & R_n + j\omega L_n + \frac{1}{j\omega C_n}
\end{bmatrix} \cdot \begin{bmatrix} i_1 \\ i_2 \\ \vdots \\ i_n \end{bmatrix} = \begin{bmatrix} e_s \\ 0 \\ \vdots \\ 0 \end{bmatrix} \tag{2-17}$$

or

$$[Z][i] = [e_s]$$

where [Z] represents an $n \times n$ impedance matrix. If the filter circuit is assumed to be synchronously tuned, this means the resonators of the filter circuit resonate at the same

frequency, called mid-band frequency $\omega_0 = 1/\sqrt{LC}$, where $L = L_1 = L_2 = \cdots L_n$ and $C = C_1 = C_2 = \cdots C_n$. The impedance matrix can be written as

$$[Z] = \omega_0 L \cdot FBW \cdot [\bar{Z}] \tag{2-18}$$

where $[\bar{Z}]$ represents the normalised impedance matrix and *FBW* is the fraction bandwidth, the $[\bar{Z}]$ of a synchronously tuned filter can be expressed as [1]

$$[\bar{Z}] = \begin{bmatrix} \frac{1}{q_{e1}} + p & -jm_{1,2} & \cdots & -jm_{1,n} \\ -jm_{2,1} & p & \cdots & -jm_{2,n} \\ \vdots & \vdots & \vdots & \vdots \\ -jm_{n,1} & -jm_{n,2} & \cdots & \frac{1}{q_{en}} + p \end{bmatrix} \tag{2-19}$$

where p is the frequency variable; m_{ij} is the normalised coupling coefficient of resonators i and j; q_{e1} and q_{en} is the normalised external quality factors of input and output resonators. These parameters (p, m_{ij}, q_{e1} and q_{en}) can be expressed as given in [1]

$$p = j\frac{1}{FBW}\left(\frac{\omega}{\omega_0} - \frac{\omega_0}{\omega}\right) \tag{2-20}$$

$$\begin{aligned} m_{i,j} &= \frac{M_{i,j}}{FBW} \\ q_{ei} &= Q_{ei} \cdot FBW \quad \text{for } i = 1, n \end{aligned} \tag{2-21}$$

where M_{ij} are de-normalised coupling coefficients and Q_{ei} are the de-normalised external quality factor of input and output resonators. These values are used for the practical design of filters and are given as [1]

$$M_{i,j} = \frac{L_{i,j}}{L} \tag{2-22}$$

$$Q_{ei} = \frac{\omega_0 L}{R_i} \tag{2-23}$$

In case when the filter is asynchronously tuned and each resonator of this filter has a different resonance frequency, an extra normalised coupling coefficient m_{ii} is added to the diagonal of the matrix and is expressed as [1]

$$\left[\bar{Z}\right] = \begin{bmatrix} \frac{1}{q_{e1}} + p - jm_{1,1} & -jm_{1,2} & \cdots & -jm_{1,n} \\ -jm_{2,1} & p - jm_{2,2} & \cdots & -jm_{2,n} \\ \vdots & \vdots & \vdots & \vdots \\ -jm_{n,1} & -jm_{n,2} & \cdots & \frac{1}{q_{en}} + p - jm_{nn} \end{bmatrix} \tag{2-24}$$

The equivalent circuit of mutual capacitance in Figure 2.9b can be analysed similar to the equivalent circuit of mutual inductance. The normalised admittance $[\bar{Y}]$ can be obtained for the equivalent circuit of electric coupling by using the Kirchhoff current law as [1]

$$\left[\bar{Y}\right] = \begin{bmatrix} \frac{1}{q_{e1}} + p - jm_{1,1} & -jm_{1,2} & \cdots & -jm_{1,n} \\ -jm_{2,1} & p - jm_{2,2} & \cdots & -jm_{2,n} \\ \vdots & \vdots & \vdots & \vdots \\ -jm_{n,1} & -jm_{n,2} & \cdots & \frac{1}{q_{en}} + p - jm_{nn} \end{bmatrix} \tag{2-25}$$

As shown in equation (2-25) the normalised admittance matrix $[\bar{Y}]$ is identical to the normalised impedance matrix $[\bar{Z}]$, and for this reason both matrices can be utilised to

represent one general coupling matrix [A] regardless type of coupling (magnetic, electric or mixed coupling) as defined in [1]

$$[A]=\begin{bmatrix} \frac{1}{q_{e1}} & 0 & \cdots & 0 \\ 0 & 0 & \cdots & 0 \\ \vdots & \vdots & \ddots & \vdots \\ 0 & 0 & \cdots & \frac{1}{q_{en}} \end{bmatrix}+p\begin{bmatrix} 1 & 0 & \cdots & 0 \\ 0 & 1 & \cdots & 0 \\ \vdots & \vdots & \ddots & \vdots \\ 0 & 0 & \cdots & 1 \end{bmatrix}-j\begin{bmatrix} m_{1,1} & m_{1,2} & \cdots & m_{1,n} \\ m_{2,1} & m_{2,2} & \cdots & m_{2,n} \\ \vdots & \vdots & \ddots & \vdots \\ m_{n,1} & m_{n,2} & \cdots & m_{n,n} \end{bmatrix} \tag{2-26}$$

or simplified as [1]

$$[A]=[q]+p[U]-j[m]$$

where [q] is the $n \times n$ matrix of normalised external quality factors, [U] represents $n \times n$ identity matrix, [m] is a n by n reciprocal matrix (m=m) which is called general an coupling matrix, in case of synchronously tuned filter the [m] have zeros diagonal entries.

For the two-port network as in Figure 2.2 the S-parameters can be obtained from [1]

$$\begin{aligned} S_{11} &= \pm\left(1-\frac{2}{\sqrt{q_{e1}}}[A]_{11}^{-1}\right) \\ S_{21} &= \frac{2}{\sqrt{q_{e1}\cdot q_{en}}}[A]_{n1}^{-1} \end{aligned} \tag{2-27}$$

The coupling matrix [m] and external quality factor q_e for a bandpass filter with standard responses (such as Chebyshev or Butterworth) directly can be synthesised according to equation (2-21) and by using the lowpass prototype filter g-values as [1]

$$
\begin{aligned}
&Q_{e1} = \frac{g_0 g_1}{FBW} \qquad Q_{en} = \frac{g_n g_{n+1}}{FBW} \\
&M_{i,i+1} = \frac{FBW}{\sqrt{g_i g_{i+1}}} \quad \text{for } i = 1 \ \textit{to}\ n \\
&q_{e1} = Q_{e1} \cdot FBW = g_0 g_1, \qquad q_{en} = Q_{en} \cdot FBW = g_n g_{n+1} \\
&m_{i,i+1} = \frac{M_{i,i+1}}{FBW} = \frac{1}{\sqrt{g_i g_{i+1}}} \quad \text{for } i = 1 \ \textit{to}\ n
\end{aligned}
\tag{2-28}
$$

These *g*-element values are determined according to the filter order and passband ripple (L_{Ar}).The *g*-element values of the common used lowpass prototype filters such as Chebyshev can be directly obtained from tables or formulae as given in [1, 10].

$$
\begin{aligned}
&g_0 = 1 \\
&g_1 = \frac{2}{\gamma}\sin\left(\frac{\pi}{2n}\right) \\
&g_i = \frac{1}{g_{i-1}} \frac{4\sin\left(\frac{(2i-1)\pi}{2n}\right)\cdot\sin\left(\frac{(2i-3)\pi}{2n}\right)}{\gamma^2 + \sin^2\left(\frac{(i-1)\pi}{n}\right)} \quad (i = 2 \text{ to } n) \\
&g_{n+1} = \begin{cases} 1 & \text{for } n \text{ odd} \\ \coth^2\left(\frac{\beta}{4}\right) & \text{for } n \text{ even} \end{cases} \\
&\beta = \ln\left[\coth\left(\frac{L_{Ar}}{17.37}\right)\right] \\
&\gamma = \sinh\left(\frac{\beta}{2n}\right)
\end{aligned}
\tag{2-29}
$$

2.4 Microwave Filter Design

The approach of design a microwave filter can be represented by three steps. The first step is synthesising the filter coupling matrix [*m*] according to the filter specifications. Then based on the values of matrix [*m*] entries can calculate the filter response and the

design parameters ($M_{i,i+1}$ and Q_e) as well as model the filter topology. An example is given later in this section for the first step of microwave filter design. The second step is extracting the physical dimensions of the filter structure based on the values of the filter design parameters ($M_{i,i+1}$ and Q_e) and by using an EM simulator. This second step of filter design is described in Chapter 4. Finally, the third step is to optimise the filter dimensions by using an EM simulator; because the filter response with the initial extracted dimensions may not be close enough for the filters ideal response. The filter is then fabricated based on the optimised dimensions and then measured by a vector network analyser (VNA). The measured response should be very close to the optimised (simulated) results. This design approach can be applied to most types of microwave filters such as waveguide, coaxial, dielectric and microstrip filters [1].

This section will now proceed with an example for the first step of the filter design procedure, this example shows synthesis of the coupling matrix [m] for a 4^{th} order bandpass Chebyshev filter. The filter response has 20 dB return loss and 0.05 *FBW* at 3 GHz. Based on these filter specifications the g-values of the lowpass prototype filter are obtained by using equation (2-29) as g_1=0.9314 g_2=1.2920 g_3=1.5775 g_4=0.7628 and g_5=1.2210. The normalised synthesised coupling matrix [m] and q_e according to equations (2-28) are given as

$$[m] = \begin{bmatrix} 0 & 0.9106 & 0 & 0 \\ 0.9106 & 0 & 0.6999 & 0 \\ 0 & 0.6999 & 0 & 0.9106 \\ 0 & 0 & 0.9106 & 0 \end{bmatrix} \qquad (2\text{-}30)$$

$$q_{e1} = 0.9331, \quad q_{e2} = 0.9331$$

The filter coupling coefficients $M_{i,i+1}$ and external quality factor Q_e are calculated by using equation (2-28) as:

$$M_{1,2}= M_{3,4}= 0.0455,\ M_{2,3}= 0.0349$$

$$Q_{e1}= Q_{e2}= 18.66$$

This result corresponds to the filter topology shown in Figure 2.10.

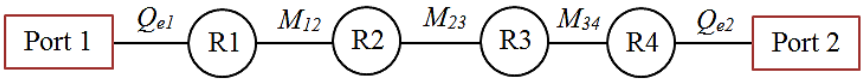

Figure 2.10 4th order filter topology

The filter response calculated from the synthesised coupling matrix and by using equation (2-27) is shown in Figure 2.11.

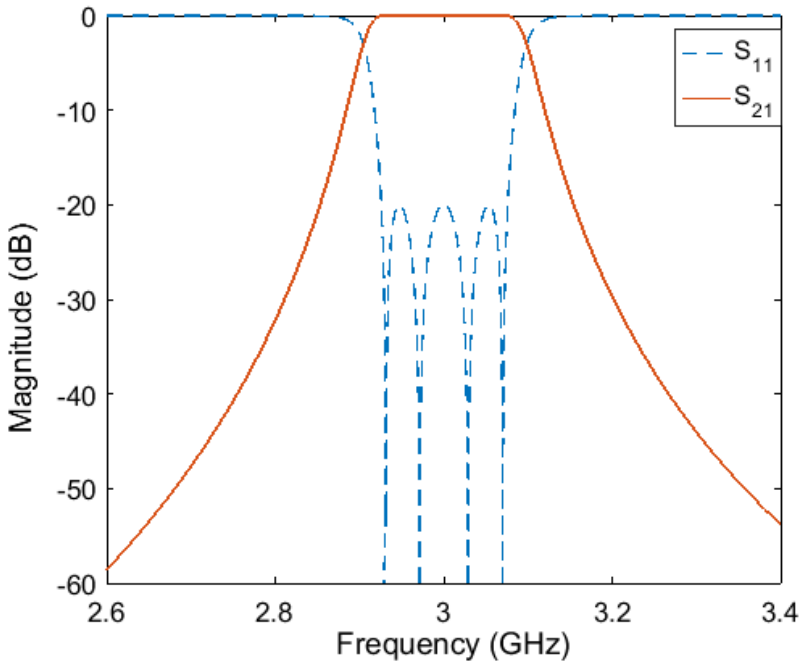

Figure 2.11 S-parameter responses for a 4th order passband filter calculated from coupling matrix

2.5 Summary

A brief explanation for the fundamental theory of microwave filters is presented in this chapter. This includes description for the transfer function of a Chebyshev response and the Chebyshev lowpass prototype filters as well as the transformation from lowpass prototype filters to bandpass filters. The representation of the $n \times n$ coupling matrix for an n^{th} order filter is described in this chapter, as well. Finally, an example for synthesis of a coupling matrix of a 6^{th} order Chebyshev filter is given.

References:

[1] J.-S. G. Hong and M. J. Lancaster, *Microstrip Filters for RF/Microwave Applications*. New York, NY, USA: Wiley, 2011.

[2] D. M. Pozar, *Microwave Engineering*. 4th ed. Hoboken, NJ, USA: Wiley, 2012.

[3] R. J. Cameron, R. Mansour, and C. M. Kudsia, *Microwave Filters for Communication Systems: Fundamentals, Design and Applications*. Hoboken, NJ, USA: Wiley, 2007.

[4] R. J. Cameron, "General coupling matrix synthesis methods for Chebyshev filtering functions," *IEEE Trans. Microw. Theory and Tech.*, vol. 47, no. 4, pp. 433-442, Apr 1999.

[5] P. Jarry, and J. Beneat, *Advanced Design Techniques and Realizations of Microwave and Rf Filters*, John Wiley & Sons, Inc., 2008.

[6] A. E. Atia and A. E. Williams, "New types of bandpass filters for satellite transponders," *COMSAT Tech. Rev.*, vol. 1, pp. 21–43, 1971.

[7] A. E. Atia and A. E. Williams, "Narrow-bandpass waveguide filters," *IEEE Trans. Microw. Theory Tech.*, vol. MTT-20, pp. 258–265, Apr. 1972.

[8] A. E. Atia, A. E. Williams, and R. W. Newcomb, "Narrow-band multiple-coupled cavity synthesis," *IEEE Trans. Circuits Syst.*, vol. CAS-21, pp. 649–655, Sept. 1974.

[9] R. J. Cameron, "Advanced coupling matrix synthesis techniques for microwave filters," *IEEE Trans. Microw. Theory and Tech.*, vol. 51, no. 1, pp. 1-10, Jan 2003.

[10] G. Matthaei, L. Young, and E. Jones, *Microwave filters, impedance-matching networks, and coupling structures*, Mcgraw-Hill, 1964.

Chapter 3 Novel Dielectric Split Ring Resonators with High Unloaded Quality Factor

3.1 Introduction

A new resonator with high unloaded quality factor Q_u called Dielectric Split Ring Resonator (Dielectric-SRR) is presented in this chapter. This resonator is utilised to design a microwave filter in the next chapters and is therefore looked into in detail. The Dielectric-SRR is made from a dielectric material of high constant (ε_r) and is of the same shape of a conventional metal Split Ring Resonator (Metal-SRR) [1-3]. The new Dielectric-SRR can achieve Q_u higher than the conventional Metal-SRR due to removing the conduction loss [4]. The Q_u of the Dielectric-SRR can be even higher than the Q_u of the conventional cylindrical Dielectric Resonators (CDRs) [5, 6] with the same dielectric constant (ε_r) and loss tangent.

An overview of the conventional Dielectric Resonators (DRs) is given in Section 3.2. The Dielectric-SRR is modelled and simulated by the CST software package in Section 3.3, the Metal-SRR is simulated in this section for comparison purposes. The simulation results include the resonators electromagnetic field distribution, resonance frequency and unloaded quality factor (Q_u). The fabrication and measurements of some Dielectric-SRRs and the Metal-SRR are described in section 3.4. Comparison between the Dielectric-SRR and the conventional CDR is given in Section 3.5.

3.2 Dielectric Resonators (DRs)

The DRs are a good choice for microwave filters with stringent requirement on the insertion loss. The DR filters have a small size and weight compared to waveguide filters and very low insertion loss compared to microstrip and coaxial filters; such filters are very suitable for many wireless applications such as satellite systems and mobile base stations [5-9].

The most common DR is a cylindrical dielectric resonator (CDR) as shown in Figure 3.1a [5, 6]. The CDRs are mounted in a metal cavity to decease the radiation loss, and supported by Teflon (or other low loss, low dielectric constant material) holders to decrease the conduction or cavity loss as shown in Figure 3.1b.

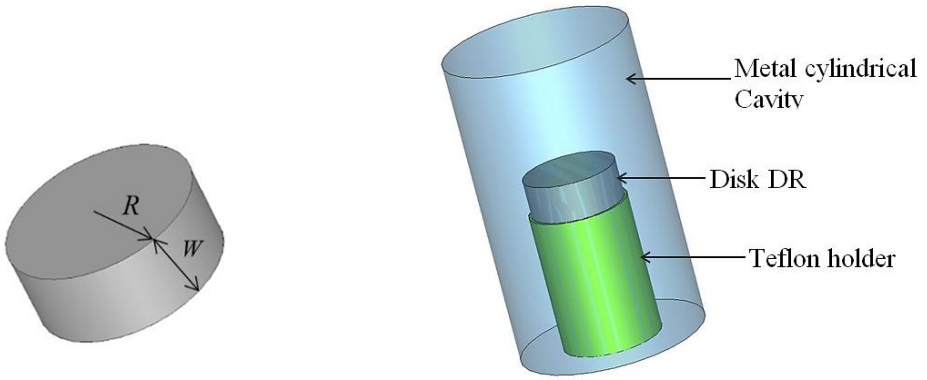

(a) (b)

Figure 3.1 Configuration of CDR, (a) CDR model with radius *R* and height *W*, and (b) CDR inside metal cavity and on the supporting holder

Most of the electromagnetic fields are stored inside the conventional DRs; the amount of stored electric fields depends on the dielectric constant (ε_r) [5, 6]. Popular ε_r for DRs are from 20 to 100 [5]; and the loss of DRs is primarily determined by the dissipated factor called loss tangent (tan δ). The DRs in some research paper are called Ceramic

Resonator because most DRs are made from ceramic material. The DR holders are usually made from dielectric material with low ε_r and loss tangent like Teflon of ε_r=2.1.

The dimensions of a DR depend on the fundamental mode wavelength (λ_d) inside the DR. The wavelength λ_d is proportional to $\lambda_o/\sqrt{\varepsilon_r}$, where λ_o is the wavelength in the air. For this reason a higher ε_r can be used with low frequencies to obtain a DR with a smaller size [5].

There are 3 other less common shapes for the DRs in the literature [5] as shown in Figure 3.2.

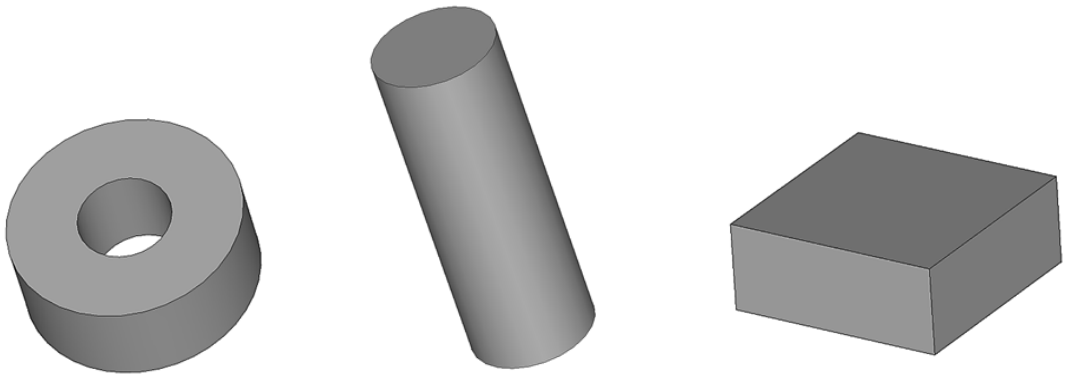

(a) (b) (c)

Figure 3.2 DRs with different shapes, (a) Ring DR, (b) Combline DR, and (c) Rectangular DR

The best achievable Q_u for conventional DRs (cylindrical, ring, combline or rectangular DR) are approximately equal in value if the DRs are made from the same material and resonate at same fundamental frequency. But these DRs have different electromagnetic (EM) field distributions, modes separation and volume [5-7].

The ring and cylindrical DRs have the same EM field distributions of TE_{01} for the fundamental mode as shown in Figure 3.3 [9]. The TE_{01} is the most common mode for designing DR filters because it has no degenerate mode [5].

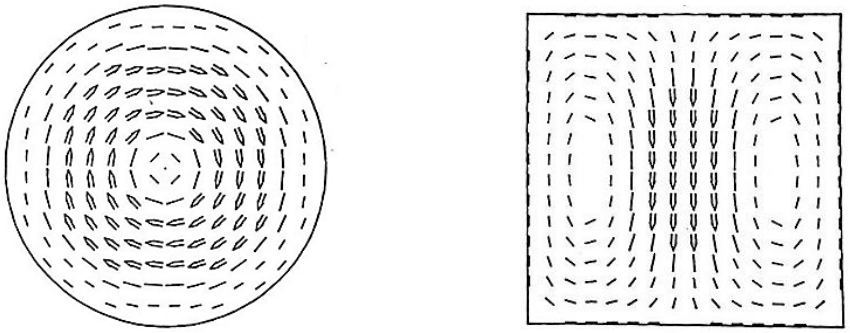

(a) (b)

Figure 3.3 TE_{01} mode of CDR, (a) electric field of top view and (b) magnetic fields of side view from [9]

In general the DRs have relatively a small separation between the fundamental mode and first higher order. For example the mode separation for the cylindrical DR with (ε_r = 97) is about 600 MHz at S band and for the ring DR with (ε_r = 97) is about 1100 MHz at S band [5, 6].

There are two common methods used in the past to design and investigate the conventional DRs: Cohn's method in 1968 and the mode-matching method in 1983 [10-12]. Recently investigating the DR characteristics such as resonance frequency and the unloaded quality factor are achieved based on an EM simulator like the CST software package [13-14].

New DRs with complex shapes compared to conventional DRs are designed by using the EM simulators. These new DRs are useful for designing low loss filters with interesting features. For example the half-cut DR with through slots is presented for dual-mode and quad-mode filters as shown in Figure 3.4a [15]. Another new DR with rectangular shape and through slots is designed for the triple-band filters as shown in Figure 3.4b [16]. A new shape of DR is presented in the next section and used to design low loss tunable filters as well as untunable filters.

(a) (b)

Figure 3.4 DR with new shapes, (a) Half-cut DR with slots [15], and (b) Rectangular DR with slots [16]

3.3 The Dielectric Split Ring Resonator (Dielectric-SRR)

This section presents a new type of microwave resonator with high Q_u. This new resonator has a shape similar to the conventional Metal-SRR and a material similar to the conventional DRs. Subsequently, this new resonator is named the Dielectric-SRR. The Dielectric-SRR can obtain Q_u higher than the Metal-SRR due to its use of dielectric material of high constant [17]. Also, the EM field distributions of the Dielectric-SRR are useful to design BW tunable filters [17]. Therefore, this new resonator is chosen to design tunable and non-tunable filters with low insertion loss later in this thesis.

The Dielectric-SRR has a cylindrical ring with a longitudinal gap, as shown in Figure 3.5. This resonator achieves EM field distributions similar to that of the conventional Metal-SRRs with a high Q_u, like the conventional DRs.

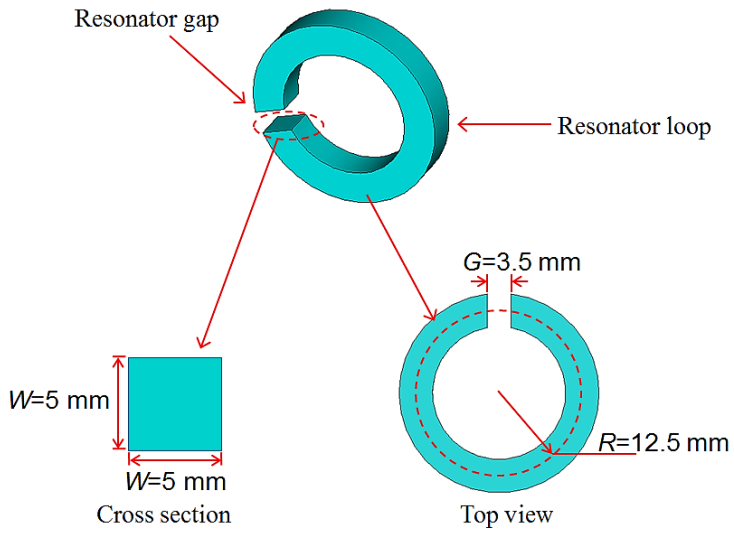

Figure 3.5 The Dielectric-SRR dimensions: the gap width (*G*), the resonator radius (*R)* and the cross section (*W*)

The Dielectric-SRR is modelled by CST software with the dimensions as shown in Figure 3.5. These dimensions can achieve high Q_u, as shown later in this section. The conventional Metal-SRR is also modelled with the same dimensions for comparison purpose. Each resonator is mounted on a Teflon holder and is inside a metal cavity, as shown in Figure 3.6. The material specifications of this model are listed in Table 3.1.

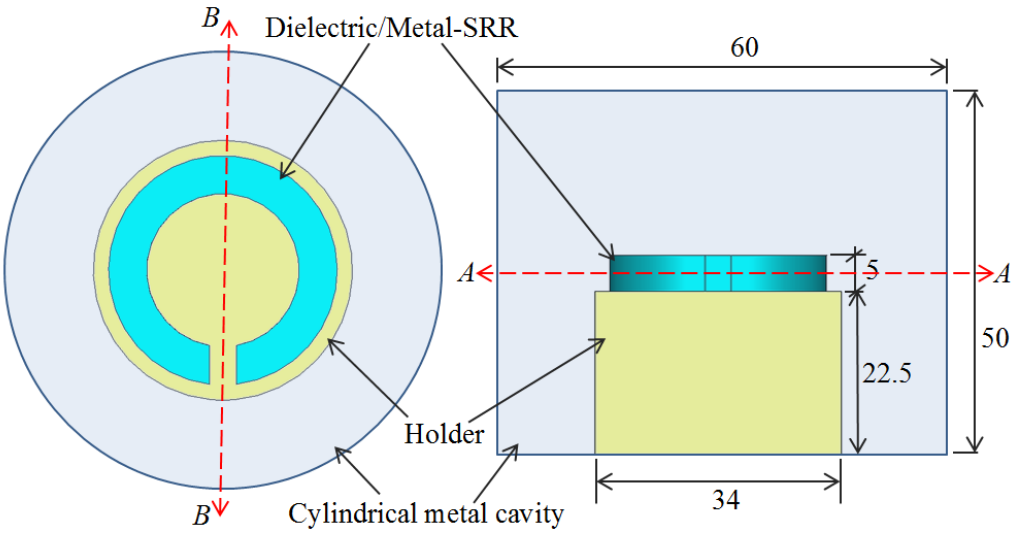

Figure 3.6 Model of single resonator inside metal cavity and on the Teflon holder, the dimensions unit in (mm)

Table 3.1 Material specifications for the model in Figure 3.6

	Dielectric-SRR	Holder	Metal-SRR and metal cavity
Material specifications	Titania ε_r =97 tan δ= 7.2×10^{-5}	Teflon ε_r =2.1 tan δ= 4.4×10^{-5}	Copper with electric conductivity of σ =5.8 × 10^{7} S/m

The CST simulated EM field distributions of the fundamental mode for the Dielectric-SRR and the Metal-SRR are shown in Table 3.2. These simulations in Table 3.2 show that the most electric field is inside the resonator gap, and most magnetic fields are at the opposite side around the resonator loop in both the Metal-SRR and Dielectric-SRR. In addition, the EM fields are not high inside the dielectric material of the Dielectric-SRR.

Table 3.2 EM field distributions for the Dielectric-SRR and the Metal-SRR. The top view for cross section AA and the side view for cross section BB (See Figure 3.6)

		Metal-SRR	Dielectric-SRR
Electric Fields	Top View	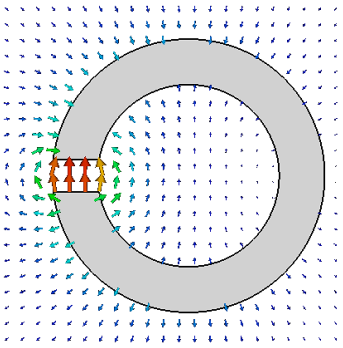	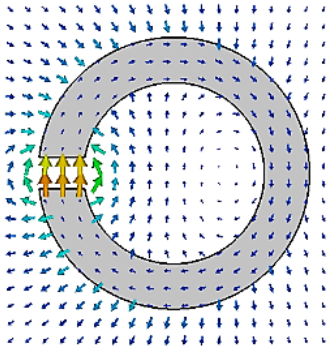
	Side View	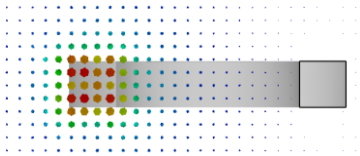	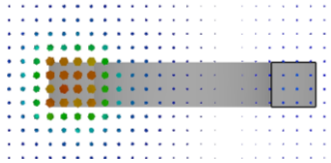
Magnetic Fields	Top View	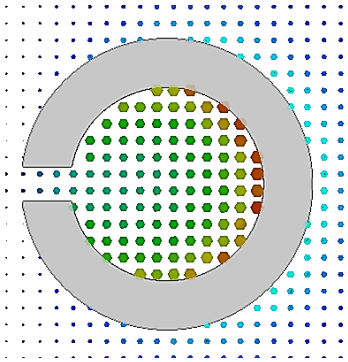	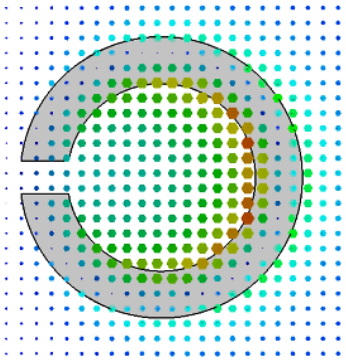
	Side View	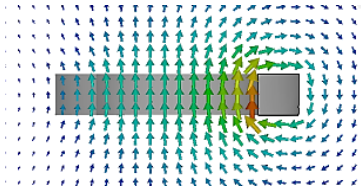	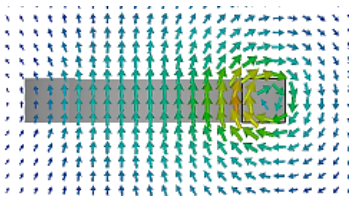

The power loss in the each part of the resonator model (in Figure 3.6) can be determined by quality factor or *Q*-factor, as given in Chapter 2 [18]. The power dissipated in the conductors of the resonator model is assessed by the conductive quality factor Q_c, and power dissipated in the dielectrics is assessed by the dielectric quality factor Q_d. The total dissipated power in the all parts of the resonator model is determined by the unloaded quality factor Q_u. When using the Metal-SRR with the model given in Figure 3.6, the Q_u can be calculated by [18]

$$\frac{1}{Q_u} = \frac{1}{Q_{c\_cavity}} + \frac{1}{Q_{c\_resonator}} + \frac{1}{Q_{d\_holder}} \tag{3-1}$$

and when using the Dielectric-SRR, the Q_u can be calculated by [18]

$$\frac{1}{Q_u} = \frac{1}{Q_{c\_cavity}} + \frac{1}{Q_{d\_resonator}} + \frac{1}{Q_{d\_holder}} \tag{3-2}$$

The lower dissipated power in the parts of the resonator model leads to achieving higher Q_u for the resonator model. Therefore, the resonators with higher Q_u are desired for designing filters with lower insertion loss. The Eigenmode analysis in CST software is used to calculate the *Q*-factors for the resonator model as given in Figure 3.6. The simulated *Q*-factors by the Eigenmode solver for the Metal-SRR and Dielectric-SRR are as shown in Figure 3.7.

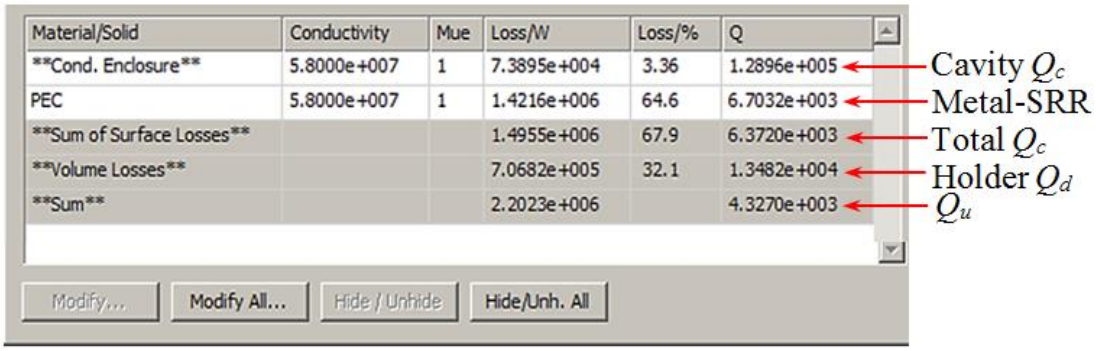

(a)

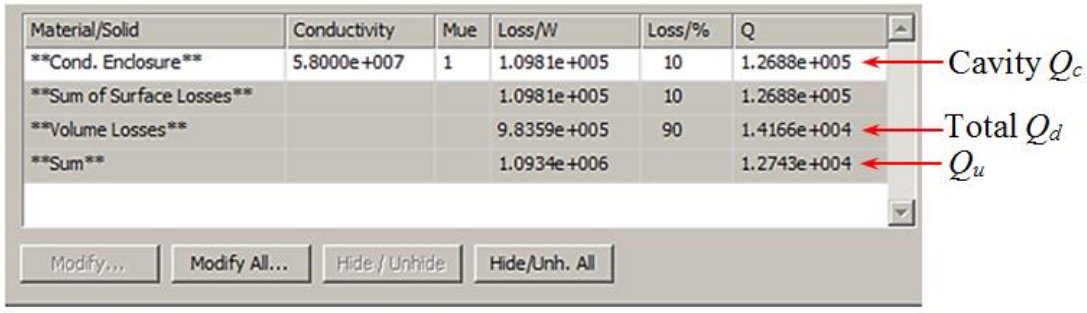

(b)

Figure 3.7 CST dialog box of the *Q*-factors calculation. (a) Results of the Metal-SRR and (b) Results of the Dielectric-SRR

The volume-loss results in the CST dialog box represent the total Q_d of the Dielectric-SRR and the Teflon holder. The Q_d of the Dielectric-SRR can be found by assuming the holder has zero loss (loss tangent = 0) and simulating the resonator model again. Holder Q_d can then be determined by subtracting the Dielectric-SRR Q_d from the total Q_d (See equation 3-2). The CST simulated results of the all *Q*-factors for the Dielectric-SRR and the Metal-SRR are listed in Table 3.3.

Table 3.3 Comparison of the CST simulated *Q*-factors for Dielectric-SRR and Metal-SRR.

	Dielectric-SRR	Metal-SRR
f_c *(GHz)*	2.19	1.51
Cavity Q_c	126,880	128,960
Metal-SRR Q_c		6,703
Total Q_c	126,880	6,372
Holder Q_d	37,100	13,482
Dielectric-SRR Q_d	22,915	
Total Q_d	14,166	13,482
Q_u	12,743	4,327

As shown in Table 3.3, the Q_u of Dielectric-SRR is three times higher than the Q_u of Metal-SRR. This is due to removing the conduction loss of the Metal-SRR by using the dielectric material of high constant.

The Metal-SSR in Table 3.3 has a slightly lower frequency than the Dielectric-SSR. However, if the Metal-SSR is reduced in size to give the same frequency as the Dielectric-SSR (2.19 GHz), the simulation result of Q_u at 2.19 GHz increases to 4,035. This Metal-SRR Q_u is still almost three times lower than the Dielectric-SSR.

The holder Q_d values (in Table 3.3) are relatively low compared to cavity *Q*-factors, and this leads to decrease the Q_u of the resonator model. In order to determine the holder effect, the resonator model is simulated again without the holder. The simulated Q_u for the Dielectric-SRR and the Metal-SRR without using holders are as given in Table 3.4.

Table 3.4 Comparison of the CST simulated Q_u and f_c for the Dielectric-SRR and Metal-SRR without using Holder.

	Without Holder		With Holder	
	Dielectric-SRR	Metal-SRR	Dielectric-SRR	Metal-SRR
f_c *(GHz)*	2.315	1.68	2.19	1.51
Q_u	20,507	7,275	12,743	4,327

The resonator Q_u, without using the holder, is increased by 60% for the Dielectric-SRR and by 68% for the Metal-SRR. These results show the cylindrical holders have significant effect on Q_u of the Dielectric-SRRs and the Metal-SRRs.

On the other hand, this cylindrical holder achieves very high Q_d with conventional DRs [4-10]. This is because the most electric fields are stored inside the dielectric material of the conventional DRs (e.g. ring, cylindrical, and rectangular DR) [4, 5]. Thus, the electric fields within holders of conventional DRs are very low. The cylindrical holder effect on the CDR Q_u is shown later in this chapter.

In the case of the Dielectric-SRR, the most electric fields are stored near and inside the gap of the resonator (as given in Table 3.2). This electric fields distribution leads to the increase of electric fields and loss within the holder because the cylindrical holder is very close to the resonator gap. Therefore, a new holder is designed for the Dielectric-SRR to increase the holder Q_d. This holder has a Y configuration with the same material of the conventional holder (in Table 3.1) and is called Y-holder. The Y-holder design

reduces the overall amount of the holder Teflon material, especially from the resonator gap as shown in Figure 3.8.

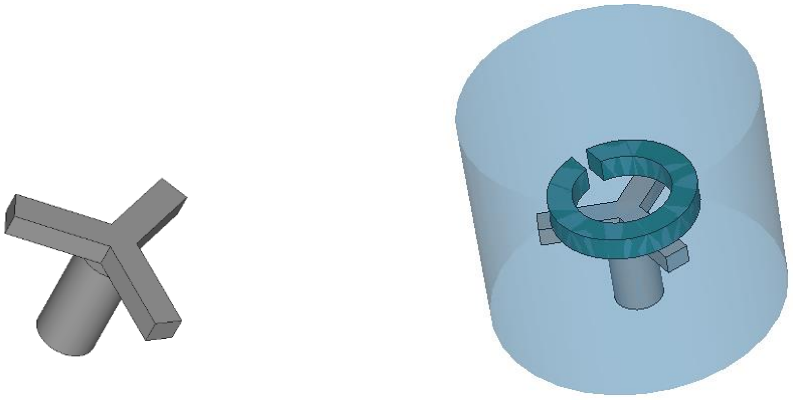

(a) (b)

Figure 3.8 Configuration of the Y-holder, (a) 3-D model of the Teflon Y-holder and (b) the single resonator inside a metal cavity and mounted on a Y-holder

The new single resonator model in Figure 3.8b is the same as the model which used in previous simulations (in Figure 3.6) except for the new Y-holder. The dimensions of the model in Figure 3.8b are as shown in Figure 3.9.

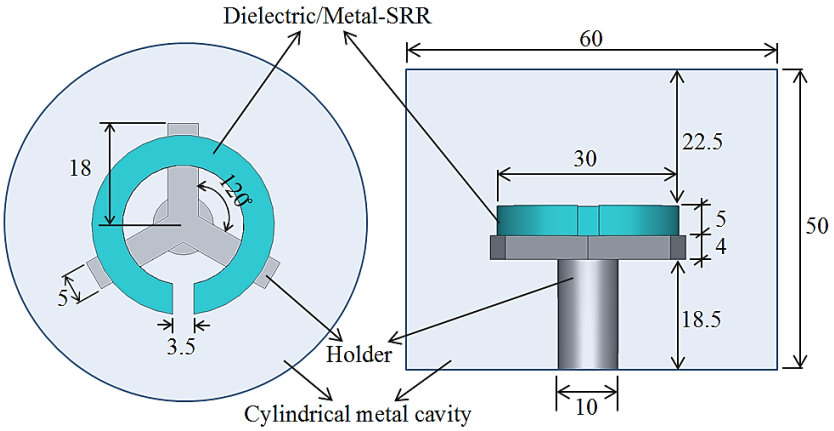

Figure 3.9 Model of a single resonator inside metal cavity and on the Teflon holder. The model material specifications are given in Table 3.1. The dimensions unit in (mm)

Comparison of CST simulated results for the model of Y-holder (Figure 3.9) and the model of the conventional holder (in Figure 3.6) are summarised below in Table 3.5.

Table 3.5 Q_u comparison for Dielectric-SRR and Metal-SRR when used conventional holder (in Figure 3.6) and Y-holder (in Figure 3.9)

	By Using Y-holder		By Using Conventional Holder	
	Dielectric-SRR	Metal-SRR	Dielectric-SRR	Metal-SRR
f (GHz)	2.3	1.66	2.19	1.51
Cavity Q_c	122,510	124,010	126,880	128,960
Metal-SRR Q_c		7,616		6,703
Total Q_c	122,510	7,176	126,880	6,372
Holder Q_d	315,080	108,810	37,100	13,482
Dielectric-SRR Q_d	24,502		22,915	
Total Q_d	22,734	108,810	14,166	13,482
Q_u	19,176	6,732	12,743	4,327

The results in Table 3.5 show that, by using the Y-holder instead of the conventional holder, the Q_u values are increased by 50% with Dielectric-SRR and by 55% with the Metal-SRR. The Q_d values of the Y-holder are increased due to eliminating the Teflon material from the resonator gap where the most electric fields are stored. The Dielectric-SRR Q_u in Table 3.5 is three times higher than the Metal-SRR Q_u when using either the Y-holder or the conventional holder.

3.3.1 The effect of the resonator gap on the Fundamental Resonance Frequency

The relationship between the gap dimensions of the Dielectric-SRR and the fundamental resonance frequency is investigated in this section by using the CST software. The same model of the Dielectric-SRR inside the cylindrical metal cavity (in Figure 3.9) and the material specifications in Table 3.1 are used in the CST simulations.

The gap dimensions *G* and *W* as shown in Figure 3.5 are varied in CST simulations. The dimension *G* is varied from 1 to 5 mm when *W*=5 mm and the resonator radius is 12.5 mm. The CST simulation results of the fundamental resonance frequency are shown in Figure 3.10.

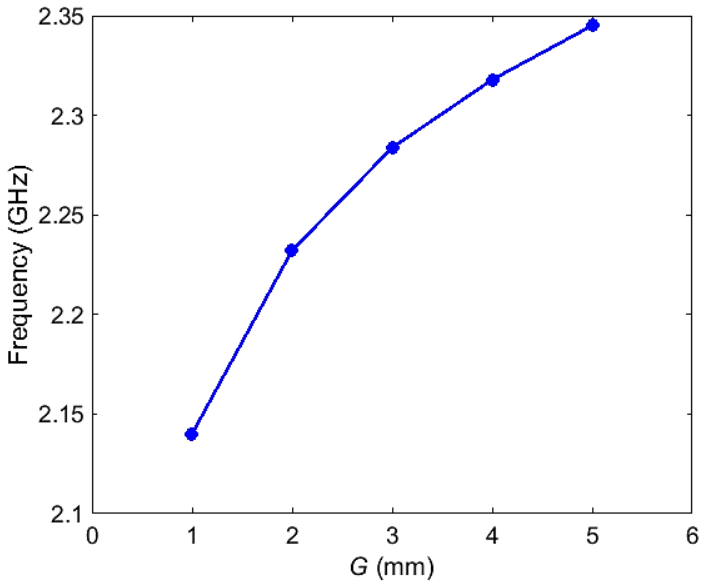

Figure 3.10 Fundamental resonance frequency against the resonator gap dimension *G*

The increasing *G* as shown in Figure 3.10 led to the decreasing of capacitance in the resonator gap where the most electric fields located and thus an increase of the resonant frequency.

In addition the gap dimension *W* is varied by the CST software from 3 to 8 mm when *G* = 3.5 mm, the results of these simulations are as shown in Figure 3.11. As expected the resonance frequency decreases when *W* increases due to the increase of capacitance in the resonator gap.

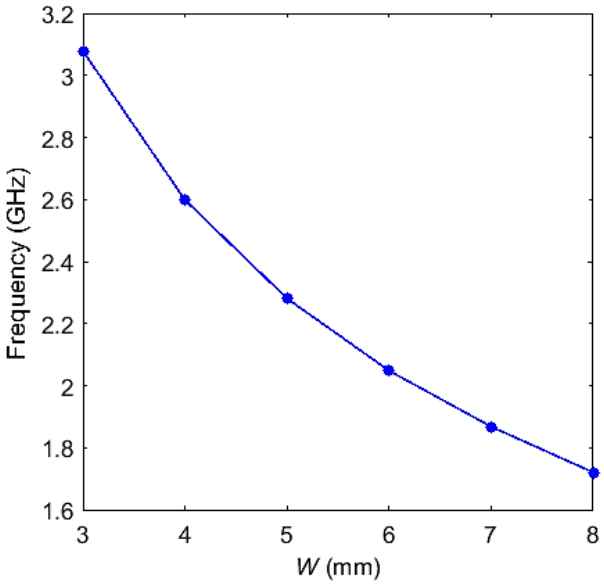

Figure 3.11 Fundamental resonance frequency against the gap dimension *W*

3.3.2 Effect of the Dielectric-SRR Dimensions on the Q_u and the Mode Separation

This section shows the effect of the Dielectric-SRR dimensions on the Q_u at 2.3 GHz, and on the separation between the fundamental mode (2.3GHz) and the first higher order. The model of the single Dielectric-SRR (in Figure 3.9) with the material specifications shown in Table 3.1 are used in the CST simulations. The resonator gap dimension *W* (in Figure 3.5) is varied with three different *G* values, and the resonator radius *R* is tuned to fix the fundamental resonance frequency at 2.3 GHz.

The CST simulated results of Q_u and the mode separation are as shown in Figure 3.12. The mode separation represents the separation between the fundamental mode (2.3 GHz) and the first higher order mode of the Dielectric-SRR. The EM field distributions of fundamental mode are given in Table 3.2 and the EM field distributions of first higher mode are as shown in Table 3.6.

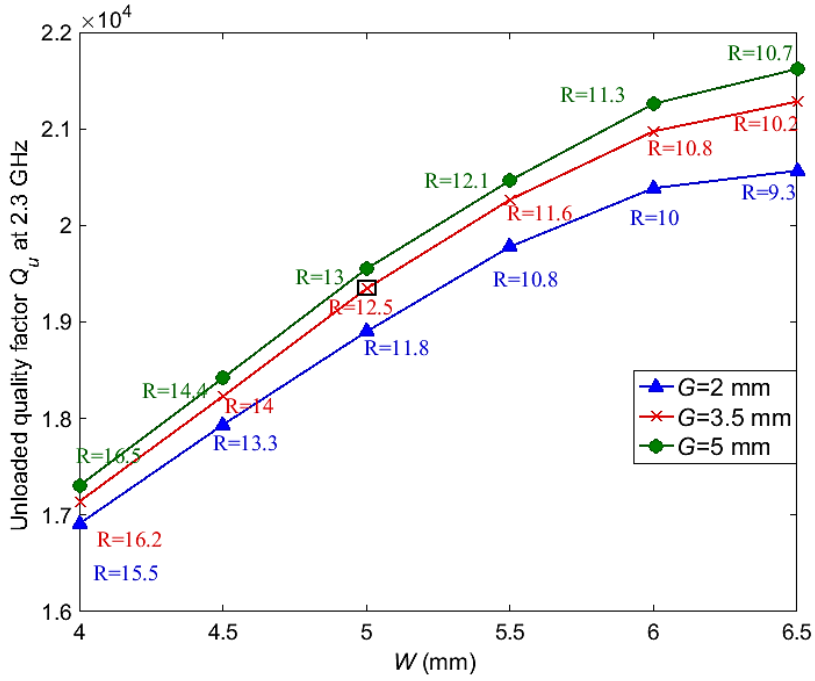

(a)

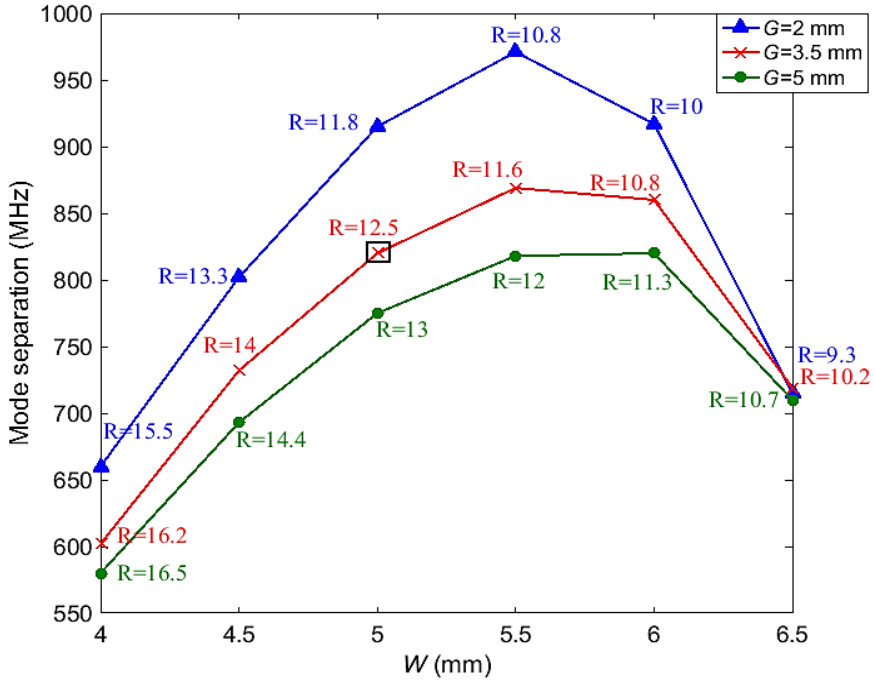

(b)

Figure 3.12 Effect of Dielectric-SRR dimensions, (a) on the Q_u and (b) on the modes separation

Table 3.6 EM field distributions for fist higher order of the Dielectric-SRR

	Top View	Side View
Electric Fields	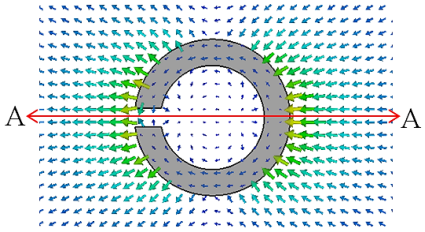	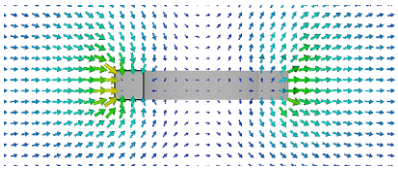 Section AA
Magnetic Fields	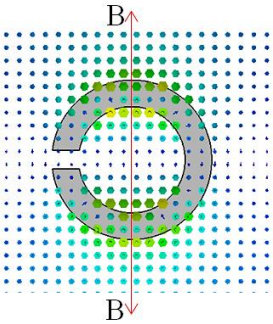	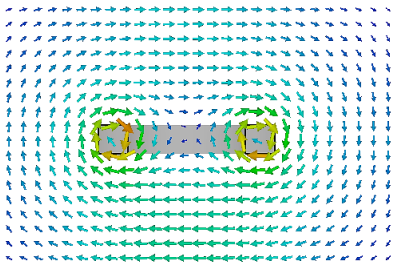 Section BB

Figure 3.12 (a) shows for the three *G* dimensions the Q_u increases when the *W* increases and *R* decreases at the same time. Also, the Q_u increases when the *G* and *R* increase at the same time and in the same *W* dimension. The varying of the Q_u values at 2.3 GHz and the mode separation as given Figure 3.12 are due to combination of two different dimensions. So, for these simulations, it is not possible to determine the effect of each dimension on the Q_u and the mode separation.

The simulated results show the best Q_u and mode separation together can be achieved at 2.3 GHz when the Dielectric-SRR dimension *W* is about 5 to 6 mm and *R is* about 10 to 12 mm, depending upon the value of *G*. The square in Figure 3.12 indicates the dimensions of *R* = 12.5 mm, *W* = 5 mm, and *G* = 3.5 mm, which are used in the previous CST simulations (in Table 3.4) and was fabricated in the next section. The fact that this is not at the best mode separation/Q_u point is due to the Dielectric-SRRs being

fabricated before this investigation of the mode separation and Q_u against the resonator dimensions.

The cavity radius is increased and decreased with the Dielectric-SRR radius (*R)* to make sure the metal cavity has a small effect on Q_u. The Q_c values of the metal cavity for all the results (in Figure 3.12a) are from 122,700 to 124,500, showing the metal cavity has a minimal effect on the total Q_u.

3.4 Fabrications and Measurements

The Dielectric-SRR, Metal-SRR, and Y-holder are fabricated with the dimensions shown in Figure 3.9 and the material specifications in Table 3.1. The fabricated Dielectric-SRR, Metal-SRR, Y-holder, and the cylindrical cavity are shown in Figure 3.13. The holder is fixed in the cylindrical cavity by inserting the holder base into a slot with 3 mm depth on the bottom of the cavity, as shown in Figure 3.14. The slot diameter is larger than the holder base diameter by about 0.2 mm to achieve a tight connection between the holder and the cavity. Due to this slotting of holder into the cavity, the length of holder base is increased by 3 mm in the fabrication. The resonator is then fixed tightly on the holder by adding three small Teflon sticks on the holder with 2 mm height and thickness, as shown in Figure 3.14. The resonator model as given in Figure is simulated with these Teflon sticks to investigate their effects on the Q_u and the resonance frequency. The CST simulations showed these sticks have no effect on the resonator Q_u and only shift the resonance frequency by 1 MHz. This is due to the very small dimensions of these sticks as well as their Teflon material of low constant and loss tangent.

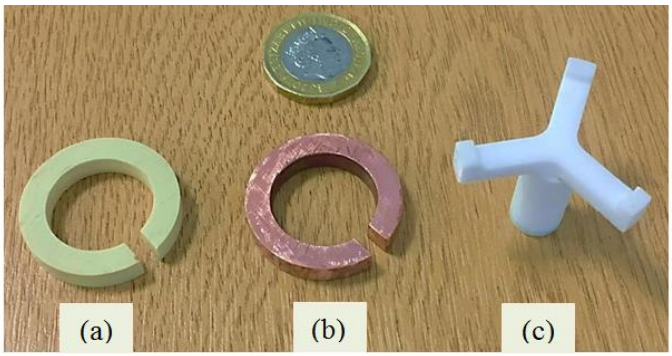

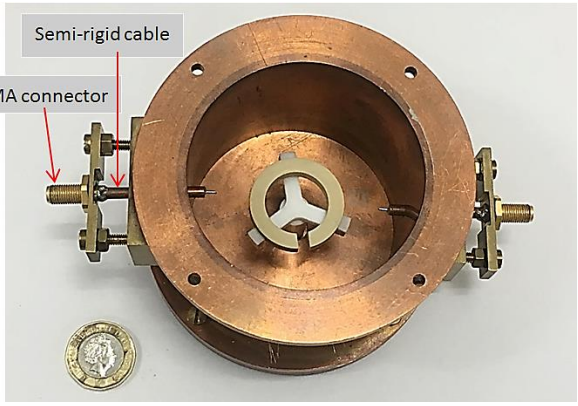

(d)

Figure 3.13 Fabrications (a) The Dielectric-SRR, (b) Metal-SRR, (c) Y-holder, and (d) Cylindrical metal cavity with the resonator, Y-holder, and removed lid

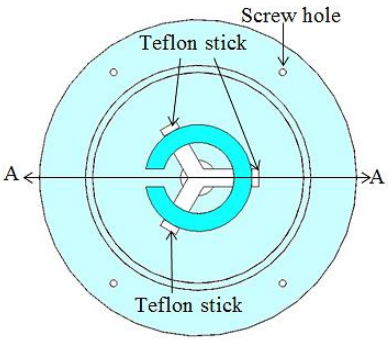

(a)

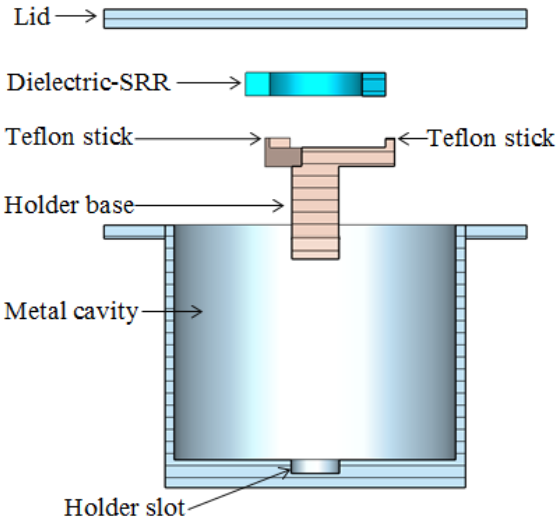

(b)

Figure 3.14 Parts of the resonator structure: (a) Top view and (b) Side view section AA

The measured S_{21} responses for the Dielectric-SRR and the Metal-SRR are shown in Figures 3.15 and 3.16, respectively.

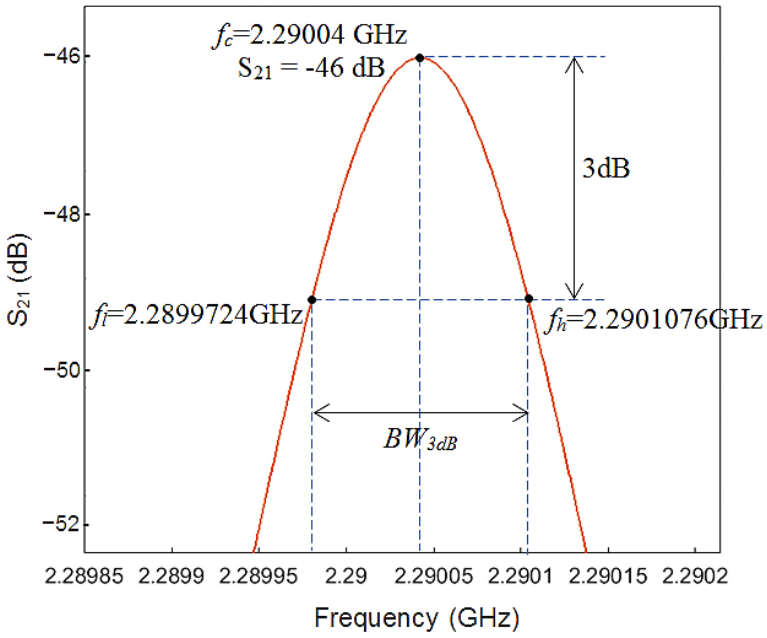

Figure 3.15 Measured S_{21} results for the Dielectric-SRR

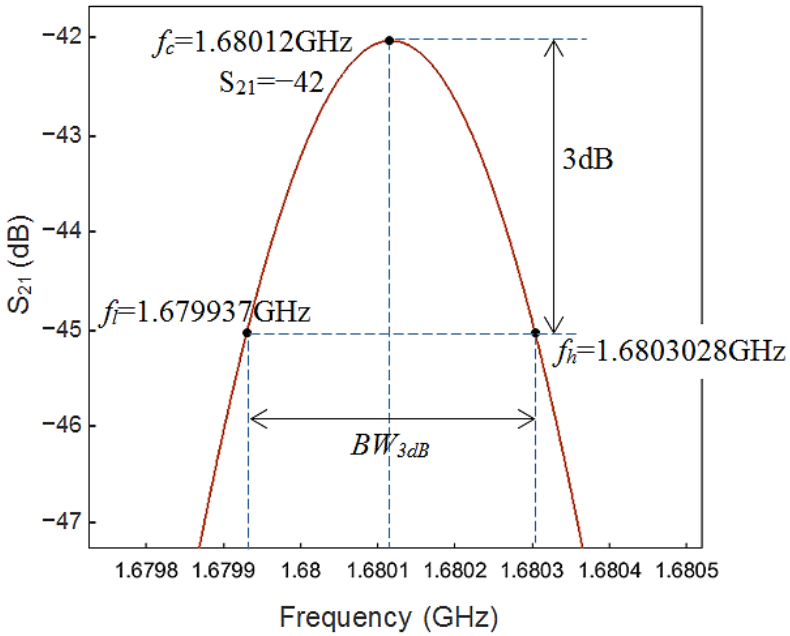

Figure 3.16 Measured S_{21} results for the Metal-SRR

The Q_u for both resonators are calculated based on the above measured results by using [18]

$$Q_u = \frac{Q_L}{1-10^{\frac{S_{21}}{20}}} \tag{3-3}$$

Here, S_{21} is the minimum measured loss at the resonance frequency f_c, and Q_L is the loaded quality factor, which is determined by using the centre frequency f_c and the 3dB bandwidth BW_{3dB} of the above measured S_{21} results as given [18]

$$Q_L = \frac{f_c}{BW_{3dB}} \tag{3-4}$$

The measured f_c and Q_u for the Dielectric-SRR and the Metal-SRR, with comparison to the simulated f_c and Q_u, are summarised in Table 3.7.

Table 3.7 Comparison between measured and simulated results for the Dielectric-SRR and the Metal-SRR

	Measurement		Simulation	
	Dielectric-SRR	Metal-SRR	Dielectric-SRR	Metal-SRR
f_c *(GHz)*	2.29	1.68	2.3	1.66
Q_u	17,021	4,630	19,176	6,732

As shown in Table 3.7, the measurements of f_c for both resonators are lower than the simulations. Also, the measurements of Q_u are lower than the simulations by about 10% for the Dielectric-SRR and 30% for the Metal-SRR. This due to the losses in the SMA connectors and the 5 cm semi-rigid cables which are not considered in the CST Eigenmode simulations. However, the measurements in Table 3.7 show that the

Dielectric-SRR Q_u is also three times higher than Metal-SRR Q_u, similar to the CST simulation results.

3.5 Q_u Comparison for Dielectric-SRR and the cylindrical DR

This section presents a comparison between the Q_u of the novel Dielectric-SRR and the Q_u of conventional CDR when both resonators have the same fundamental resonance frequency and material specifications (ε_r and tan δ). This comparison contains only CST simulation results. There are more shapes for the conventional DRs, such as the ring, combline, and rectangular DR (in Figure 3.2), but only the CDR is chosen for the comparison here because it is the most widely used [4-11], and the conventional DRs with these different shapes have approximately the same Q_u [5].

The best Q_u and mode separation for the CDR, as shown in Figure can be achieved by using the ratio of $W/2R$ = 0.4. This ratio can achieve the strongest magnetic fields with a sufficient distance outside the CDR [5, 10]. As a result, this ratio is adopted to model the CDR in this section.

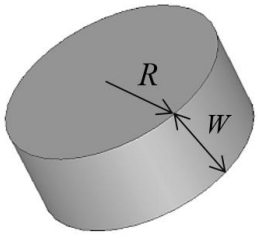

Figure 3.17 Configuration of CDR R is the resonator radius, and W is the height.

The Dielectric-SRR and the CDR are mounted on the Teflon holder and inside a cylindrical copper cavity, as shown in Figure 3.18. Both these resonators in Figure 3.18

are modelled to achieve the same fundamental resonance frequency of 2.3 GHz with the same material specifications (in Table 3.1). The CST simulation results of Q_u are summarised in Table 3.8.

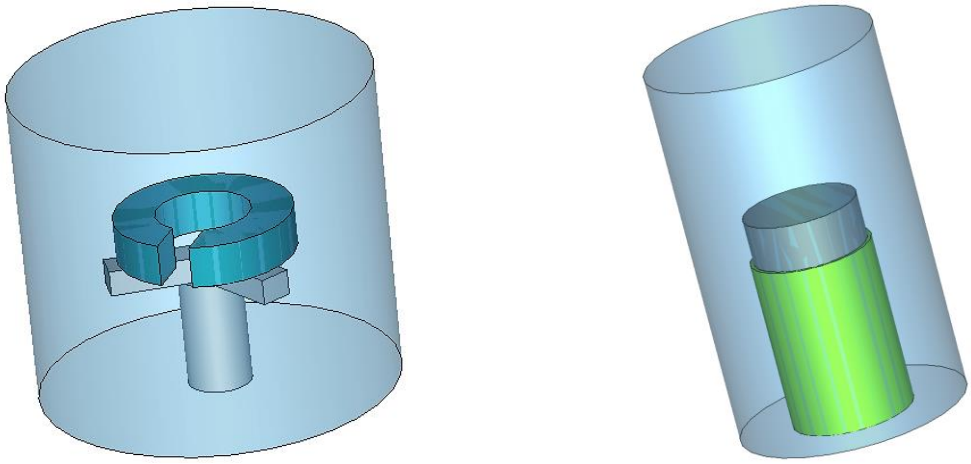

(a) (b)

Figure 3.18 Model of single resonator inside the cavity and on the Teflon holder. (a) the Dielectric-SRR and (b) the conventional CDR.

Table 3.8 CST simulation results for comparison between Dielectric-SRR and DR, both resonators have same material specifications (in Table 3.1)

	Dielectric-SRR	DR
Resonator Dimensions (mm): Radius (R), Height (W), Gap Width (G)	R=10.7, W=6.5, G=5	R=7.5, W=6
Cavity Dimensions	Radius= 30, Height= 50	Radius= 15, Height=50
Resonance Frequency f_c	2.3 GHz	2.3 GHz
Cavity Q_c	106,710	112,430
Holder Q_d	247,110	14×10^5
Resonator Q_d	30,453	14,108
Unloaded Quality Factor Q_u	21,621	12,423

The comparison in Table 3.8 shows the Q_u of the Dielectric-SRR is two times higher than the Q_u of the CDR. This is a result of the most electric fields with Dielectric-SRR being stored near and inside the resonator gap (see Table 3.2), while the most electric fields of CDR are stored inside the dielectric material [5]. On the other hand, the radius of the Dielectric-SRR is about twice the radius of CDR. The high Q_u property of the Dielectric-SRR is very important to design low loss filters, and the fact that the Dielectric-SRR is slightly larger than CDR is of less importance. The Dielectric-SRR also has the advantage that the shape and the EM field distributions are very useful to design tunable filters, as will be seen in later chapters.

The CDR model in Figure 3.18b is further simulated by CST software with holders having three different diameters to investigate the effect of the conventional holder on the Q_u of the CDR. The three holders are as shown in Figure 3.19.

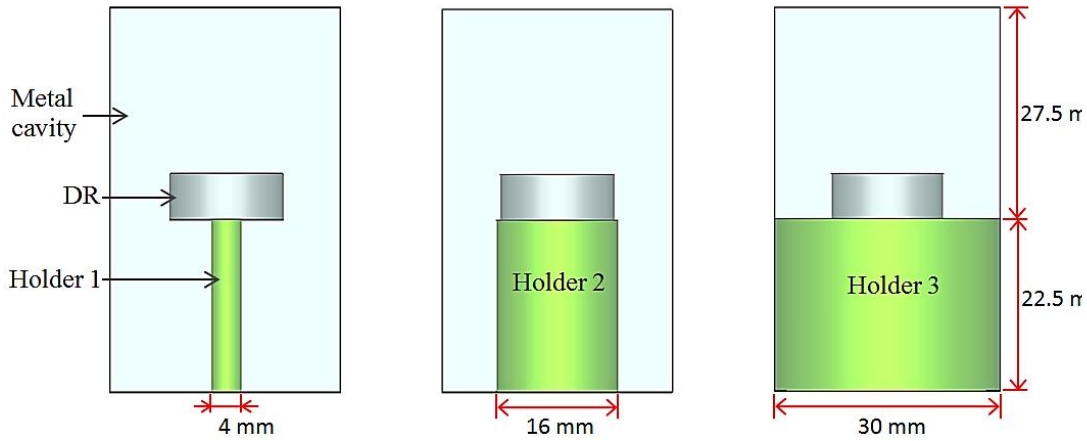

Figure 3.19 DR inside metal cavity and mounted on a cylindrical holder. (a) Holder 1 of diameter=4mm, (b) Holder 2 of diameter of 16mm, and (c) Holder 3 of diameter of 30mm.

The CST simulation results of the Q_u and f_c for the three models in Figure 3.19 are given in Table 3.9.

Table 3.9 CST simulation results for CDR with 3 holders of different size

	Holder 1	Holder 2	Holder 3
Holder Diameter (mm)	8	16	30
Frequency f_c (GHz)	2.301	2.3	2.298
Cavity Q_c	112,690	112,430	110,470
Dielectric Q_d	14,084	13,967	13,899
Unloaded Quality Factor Q_u	12,520	12,423	12,345

As shown in Table 3.9, the holder size has a very small effect on Q_u of the CDR. This is because most of the electric fields of the conventional CDR are stored inside the dielectric material [5]. As a result, the electric fields and losses within CDR holder are very small. While the Dielectric-SRR stores the most electric fields inside and surrounding its gap, some of electric fields are stored inside dielectric material, as given in Table 3.2. This leads to an increase in the electric fields and losses within the holder of Dielectric-SRR, as given in Table 3.5. In the case of the Metal-SRR, the holder has a much higher effect on the Q_u, as given in Table 3.5. This is due to the Metal-SRR stores the electric fields outside the metal material, and this implies much higher electric fields and losses within the holder of Metal-SRR.

3.6 Summary

This chapter presented a new high Q_u resonator called Dielectric-SRR. This new resonator has the shape and EM field distributions similar to the conventional Metal-SRR but is made from dielectric material of high constant.

The Dielectric-SRR was designed and investigated based on the CST software package and the resonator EM field distributions and Q_u as well as the effect of resonator dimensions on the resonance frequency, mode separation were presented in this chapter.

The Dielectric-SRR and the conventional Metal-SRR are fabricated and measured. The simulated and the measured results showed the Dielectric-SRR Q_u is 3 times higher than the Metal-SRR.

The CST simulated results of Dielectric-SRR were compared to the conventional CDR as well; the comparison showed the Dielectric-SRR Q_u is 2 times higher than the CDR Q_u but the radius of CDR is about half the radius of Dielectric-SRR.

The Dielectric-SRRs not only have a high Q_u, but also a shape and EM field distributions which are very useful to design low loss tunable filters as well as non-tunable filters as given in the next chapters.

References:

[1] M. Mehdizadeh, T. K. Ishii, J. S. Hyde and W. Froncisz, "Loop-Gap Resonator: A Lumped Mode Microwave Resonant Structure," *IEEE Trans. Microw. Theory and Tech.*, vol. 31, no. 12, pp. 1059-1064, Dec. 1983.

[2] R. F. Mostafavi, D. Mirshekar-Syahkal and Y. C. M. Lim, "Small filters based on slotted cylindrical-ring resonators," *IEEE Trans. Microw. Theory and Tech.*, vol. 49, no. 12, pp. 2369-2375, Dec 2001.

[3] H. Salehi, R. R. Mansour, and V. Dokas, “Lumped-element conductorloaded cavity resonators,” *IEEE MTT-S Int. Microw. Symp. Dig.*, vol. 3, Seattle, WA, Jun. 2002, pp. 1601–1604.

[4] Chi Wang, K. A. Zaki, A. E. Atia and T. G. Dolan, "Dielectric combline resonators and filters," *IEEE Trans. Microw. Theory and Tech.*, vol. 46, no. 12, pp. 2501-2506, Dec 1998.

[5] C. Wang and K. A. Zaki, "Dielectric resonators and filters," *IEEE Microw. Mag.*, vol. 8, no. 5, pp. 115-127, Oct. 2007.

[6] S. J. Fiedziuszko, I.C. Hunter, T. Itoh, *et al*., "Dielectric materials, devices, and circuits," *IEEE Trans. Microw. Theory and Tech.*, vol. 50, no. 3, pp. 706-720, Mar 2002.

[7] R. R. Mansour, "Filter technologies for wireless base stations," *IEEE Microw. Mag.*, vol. 5, no. 1, pp. 68-74, Mar 2004.

[8] R. R. Mansour, "High-Q tunable dielectric resonator filters," *IEEE Microw. Mag.*, vol. 10, no. 6, pp. 84-98, Oct. 2009.

[9] D. Kajtez, P. Guillon, *Dielectric Resonators*. 2nd ed., Atlanta, GA: Noble, 1998.

[10] S. B. Cohn, "Microwave Bandpass Filters Containing High-Q Dielectric Resonators," *IEEE Trans. Microw. Theory and Tech.*, vol. 16, no. 4, pp. 218-227, Apr 1968.

[11] K. A. Zaki and A. E. Atia, "Modes in Dielectric-Loaded Waveguides and Resonators," *IEEE Trans. Microw. Theory and Tech.*, vol. 31, no. 12, pp. 1039-1045, Dec. 1983.

[12] S. W. Chen and K. A. Zaki, "Dielectric ring resonators loaded in waveguide and on substrate," *IEEE Trans. Microw. Theory and Tech.*, vol. 39, no. 12, pp. 2069-2076, Dec 1991.

[13] R. R. Mansour, F. Huang, S. Fouladi, W. D. Yan and M. Nasr, "High-Q Tunable Filters: Challenges and Potential," *IEEE Microw. Mag.*, vol. 15, no. 5, pp. 70-82, July-Aug. 2014.

[14] CST Computer Simulation Technology AG., USA, (Jul. 2015). [Online]. Available: www.cst.com.

[15] M. Memarian and R. R. Mansour, "Quad-mode and dual-mode dielectric resonator filters," *IEEE Trans. Microw. Theory and Tech.*, vol. 57, no. 12, pp. 3418-3426, Dec. 2009.

[16] L. Zhu, R. R. Mansour and M. Yu, "Triple-band dielectric resonator bandpass filters," *IEEE MTT-S Int. Microw. Symp.*, Honololu, HI, 2017, pp. 745-747.

[17] A. S. Noori, X. Shang, C. Guo, T. J. Jackson, P. A. Smith and M. J. Lancaster, “Microwave filters based on novel dielectric split-ring resonators with high unloaded quality factors,” *IET Microw., Antennas & Propag.*, vol. 12, no. 8, pp. 1389-1394, July, 2018.

[18] D. M. Pozar, *Microwave Engineering*. 4th ed. Hoboken, NJ, USA: Wiley, 2012.

Chapter 4 Passband Cavity Filter Design Based on the Novel Dielectric-SRRs

4.1 Introduction

The novel Dielectric-SRRs investigated in pervious chapters are utilised to design new types of microwave filters in this chapter. Low insertion loss can be achieved for these new filters due to the use of the high Q_u Dielectric-SRRs. Filters with low insertion loss are in demand for many wireless applications, such as satellite systems and mobile base stations [1-3].

The coupling matrix [m] is applied to design two filters based on the Dielectric-SRRs in this chapter. The coupling matrix can be applied to design microwave filters regardless of their physical structure, such as the cavity, waveguide, or microstrip [4-8]. According to the desired filter specifications, the coupling matrix [m] is synthesised for the ideal filter response, as explained in Chapter 2. There are two important steps for realising the filter structure based on the synthesised coupling matrix values [4]. The first step is extracting the internal coupling coefficients between two adjacent resonators and the corresponding dimensions, as described in Section 4.2. The second step is extracting the external quality factor and the corresponding dimensions, as described in Section 4.3. By using these two steps of realising the filter structure in Sections 4.2 and 4.3, two passband filters with different specifications are reported in this chapter. These novel filters are simulated and optimized in sections 4.4.3 and 4.5.3, and discussion on fabrication and measurements is given in Sections 4.4.4 and 4.5.4.

4.2 Extraction of the Internal Coupling Coefficient K_c

The internal coupling coefficient K_c between two adjacent Dielectric-SRRs is described in this section. The EM simulator (CST software [9]) is used to model and simulate these two adjacent resonators. Two different configurations are possible for the coupling between two adjacent Dielectric-SRRs as shown in Figure 4.1.

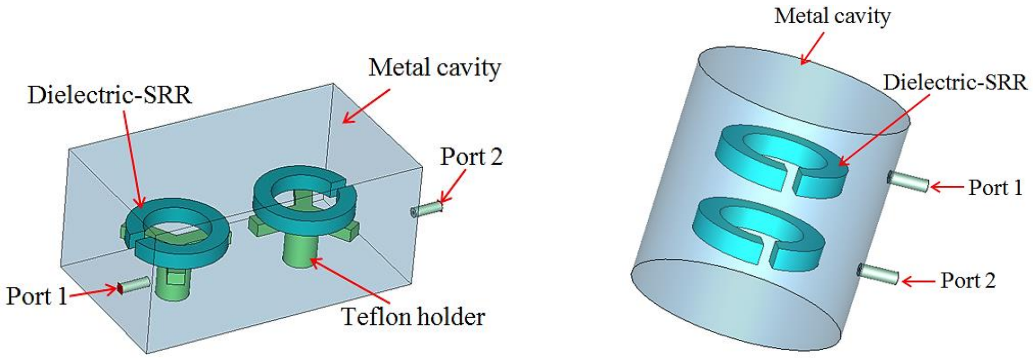

(a) (b)

Figure 4.1 Models for extracting K_c, (a) planar configuration, and (b) coaxial configuration

The planar configuration in Figure 4.1a is adopted in this section to be investigated. This because of with the planar configuration can easily rotate the Dielectric-SRRs to tune the filter internal and external couplings as will be described in the next chapter.

The feeding probes of the external ports, as shown in Figure 4.1, are modelled with very small length (0.05 mm) to achieve very weak coupling to the resonators [4]. The metal cavity of the above model (Figure 4.1a) has a PEC background and the material specifications of the Dielectric-SRRs and holders are given in Table 3.1.

The dimensions of the Dielectric-SRRs and holders (Figure 4.1a) are shown in Figure 4.2, and the cavity dimensions are shown in Figure 4.3.

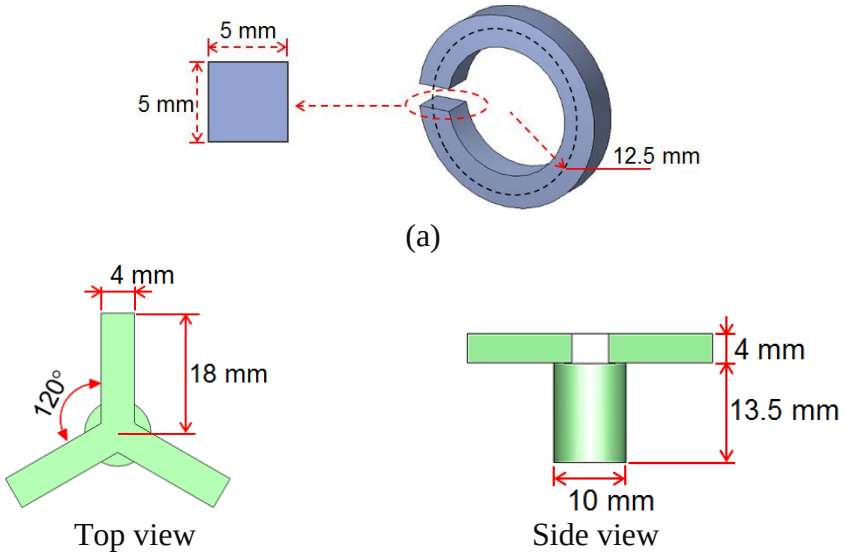

Figure 4.2 Models and dimensions, (a) Dielectric-SRR, and (b) Holder

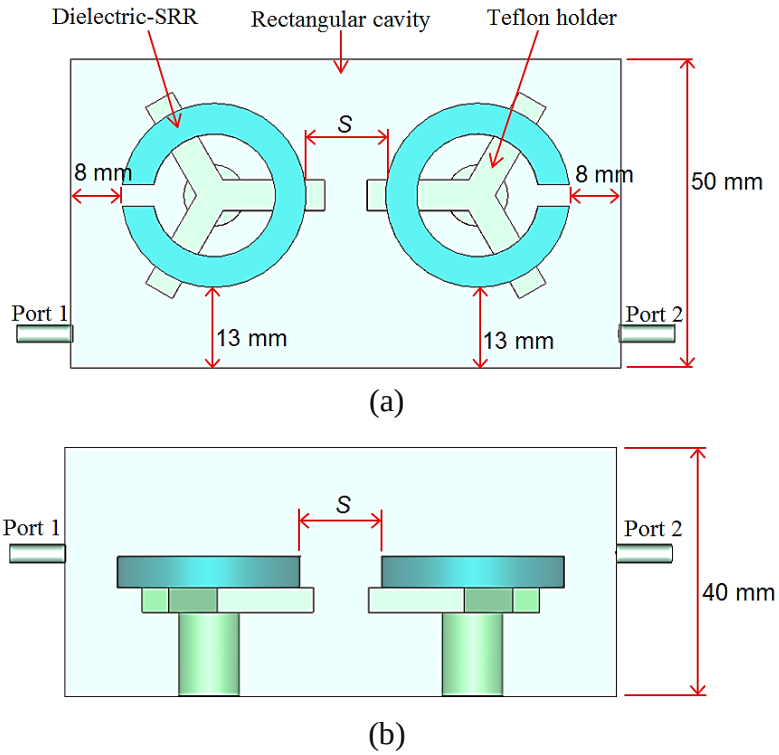

Figure 4.3 Model for extracting K_c against S, (a) Top view and (b) Side view

The simulated S_{21} response for the model given in Figure 4.3 is shown in Figure 4.4.

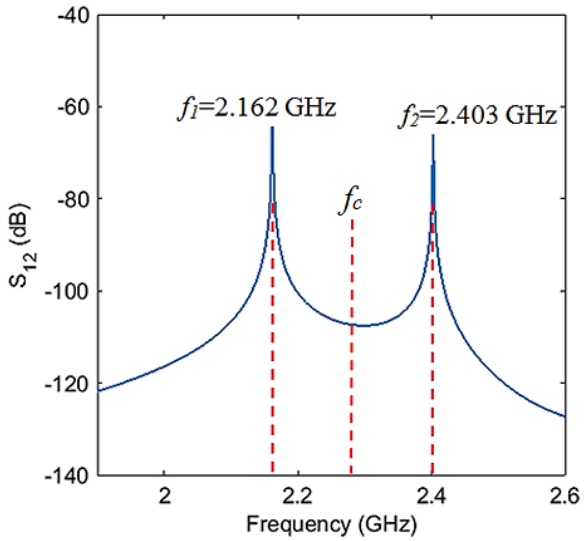

Figure 4.4 S_{21} results of the two coupled Dielectric-SRRs when S=6

The frequency peaks f_1 and f_2 in above figure are utilised to extract the K_c value between the two Dielectric-SRRs by using [4]

$$K_c = \frac{f_2^2 - f_1^2}{f_2^2 + f_1^2} \tag{4-1}$$

The K_c is calculated based on equation (4-1) and the above S_{21} response (in Figure 4.4) as

$$K_c = \frac{2.403^2 - 2.162^2}{2.403^2 + 2.162^2} = 0.1053$$

The coupling coefficient K_c and the middle frequency f_c were extracted against the distance S between the resonators (See Figure 4.3) and given in Figure 4.5.

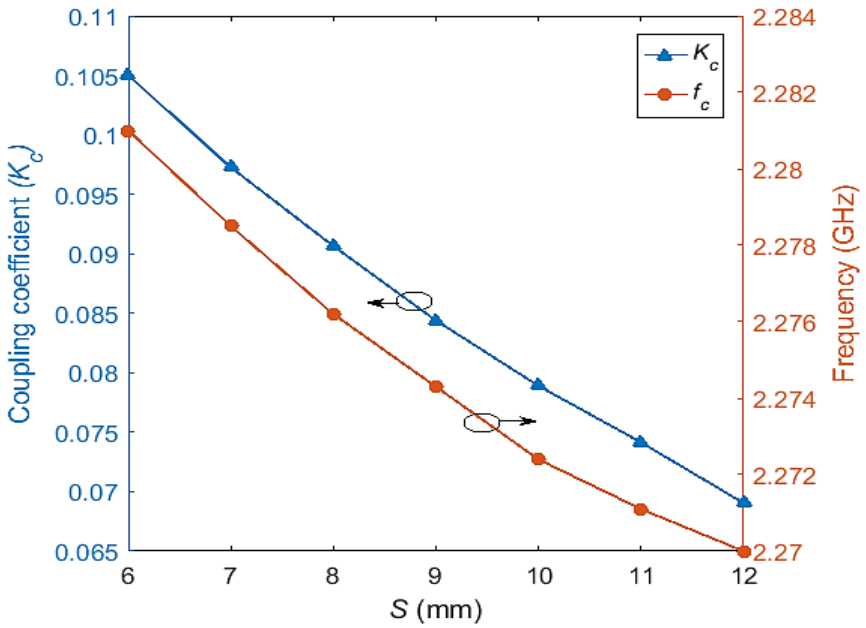

Figure 4.5 K_c and f_c against distance S

The results in Figure 4.5 show the K_c and f_c get smaller by increasing the space S between the two adjacent resonators.

The model of two resonators in Figure 4.3 can achieve other configurations by rotating the Dielectric-SRRs, these configurations allow significant flexibility to design filters with different topologies and cross-couplings. Figure 4.6 shows three new configurations obtained by rotating the Dielectric-SRRs (in Figure 4.3) with angles of θ_1 and θ_2. It should be noted there are many more possibilities for coupling between the Dielectric-SRRs as a function of the rotation angles θ_1 and θ_2. The relationship between K_c and the resonator rotation angles is described more in the next chapter.

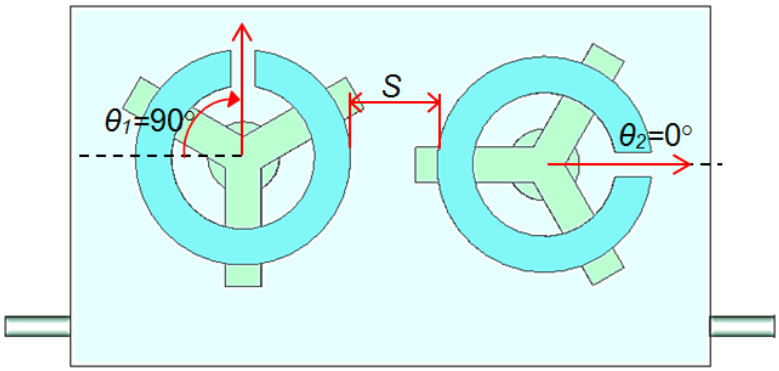

(a)

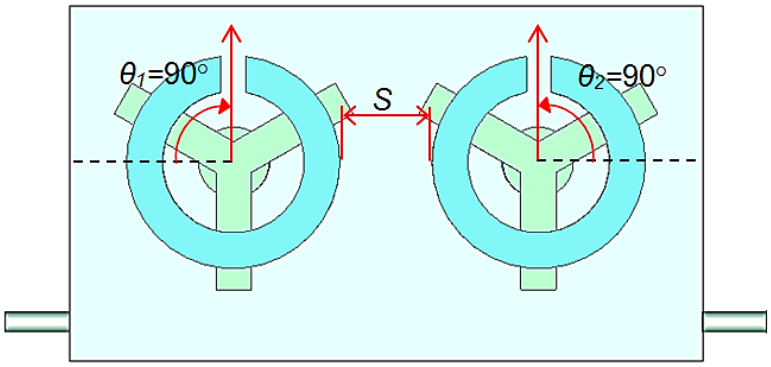

(b)

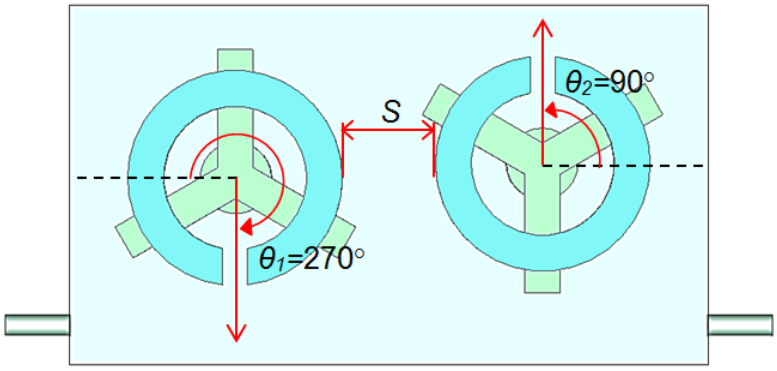

(c)

Figure 4.6 Model for extracting K_c against S, (a) θ_1=90° & θ_2=0° (b) θ_1=90° & θ_2=90° and (c) θ_1=270° & θ_2=90°

The K_c extracted against the distance S for the 3 models (in Figure 4.6) is shown in Figure 4.7.

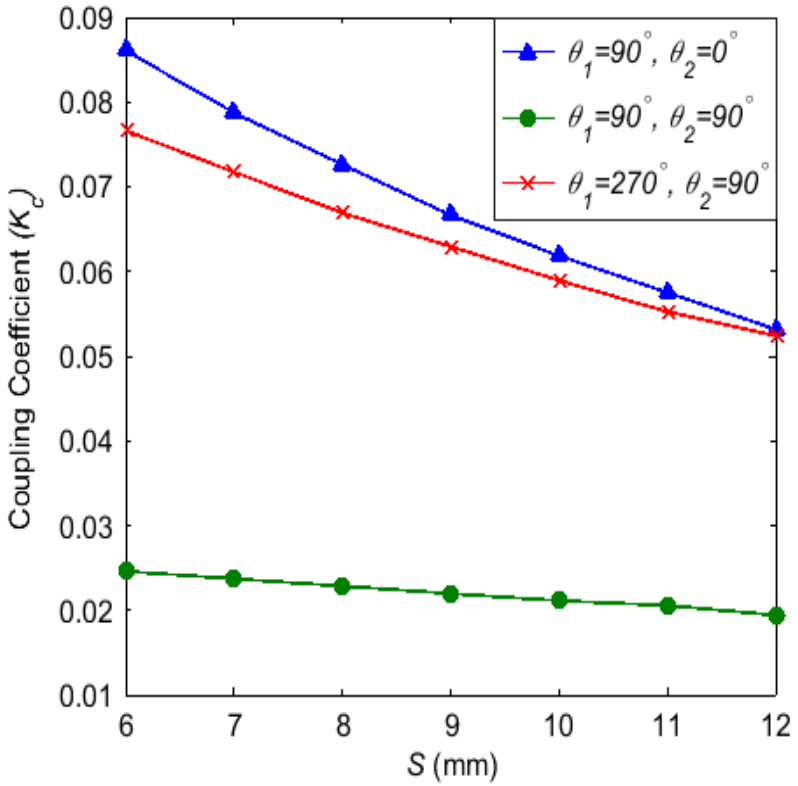

Figure 4.7 K_c against distance S for 3 different angles pairs

Figure 4.7 shows when the θ_1 and θ_2 = 90° the K_c values are small and nearly independent of the distance S between resonators. This is due to the K_c between two adjacent resonators is the total of the magnetic fields coupling K_m and the electric fields coupling K_e, these two couplings (K_m and K_e) are out of phase with each other, so K_c can be defined as the magnetic fields coupling less the electric fields coupling as given [11,12],

$$K_c = K_m - K_e \tag{4-2}$$

The coupling of this particular configuration (in Figure 4.6b) is manipulated by having a partial metal wall between resonators where most of the electric fields are located to decrease the electric coupling K_e and increase the overall coupling K_c as shown in Figure 4.8, the EM field distributions of the Dielectric-SRR are presented in Chapter 3 (Table 3.2).

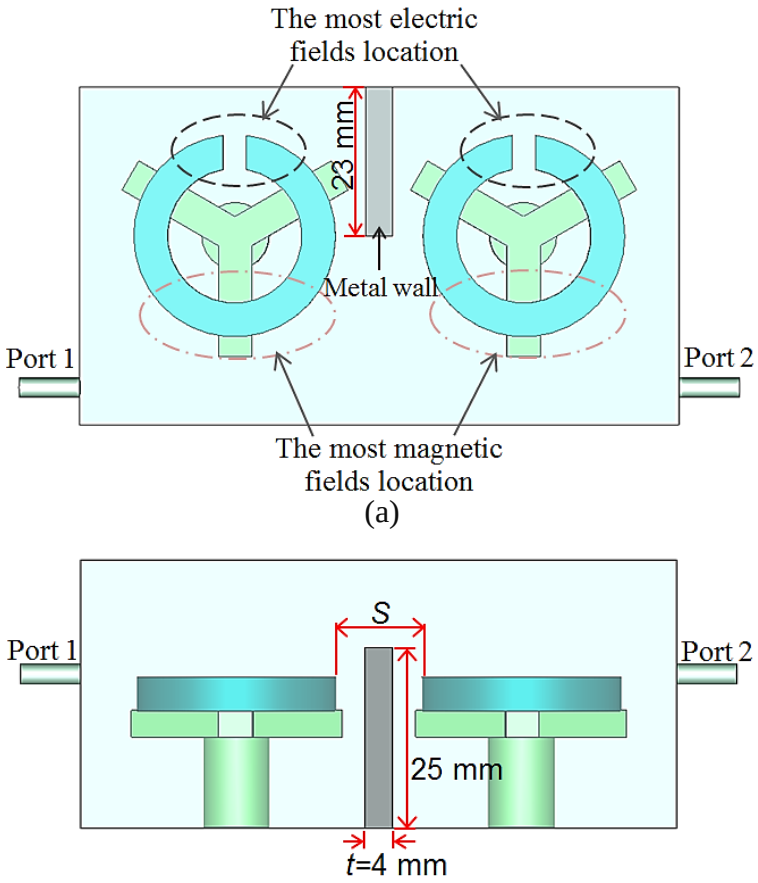

Figure 4.8 Model for extracting K_c against S, w and h, (a) Top view and (b) Side view

The K_c is extracted against S for the model with wall and compared to the results of the model without wall as shown in Figure 4.9.

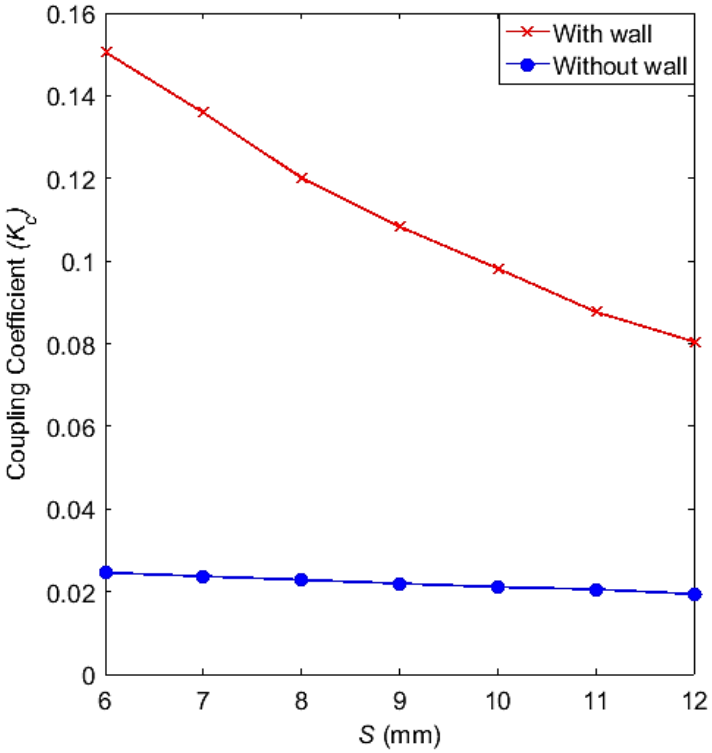

Figure 4.9 K_c against distance S with and without using wall

The above K_c results show the model with wall are much higher due to the wall decreased the electric K_e coupling and increased the overall coupling K_c. Also, this added wall can prevent unwanted cross-coupling between nonadjacent resonators in real filter.

Another wall is added with aperture between the resonators loops to control the K_c as shown in Figure 4.10. This model is simulated to extract the K_c against S with 2 different aperture sizes, the extracted K_c are as shown in Figure 4.11. The simulated results show the K_c decreases with the smaller aperture size and the higher space between resonators.

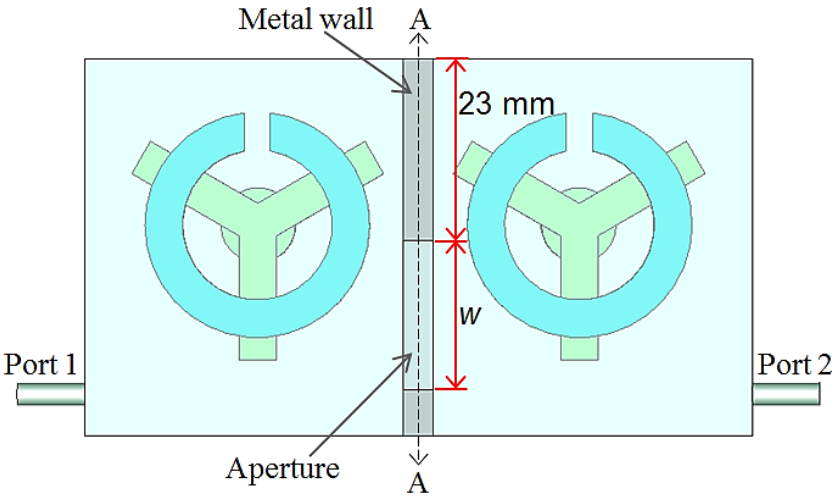

(a)

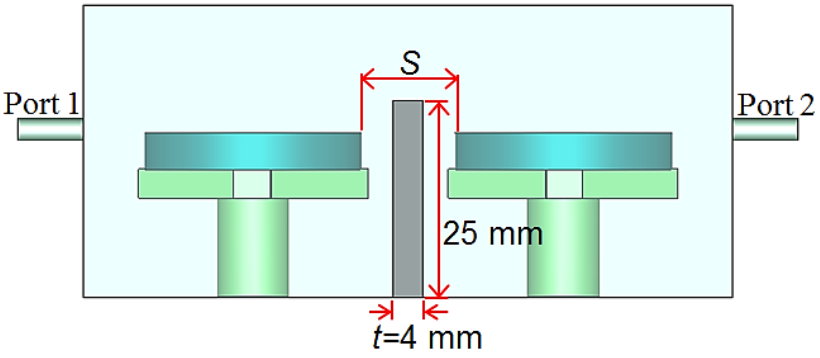

(b)

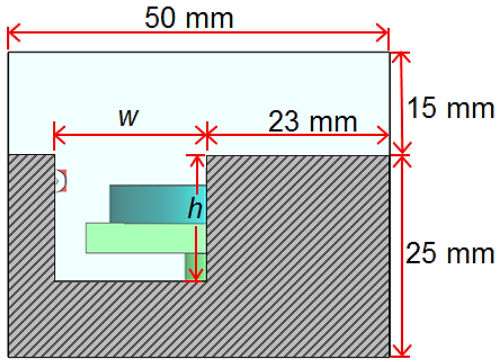

(c)

Figure 4.10 Model for extracting K_c against S, w and h, (a) Top view and (b) Side view

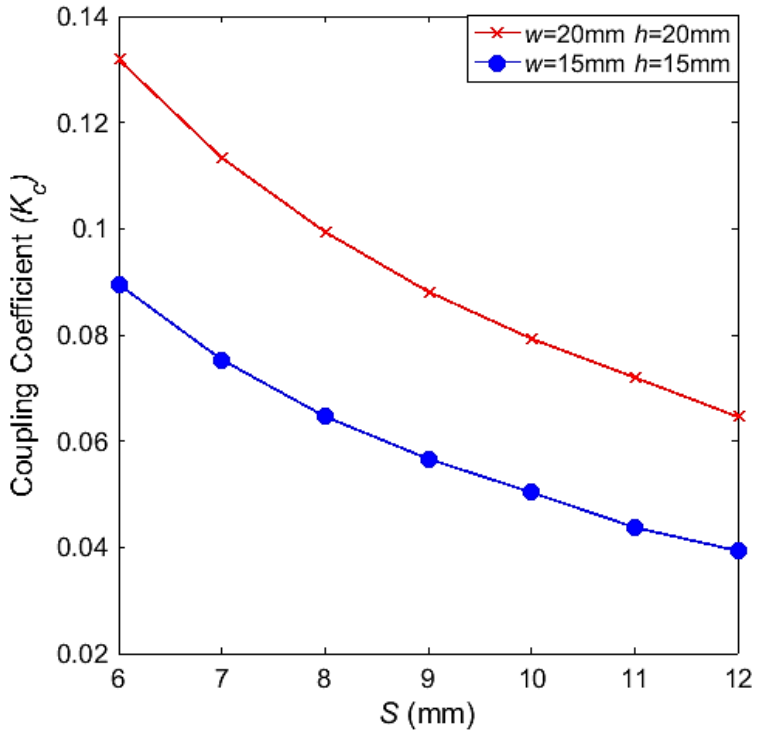

Figure 4.11 K_c against distance S and aperture size

Another new configuration is obtained by rotating the Dielectric-SRRs by 180° as shown in Figure 4.12.

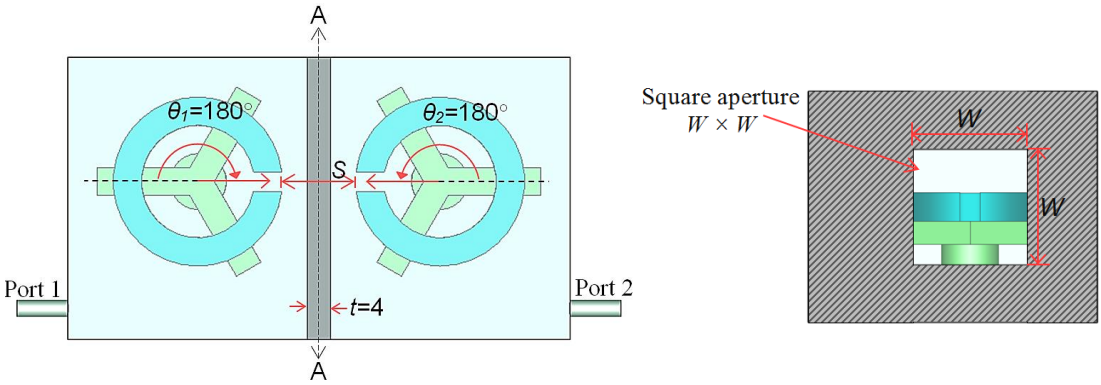

(a) (b)

Figure 4.12 Model for extracting K_c, (a) Top view, and (b) Side view cross section AA

As shown in Figure 4.12 the gaps of two adjacent Dielectric-SRRs face each other with a wall coming down from the top and side of the cavity housing, giving a square aperture in the centre to allow and control the coupling coefficient between resonators gaps. The relationship between K_c and S with 3 different aperture dimensions is shown in Figure 4.13, the K_c results are labelled with negative sign due to the most coupling between resonators is electric coupling.

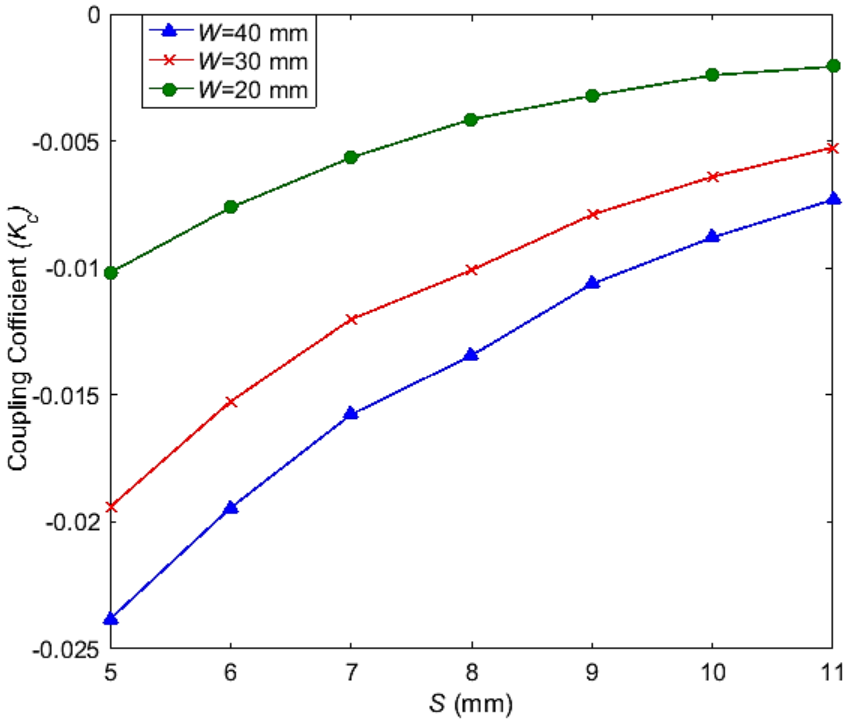

Figure 4.13 K_c against distance S and aperture dimension W

The K_c in Figure 413 increases by increasing the aperture size between the two Dielectric-SRRs.

4.3 Extraction of the External Quality Factor Q_e

The resonator coupling to the input and output is defined though the external quality factor Q_e. Figure 4.14 shows model used to extract Q_e; this model has a single resonator inside a metal cavity, the resonator is strongly coupled to port 1 and very weakly coupled to port 2. The typical S_{21} result for such model of single resonator with 2 external ports (source and load) [4] is given in Figure 4.15.

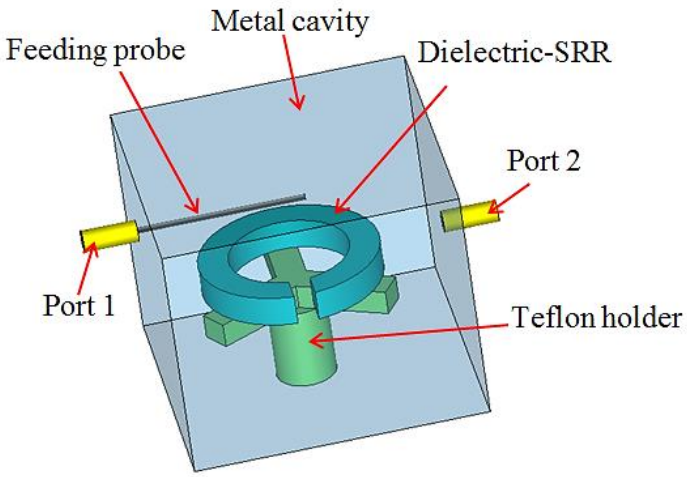

Figure 4.14 Model for extracting Q_e-factor

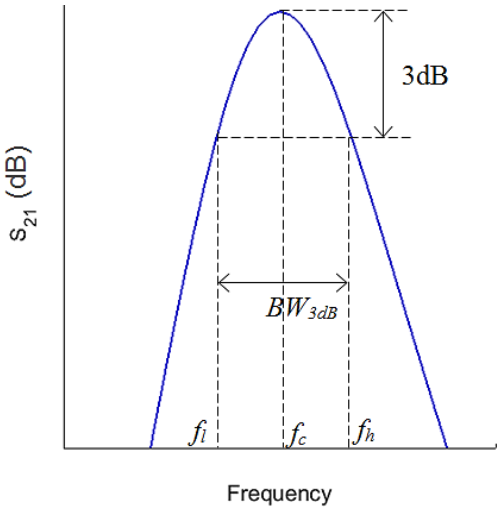

Figure 4.15 S_{21} response in dB of a loaded single resonator

The loaded quality factor Q_L can be defined from the centre frequency f_c and the 3dB bandwidth (BW_{3dB}) of the above S_{21} response as given in equation (3-4) [4]. Also the Q_L for the same model (Figure 4.14) can be calculated in term of unloaded quality factor Q_u and external quality factor Q_e [12],

$$\frac{1}{Q_L} = \frac{1}{Q_u} + \frac{1}{Q_e} = \left(\frac{1}{Q_r} + \frac{1}{Q_d} + \frac{1}{Q_c} \right) + \frac{1}{Q_e} \tag{4-3}$$

The Q_u is the unloaded quality factor, the Q_r is the radiation quality factor, Q_d is the dielectric quality factor and the Q_c is the cavity quality factor.

The CST simulated models in this section are considered the following:

The resonator inside closed enclosure, so $\frac{1}{Q_r} = 0$

The dielectric material is considered as loss free, so $\frac{1}{Q_d} = 0$

The metal cavity considered as PEC, so $\frac{1}{Q_c} = 0$

Therefore, $\frac{1}{Q_u} = 0$, this leads to $Q_L = \frac{1}{Q_e} = \frac{f_c}{BW_{3dB}}$,

Then,

$$Q_e = \frac{BW_{3dB}}{f_c} \tag{4-4}$$

The Q_e for each external port of the above model (in Figure 4.14) is defined by Q_{e1} (for por1) and Q_{e2} (for port 2), so

$$\frac{1}{Q_e} = \frac{1}{Q_{e1}} + \frac{1}{Q_{e2}} \tag{4-5}$$

The Q_{e2} is very large due to the port 2 being very weakly coupled to the Dielectric-SRR, this leads to ($1/Q_{e2} \approx 0$) and ($Q_e \approx Q_{e1}$). So, port 1 dimensions are varied to determine the Q_e which can be found directly from the CST plot of S_{12}.

Figure 4.16 shows the model used for extracting Q_e, port 1 in this model has feeding probe with length L, height H and distance C from resonator. The Q_e extracted against these port 1 parameters (L, H and C) as shown in Figure 4.17

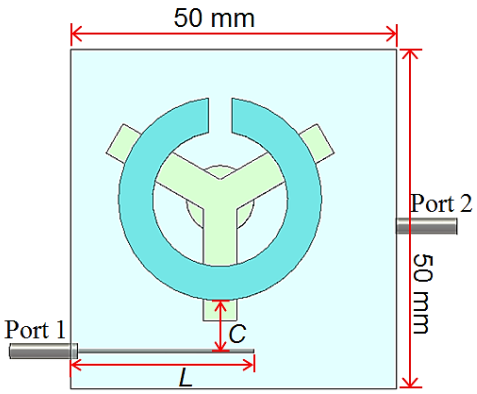

(a)

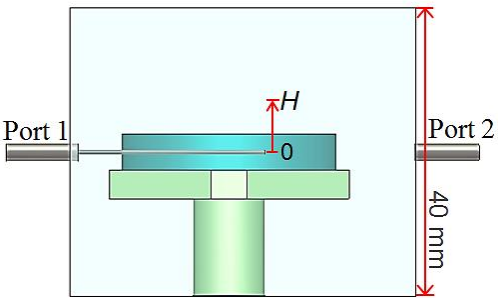

(b)

Figure 4.16 Model for extracting Q_e, (a) Top view and (b) Side view

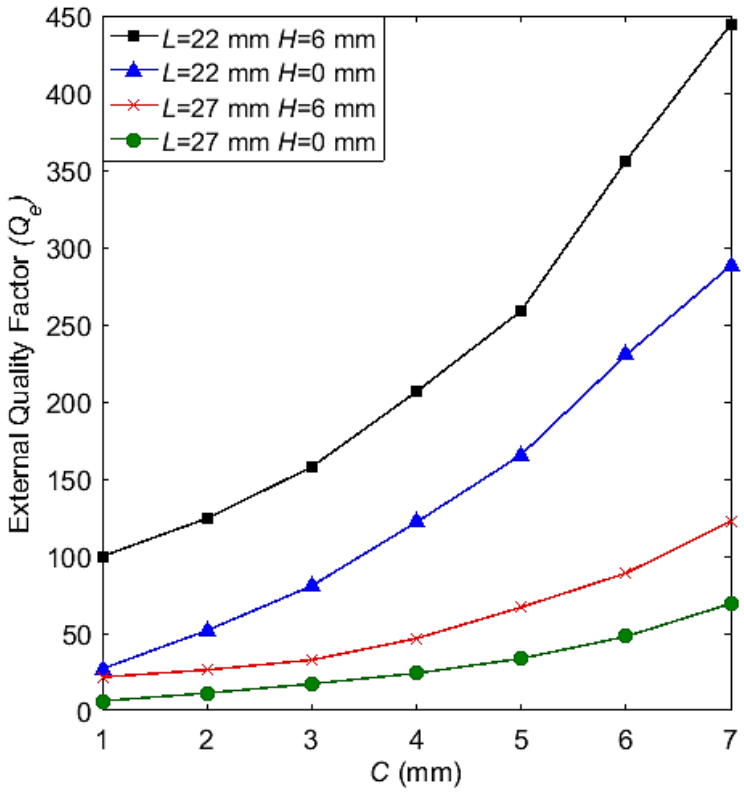

Figure 4.17 Q_e against the port 1 parameters (L, H and C)

As shown in Figure 4.17, the Q_e increases with increasing the distance C and the port height H, while Q_e decreases by increasing feeding probe length L.

Varying the port 1 position or dimension changes the centre frequency f_c (See Figure 4.15) as well as the Q_e value; this frequency change can be adjusted by varying the resonator dimensions to obtain Q_e values at same f_c. However, the resonator is left fixed in the CST simulations in this section because the Dielectric-SRRs are designed and fabricated as given in Chapter 3 (Figure 3.12). The frequency f_c for each extracted Q_e (in Figure 4.17) is shown in Figure 4.18.

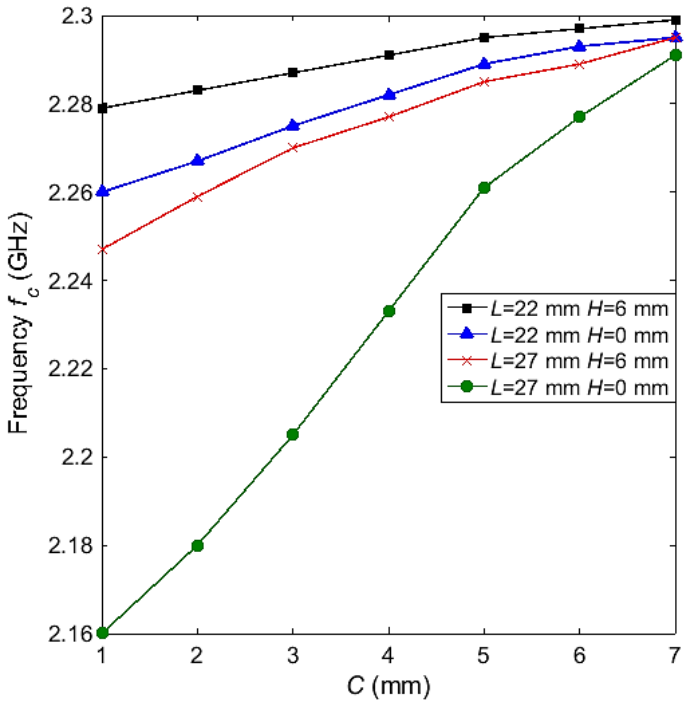

Figure 4.18 Centre frequency f_c against the port 1 parameters (L, H and C)

In addition, the Q_e is extracted when feeding probe close to the resonator gap where the most electric fields located as shown in Figure 4.19.

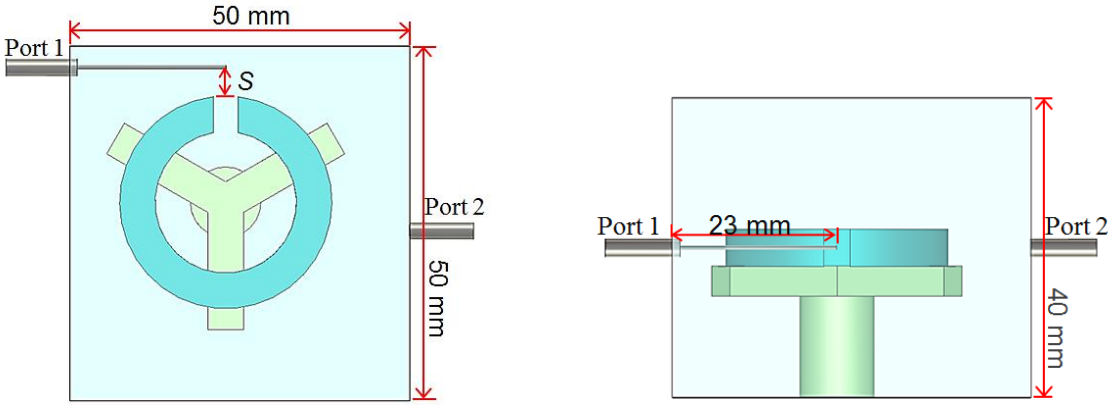

(a) (b)

Figure 4.19 Model for extracting Q_e (a) Top view and (b) Side view

The extracted Q_e and its centre frequency against the distance S are shown in Figure 4.20.

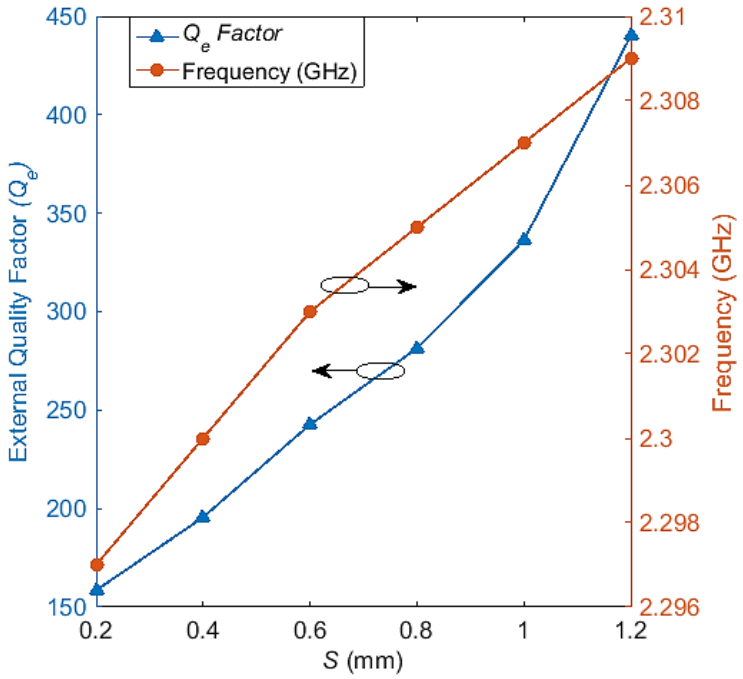

Figure 4.20 Q_e and centre frequency for the probe moved from resonator centre to its gap

The Q_e and its centre frequency (in Figure 4.20) get higher by increasing the distance S between the feeding probe and resonator gap.

There are many other possibilities of coupling to the Dielectric-SRR, but the discussion is limited to this particular structure which found suitable for the filter described in next section.

4.4 Third order Passband Cavity Filter with Chebyshev Response Based on Dielectric-SRRs

A new class of cavity filter is implemented in this section based on the novel Dielectric-SRRs.

4.4.1 The filter topology and ideal response

The filter is designed to have a Chebyshev response, with a centre frequency of 2.2 GHz, fractional bandwidth (FBW) of 5% and return loss of 20 dB. Figure 4.21 shows the filter topology, each circle represents a resonator and the lines are the internal and external coupling.

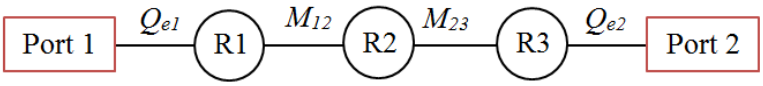

Figure 4.21 3rd order filter topology

The g values of the lowpass prototype filter obtained by equations (2.29) as g_0=1.0, g_1 = 0.8516, g_2 = 1.1032, g_3 = 0.8516, and g_4 = 1. The g-element values utilised to calculate the coupling coefficient $[m]$ and external quality factor q_e as described in Chapter 2

$$[m] = \begin{bmatrix} 0 & 1.0303 & 0 \\ 1.0303 & 0 & 1.0303 \\ 0 & 1.0303 & 0 \end{bmatrix}, \quad q_{e1} = q_{e2} = 0.9611 \tag{4-6}$$

The filter coupling coefficients $M_{i,i+1}$ and external quality factor Q_e are calculated by using equations (2-28) as:

$$M_{1,2} = M_{2,3} = 0.05$$
$$Q_{e1} = Q_{e2} = 17 \tag{4-7}$$

The corresponding S-parameters of the above design values calculated by equations (2-27) and are shown in Figure 4.22.

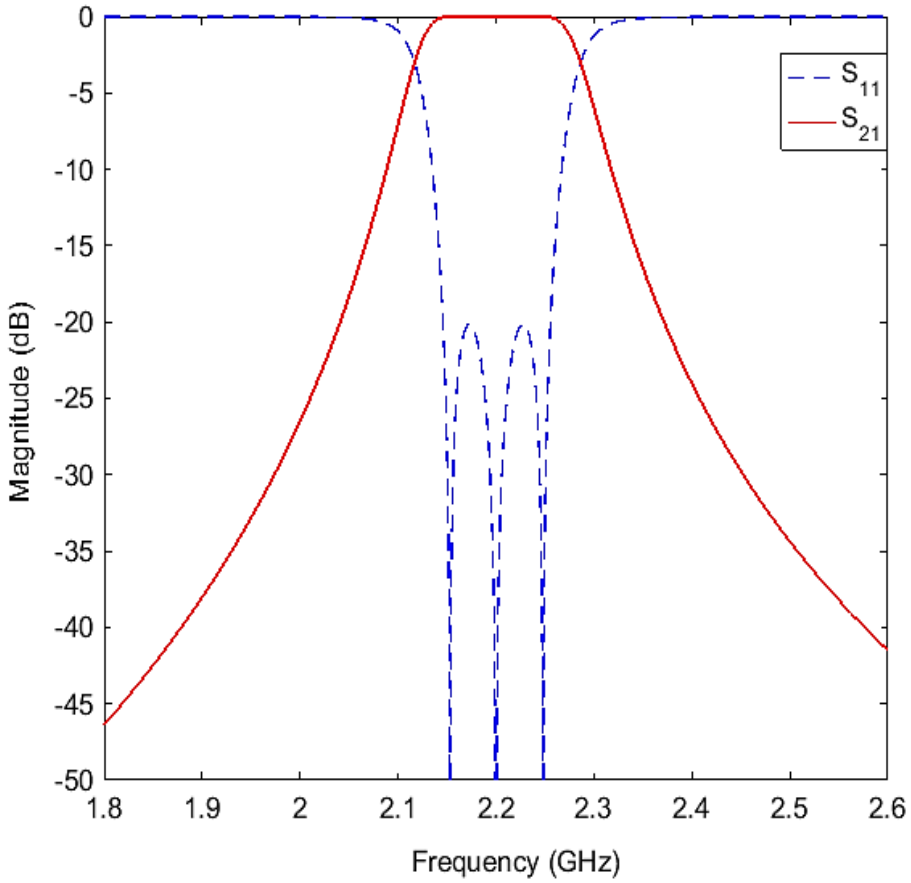

Figure 4.22 S-parameter responses for 3rd order passband filter calculated from coupling matrix

4.4.2 The Filter Configuration

The dimensions of the physical filter are obtained based on the filter coupling matrix and the method of extracting the coupling coefficient in Section 4.2 and external quality factor in Sections 4.3. The filter structure modelled by CST software and the overall dimensions are as shown in Figure 4.23. The Dielectric-SRRs and holders specifications and dimensions are as given in Section 4.2 (Figure 4.2 and Table 3.1). The filter cavity and the walls between resonators are copper with electric of conductivity of 5.8×10^7 S/m.

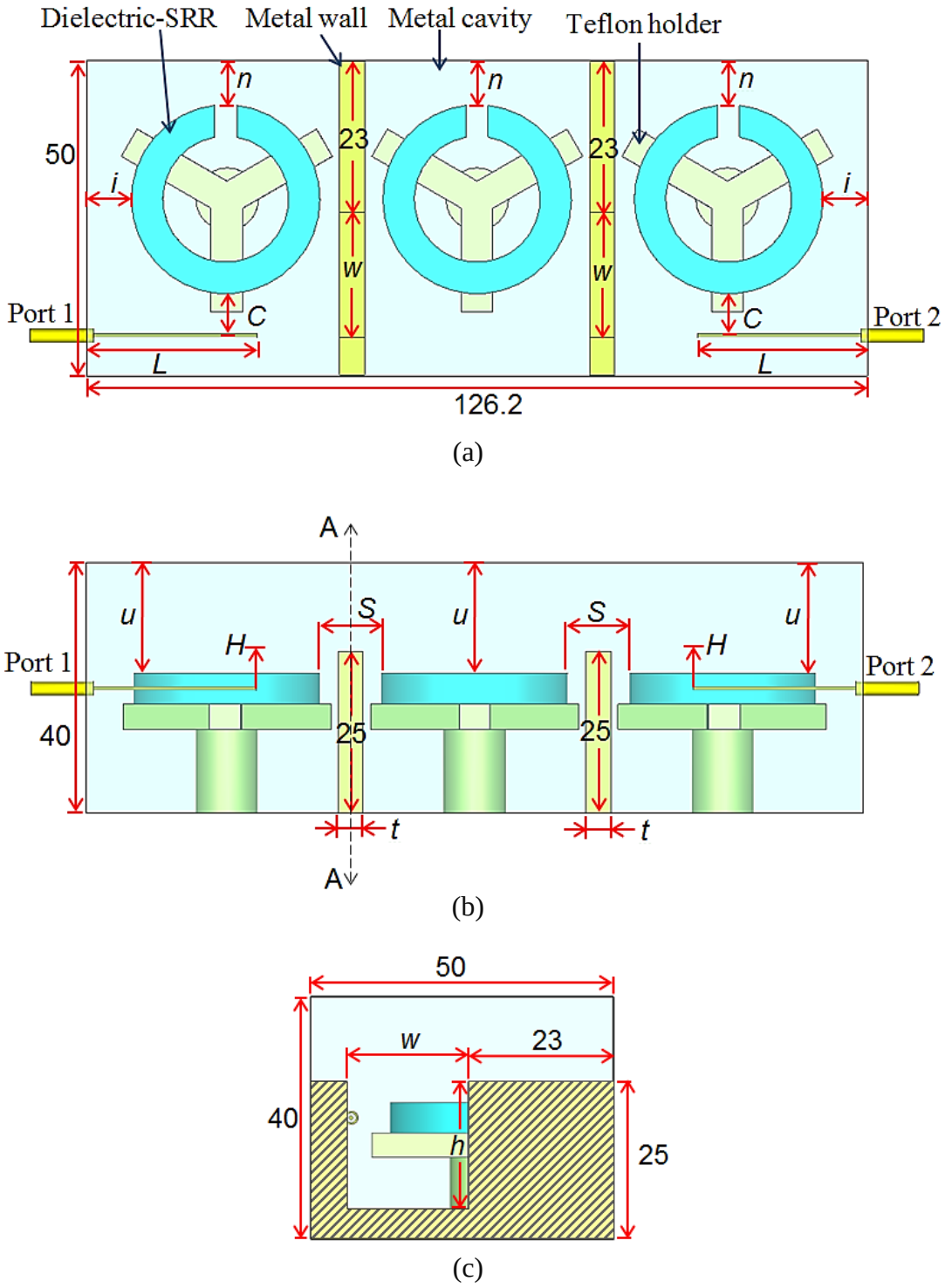

Figure 4.23 3rd order filter model based on Dielectric-SRRs, (a) Top view, (b) Side view, and (c) Side view cross section AA. Dimensions unit (mm)

4.4.3 The Filter Simulation Results

The above filter model shown in Figure 4.23 is simulated by the CST software with initial dimensions taken directly from extracted K_c results (in Figure 4.11) and the Q_e results (in Figure 4.17). The initial dimensions of the filter are then optimized by the CST software to meet the desired filter specifications. The dimensions of resonators are not optimised because these components are already designed/fabricated, as given in Chapter 3 (in Figure 3.12). The dimensions of the cavity, apertures, ports, and the space between resonators are selected to be optimised. The physical dimensions of the filter before and after optimisation are listed in Table 4.1, and the filter responses before and after the CST optimisation are shown in Figure 2.24.

Table 4.1 Dimensions of the 3rd order filter model (in Figure 4.23)

	S	*w*	*h*	*t*	*C*
Dimension before optimisation(mm)	10.1	15	15	4	3
Dimension after optimisation (mm)	10	15.8	15.4	4	3.9
	L	*H*	*n*	*u*	*i*
Dimension before optimisation (mm)	27	0	7	17.5	8
Dimension after optimisation (mm)	27.6	0	6.1	16.3	7.4

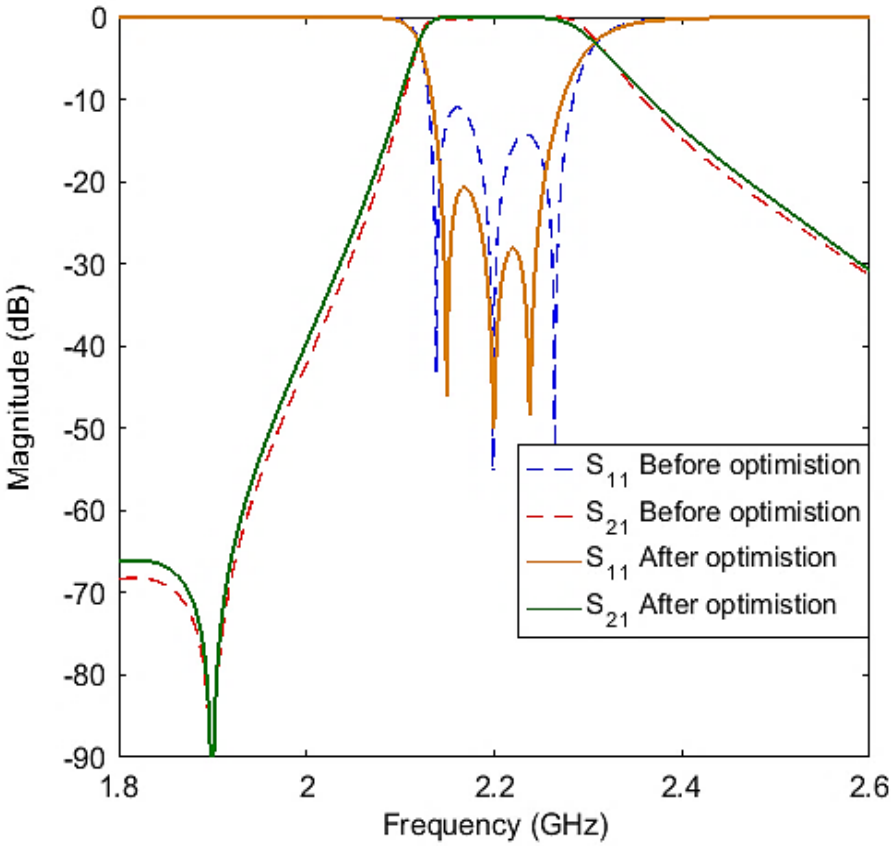

Figure 4.24 CST- simulated responses before and after optimisation

As shown in Figure 4.24, the results before optimisation are close to the after optimisation results, which show the filter design technique is good. Figure 4.24 also shows that the S_{21} response is not symmetrical due to the appearance of a transmission zero. This transmission zero is attributed to the unwanted cross-coupling between the input and output coaxial cables. This cross-coupling is proofed by varying length *L* of the feeding probes. Figure 4.25 shows the transmission zero pushed up towards the filter passband when *L* increases. This is because the increasing of *L* leads to an increase cross-coupling between ports 1 and 2. The filter optimised results compared to the filter calculated results, as shown in Figure 4.26.

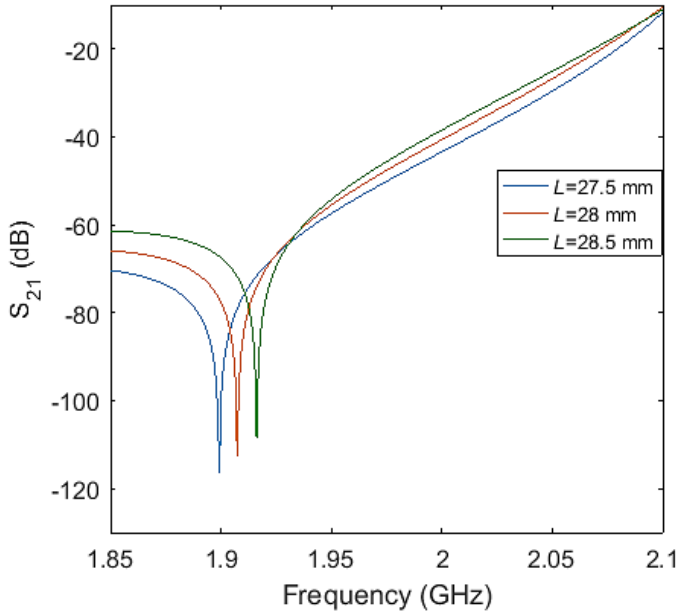

Figure 4.25 S_{21} results with three different probe lengths L

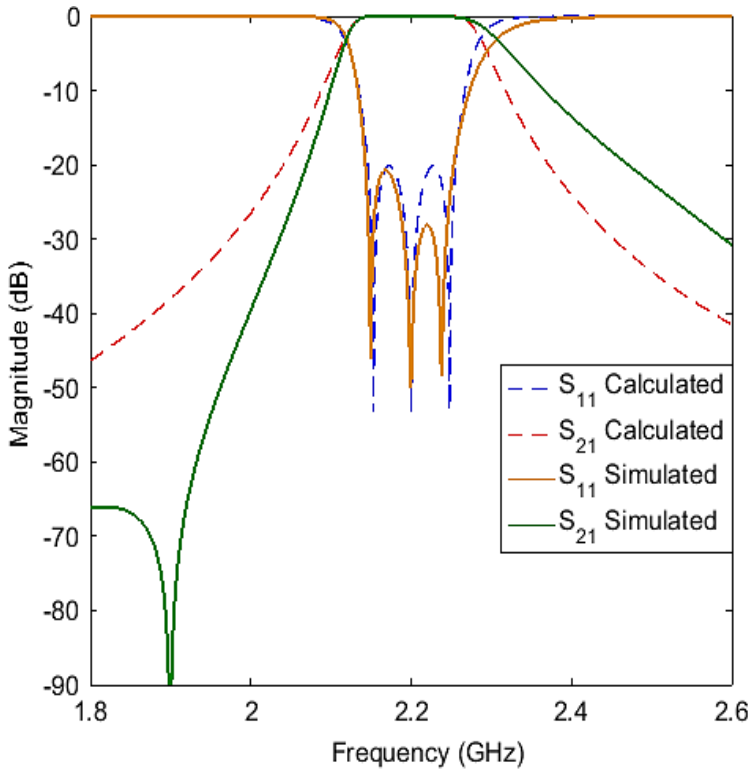

Figure 4.26 Filter responses comparison between calculated results and CST simulated results

As shown in Figure 4.26 the simulated filter response has a distortion caused by the transmission zero. Otherwise, the simulated results agree well with the calculated results in term of filter centre frequency, bandwidth, and return loss.

4.4.4 Fabrication and Measurements

Figure 4.27 shows the fabricated filter with the cavity lid removed. The filter cavity is made by soldering copper plates together, and then the Dielectric-SRRs and holders are fixed inside the copper cavity as given in Section 3.4. The filter has two SMA coaxial connectors. The small holes around the enclosure and its lid edges are for the screw assembly. The filter is tested by the Vector Network Analyser (VNA). Both the measured results and the simulated results are shown in Figure 4.28.

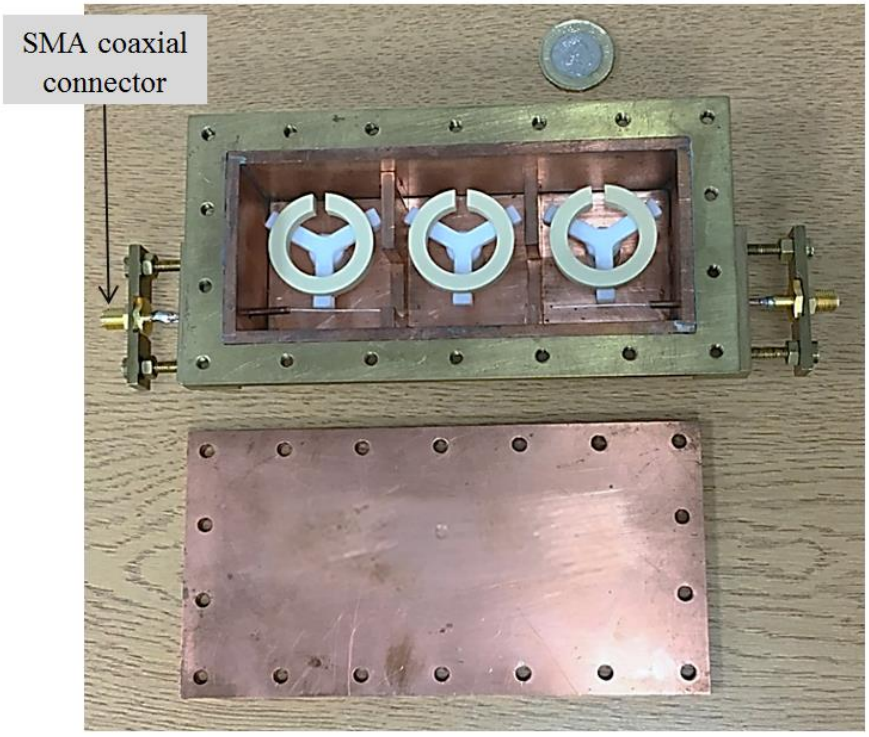

Figure 4.27 Fabricated cavity filter based on Dielectric-SRRs

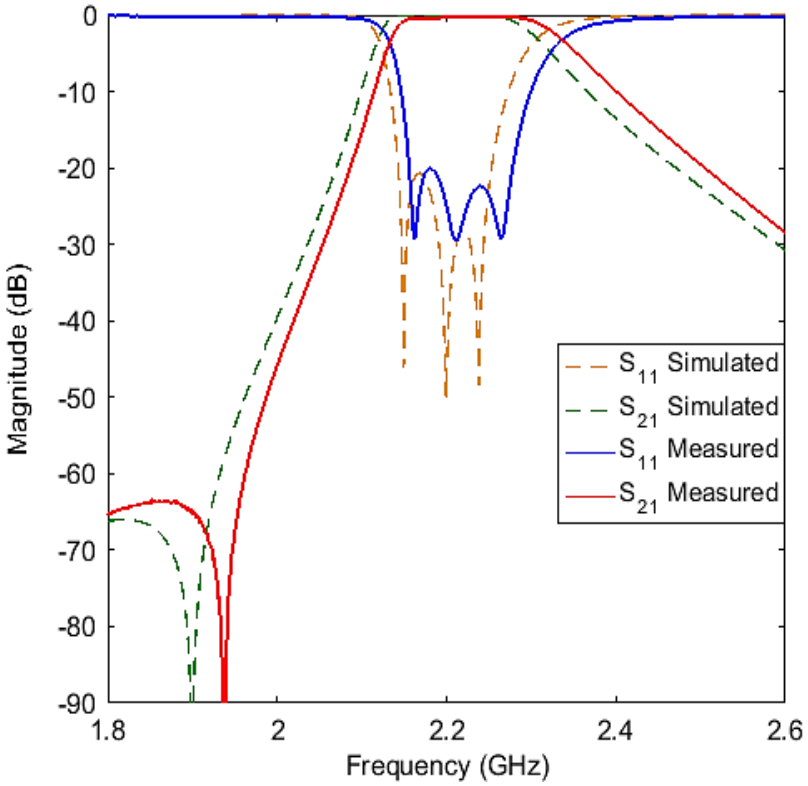

Figure 4.28 Filter responses comparison between CST simulation and measured results

As shown in Figure 4.28 the measured S_{11} has return loss greater than 20 dB which is an excellent result. There is a small frequency shift and the bandwidth larger by 12 MHz in the measured results. This is due to very small errors in the fabrication process such as the accuracy of the cutting machine and the soldering quality for the filter cavity plates and walls. Note that there has been no tuning of the filter. Tuning screws are able to correct this small frequency shift, however the agreement is good and therefore this tuning has not done. The passband insertion losses for the simulated and measured results are shown in Figure 4.29.

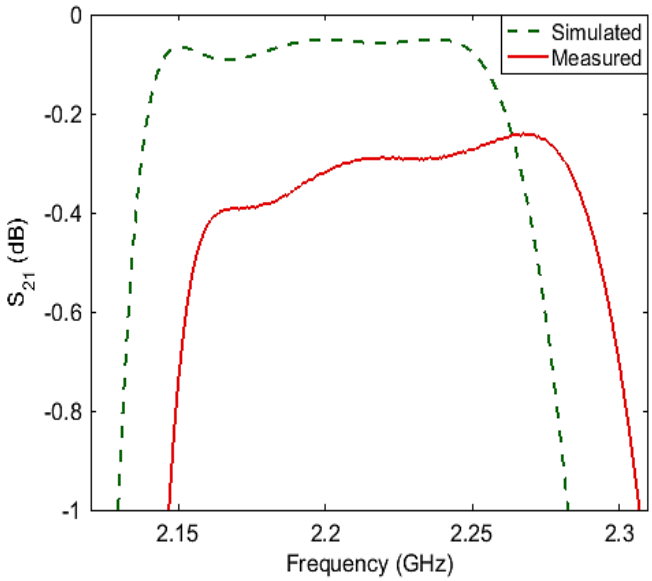

Figure 4.29 Passband insertion losses for the simulated and measured responses

The above results show the measured insertion loss is about 0.3 dB higher than simulated results. This can be attributed to (i) potential small errors in the assumed material parameters such as the loss tangent, (ii) the losses in the 3 cm semi-rigid cables connecting to the devices and in the SMA connectors, (iii) loss also could be from the leakage at gaps at the input/output ports, and/or between the filter enclosure and its lid, and (iv) the manufacturing problems, particularly with the cables and earth connection to the outer cavity. Some of these errors are small, some are difficult to quantify but the expectation is that the additional loss is a combination.

4.5 Fourth order Passband Cavity filter with symmetric transmission zeros

Another passband cavity filter based on Dielectric-SRRs is presented in this section to investigate more about the ability of the novel Dielectric-SRRs for the design of filters with different performance and configuration.

A cross-coupling is added to the filter design in this section; this cross-coupling is utilized to introduce a pair of symmetric transmission zeros and improve the filter attenuation performance.

4.5.1 The Filter Topology and Ideal Response

The filter is designed to have a centre frequency of 2.3 GHz, fractional bandwidth (FBW) of 4%, and return loss of 20 dB. Figure 4.30 shows the filter topology, the red dashed line represent a cross-coupling between resonators R1 and R4.

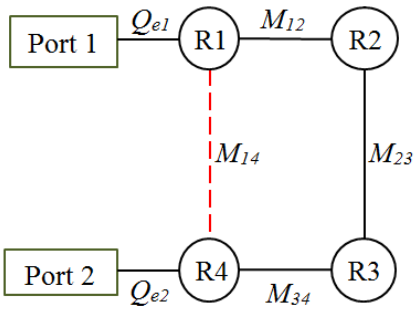

Figure 4.30 Topology of 4th order filter with cross-coupling

The cross-coupling is added to provide a pair of transmission zeros at the frequencies of 2.227 GHz and 2.374 GHz. These frequencies locations are calculated by using [4]

$$\omega_{a1} = \omega_0 \frac{-\Omega_a FBW + \sqrt{(\Omega_a FBW)^2 + 4}}{2}$$
$$\omega_{a2} = \omega_0 \frac{\Omega_a FBW + \sqrt{(\Omega_a FBW)^2 + 4}}{2} \quad (4\text{-}8)$$

where ω_0 is desired centre frequency of the passband filter and Ω_a is the location for a attenuation poles in the response of the lowpass prototype filter [4]. Figure 4.31 shows 4th order lowpass prototype filter with one cross-coupling [4].

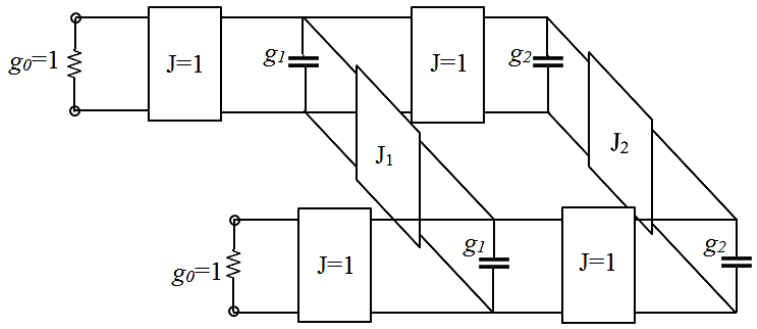

Figure 4.31 lowpass prototype filter for 4th order filter with one cross-coupling [4]

The element values g_1, g_2, J_1 and J_2 of the 4th order lowpass prototype filter can be calculated by [4]

$$\begin{aligned} g_1(\Omega_a) &= 1.22147 - 0.35534\cdot\Omega_a + 0.18337\cdot\Omega_a^2 - 0.0447\cdot\Omega_a^3 + 0.00425\cdot\Omega_a^4 \\ g_2(\Omega_a) &= 7.22106 - 9.48678\cdot\Omega_a + 5.89032\cdot\Omega_a^2 - 1.6577\cdot\Omega_a^3 + 0.10317\cdot\Omega_a^4 \\ J_1(\Omega_a) &= -4.30192 + 6.26745\cdot\Omega_a - 3.67345\cdot\Omega_a^2 + 0.9936\cdot\Omega_a^3 - 0.10317\cdot\Omega_a^4 \\ J_2(\Omega_a) &= 8.17573 - 11.36315\cdot\Omega_a + 6.96223\cdot\Omega_a^2 - 1.94244\cdot\Omega_a^3 + 0.20636\cdot\Omega_a^4 \end{aligned} \quad (4\text{-}9)$$

The filter coupling coefficients (M_{12}, M_{23}, M_{34} and M_{14}) and external quality factors (Q_{e1} and Q_{e2}) as given in the filter topology can be determined by [4]

$$\begin{aligned} Q_{e1} &= Q_{e2} = \frac{g_1}{FBW} \\ M_{12} &= M_{34} = \frac{FBW}{\sqrt{g_1 g_2}} \\ M_{23} &= \frac{FBW\cdot J_2}{g_2} \\ M_{14} &= \frac{FBW\cdot J_1}{g_1} \end{aligned} \quad (4\text{-}10)$$

The filter normalised coupling matrix [m] and the filter design parameters ($M_{i,i+1}$ and Q_e) are obtained by using equations (4-9) and (4-10) as

$$[m]=\begin{bmatrix} 0 & 0.8306 & 0 & -0.2963 \\ 0.8306 & 0 & 0.8145 & 0 \\ 0 & 0.8145 & 0 & 0.8306 \\ -0.2963 & 0 & 0.8306 & 0 \end{bmatrix} \tag{4-11}$$

$$q_{e1}=0.9668, \quad q_{e2}=0.9668$$

$$\begin{aligned} M_{1,2} &= M_{3,4} = 0.033 \\ M_{2,3} &= 0.032, M_{14} = 0.01 \\ Q_{e1} &= Q_{e2} = 24 \end{aligned} \tag{12}$$

The above design values are used to calculate the ideal filter response as shown in Figure 4.32.

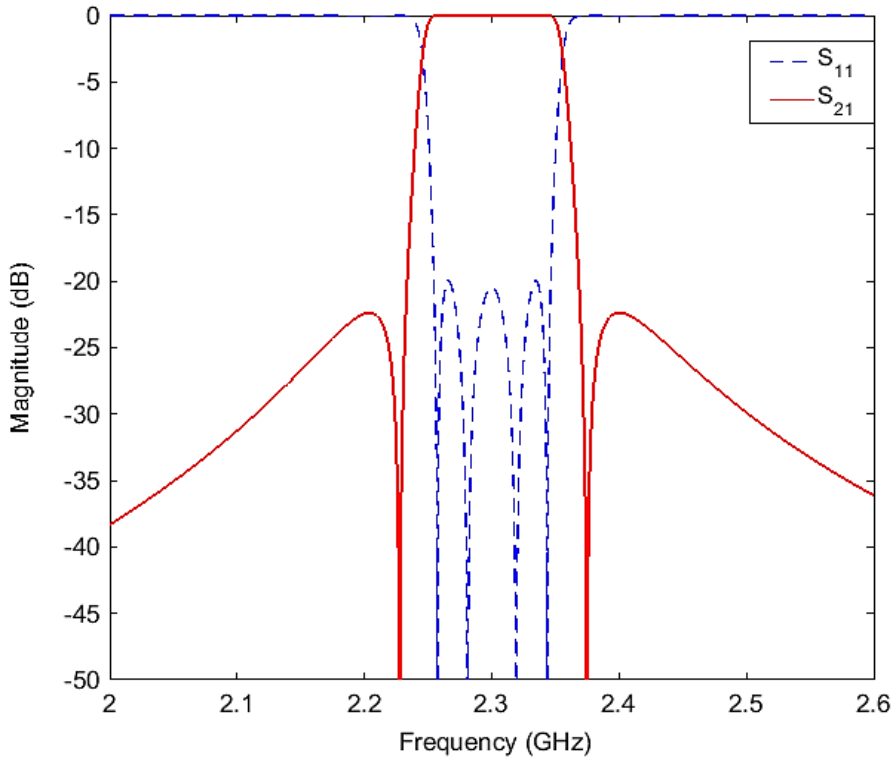

Figure 4.32 S-parameter responses for 4th order filter with symmetric transmission

4.5.2 The Filter Configuration

The filter physical dimensions are obtained based on the filter coupling values and by using the technique of extracting K_c and Q_e as described in Sections 4.2 and 4.3. The filter structure is modelled by the CST software as shown in Figure 4.33. The Dielectric-SRRs and holders are the same as given in Section 4.2, and filter cavity and walls are aluminium with an electrical conductivity of 3.56×10^7 S/m.

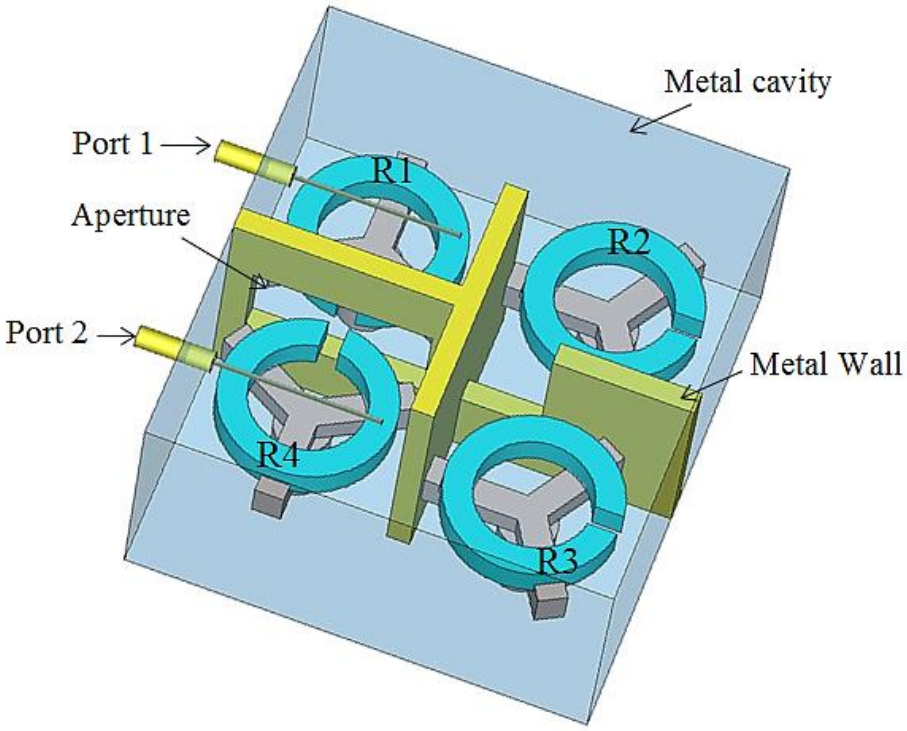

Figure 4.33 3-D structure of the 4th order filter

4.5.3 The Filter CST Simulation

The CST simulated results of the above filter model for both after and before optimization are shown in Figure 4.34.

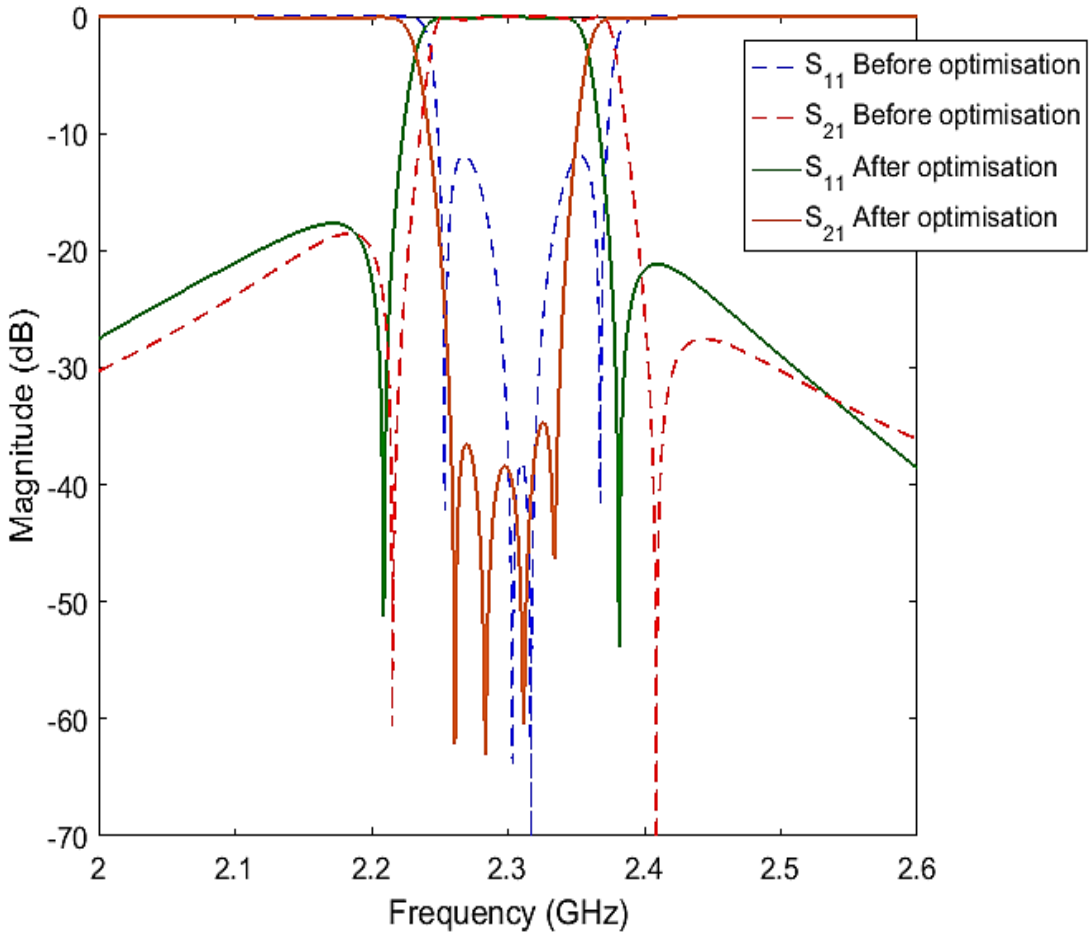

Figure 4.34 CST simulated responses before and after optimisation

The physical dimensions of the filter after CST optimisation are shown in Figure 4.35. The Dielectric-SRRs and holders dimensions are as given in Figure 4.2, again these resonators dimensions are not optimised because the Dielectric-SRRs are already fabricated as given in Chapter 3 (in Figure 3.13).

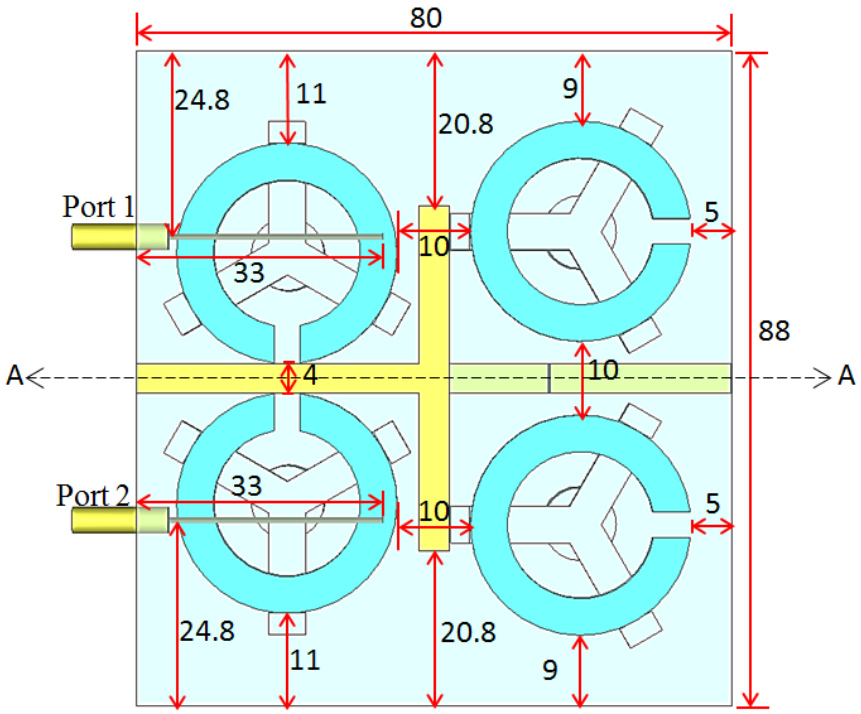

(a)

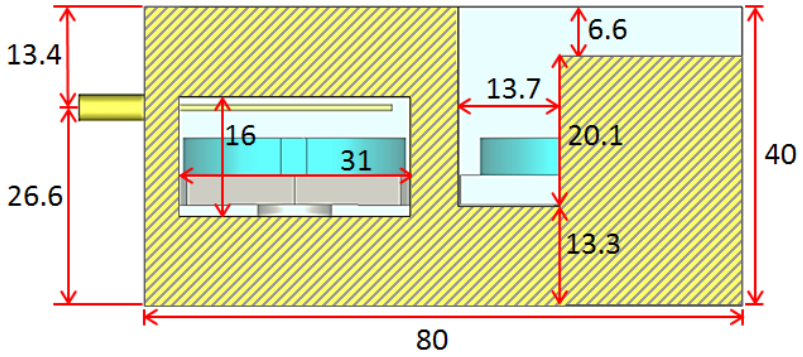

(b)

Figure 4.35 Model of the 4th order filter model, (a) Top view, and (b) Side view cross section AA. The dimensions unit in (mm)

Figure 4.36 shows the optimised results of the 4th order filter have return loss much greater than the calculated results; otherwise both results agree well in term of filter centre frequency, bandwidth and the locations of transmission zeros.

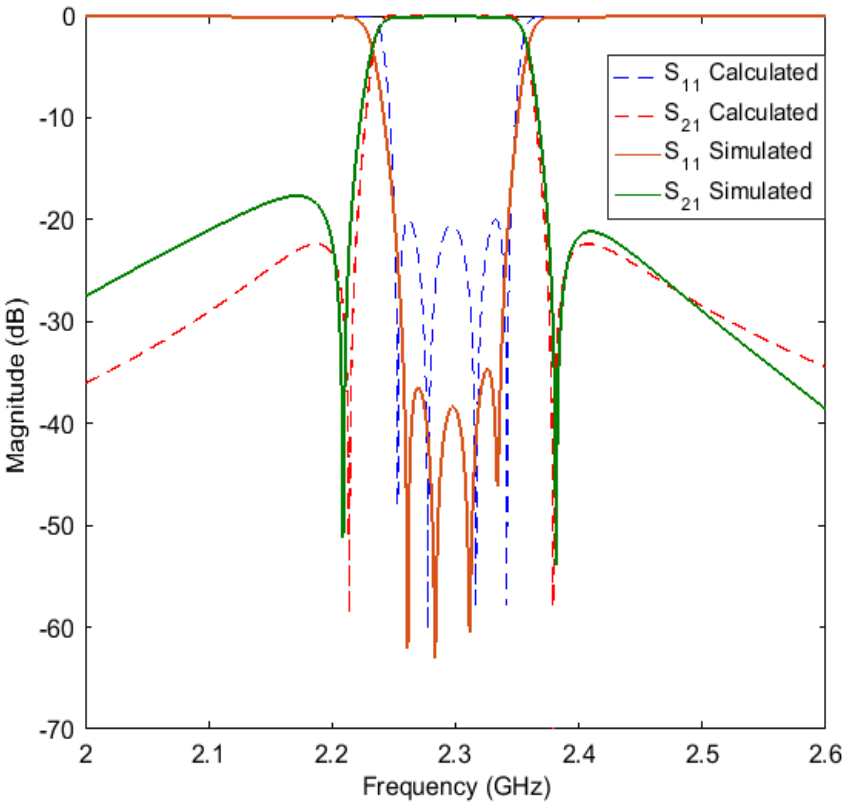

Figure 4.36 Filter responses comparison between calculated and simulated results

4.5.4 Fabrication and Measurements

The filter cavity is made by a CNC milling machine and from aluminium with an electrical conductivity of 3.56×10^7 S/m. The fabricated Dielectric-SRRs and holders have the same material specifications as in Table 3.1. The fabricated parts of the filter are assembled as shown in Figure 4.37. The holders are fixed tightly inside the filter cavity by inserting each holder inside a slot with 3 mm depth at the bottom of the filter cavity. The Dielectric-SRRs are fixed tightly onto the holders by using very small Teflon sticks with the holders, as given in Section 3.4. Each resonator holder is pressed strongly inside the cavity slot until it touches the bottom surface of the slot.

Additionally, each Dielectric-SRR is pressed strongly between the three holder sticks until it touches the top surface of holder. Otherwise, if these parts are not fitted well inside their positions, this can have an effect on the filter performance. However, these easy steps of pressing the holders inside the slots and the Dielectric-SRRs between the holder sticks can achieve enough rigidity for the assembled filter to be moved and tested. They can also present good repeatability for the filter assembly. An adhesive material is better to be used with this assembled filter to ensure more reliability for strong movements and practical work in the wireless systems.

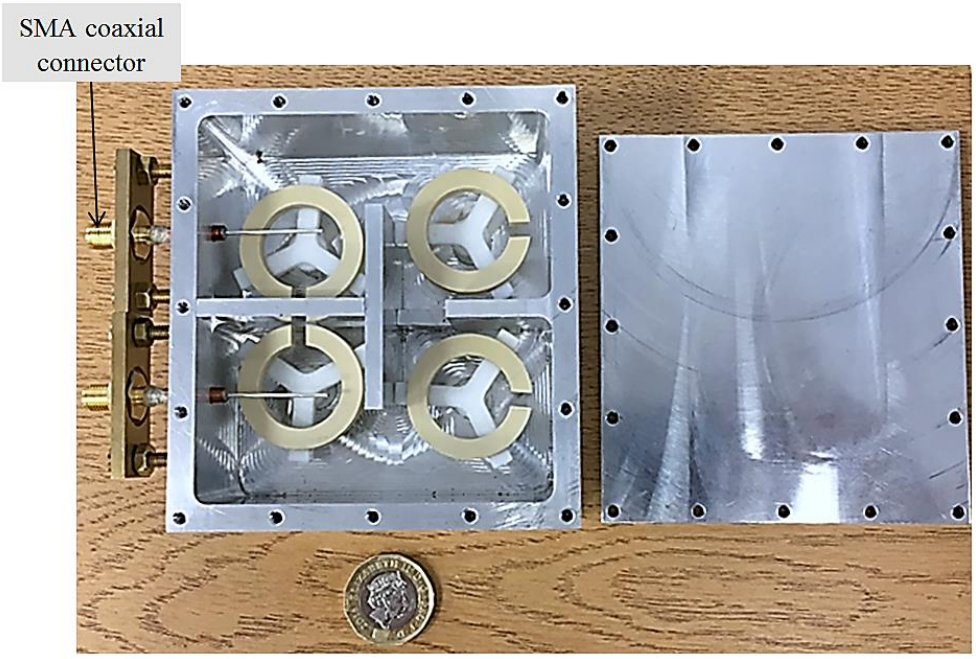

Figure 4.37 Fabricated cavity filter based on Dielectric-SRRs

The filter is tested by the Vector Network Analyser (VNA), and the measured and simulated results are shown in Figure 4.28.

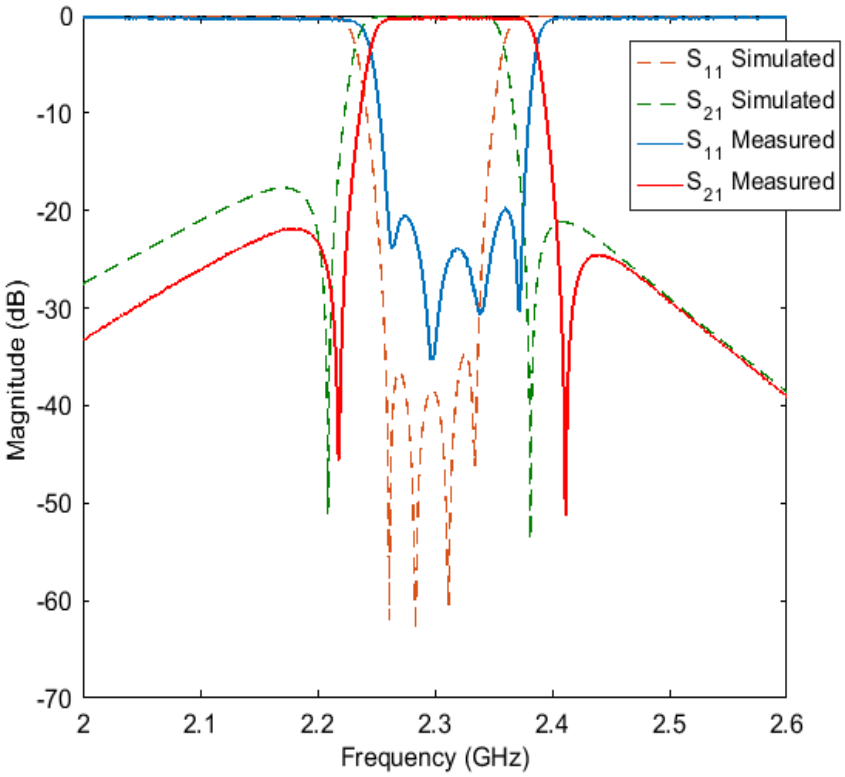

(a)

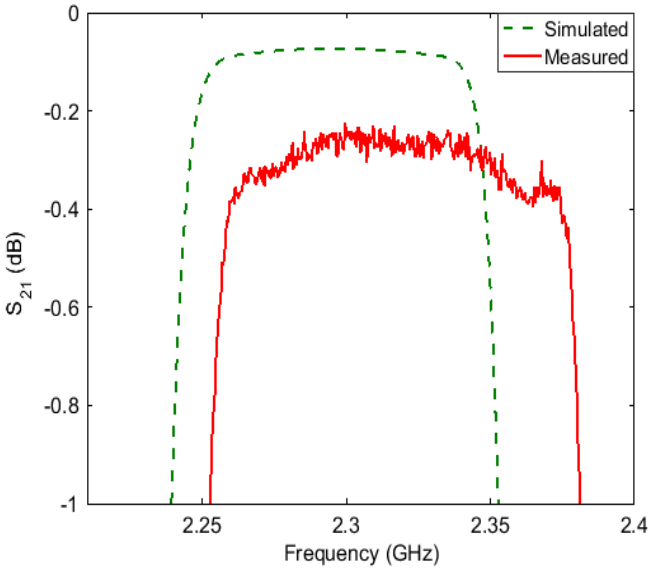

(b)

Figure 4.38 Simulated and measured results of the 4th order filter (a) S_{11} and S_{21} filter results and (b) Passband insertion losses

Again, the filter measured results have an excellent return loss of greater than 20 dB with a minimum insertion loss of only about 0.3 dB. The measured results have a small frequency shift which also moves the position of the transmission zeros slightly and increases the bandwidth by 20 MHz. The filter is tested without using any tuning screws for resonators or coupling. These filter measured results have a frequency shift and insertion loss approximately the same as the measured results of the 3rd order filter in Section 4.4.4.

4.6 Summary

A new class of non-tunable filter with two different configurations are presented in this chapter. The first filter is a 3rd order Chebyshev filter, and the second is a 4th order filter with two symmetric transmission zeros. The filters realisation began by synthesising the filter coupling matrix based on the desired specifications. The filter coupling coefficients $M_{i,i+1}$ and the external quality factors Q_e are then extracted with the corresponding dimensions by using the CST software. The filters are modelled based on the extracted dimensions then simulated and optimised by using the CST software. Finally, the filters are fabricated based on the optimised dimensions and measured. Both filters achieved excellent measured performance, as the passband insertion loss is about 0.3 dB and return loss 20 dB. The measurements and simulations of the filters, in general, agree well with each other except a small frequency shift in the measured results.

References:

[1] R. R. Mansour, F. Huang, S. Fouladi, W. D. Yan and M. Nasr, "High-Q Tunable Filters: Challenges and Potential," *IEEE Microw. Mag.*, vol. 15, no. 5, pp. 70-82, July-Aug. 2014.

[2] S. J. Fiedziuszko, I.C. Hunter, T. Itoh, *et al*., "Dielectric materials, devices, and circuits," *IEEE Trans. Microw. Theory and Tech.*, vol. 50, no. 3, pp. 706-720, Mar 2002.

[3] R. R. Mansour, "Filter technologies for wireless base stations," *IEEE Microw. Mag.*, vol. 5, no. 1, pp. 68-74, Mar 2004.

[4] J.-S. G. Hong and M. J. Lancaster, *Microstrip Filters for RF/Microwave Applications*. New York, NY, USA: Wiley, 2011.

[5] Jiafeng Zhou, M. J. Lancaster and Frederick Huang, "Coplanar quarter-wavelength quasi-elliptic filters without bond-wire bridges," *IEEE Trans. Microw. Theory and Tech.*, vol. 52, no. 4, pp. 1150-1156, April 2004.

[6] Q. X. Chu, X. Ouyang, H. Wang and F. C. Chen, "TE01δ-Mode Dielectric-Resonator Filters with Controllable Transmission Zeros" *IEEE Trans. Microw. Theory and Tech.*, vol. 61, no. 3, pp. 1086-1094, March 2013.

[7] X. Shang, M. Lancaster and Y. L. Dong, "W-band waveguide filter based on large TM_{120} resonators to ease CNC milling," *Electron. Lett.*, vol. 53, no. 7, pp. 488-490, Mar. 2017.

[8] C. Guo, X. Shang, M. J. Lancaster and J. Xu, "A 3-D Printed Lightweight X-Band Waveguide Filter Based on Spherical Resonators," *IEEE Microw. and Wireless Compon. Lett.*, vol. 25, no. 7, pp. 442-444, July 2015.

[9] CST Computer Simulation Technology AG., USA, (Jul. 2015). [Online]. Available: www.cst.com.

[10] C. Wang and K. A. Zaki, "Dielectric resonators and filters," *IEEE Microw. Mag.*, vol. 8, no. 5, pp. 115-127, Oct. 2007.

[11] J. B. Thomas, "Cross-coupling in coaxial cavity filters-a tutorial overview," *IEEE Trans. Microw. Theory Tech.*, vol. 51, no. 10, pp. 1368–1376, Apr. 2003.

[12] D. M. Pozar, *Microwave Engineering*. 4th ed. Hoboken, NJ, USA: Wiley, 2012.

Chapter 5 Tunable Bandpass Filter Design Based on Dielectric-SRRs

5.1 Introduction

In this chapter, the same Dielectric-SRRs as investigated in Chapter 3 are utilised to achieve a new type of bandwidth tunable filter. The bandwidth tunable filter is designed by using the same design approach as used with the fixed filters in Chapter 4 [1]. Filter bandwidth is tuned based on tuning the internal and external coupling of filters. Some of the published papers on BW tunable filters are reviewed in Section 5.2. The tuning of the internal coupling between two adjacent resonators is given in Section 5.3. The tuning of the external coupling is given in Sections 5.4 and 5.5. This is followed by the design of the bandwidth tunable bandpass filter.

The filter's internal and external couplings are tuned by rotating the Dielectric-SRRs mechanically without extra tuning elements, such as diodes of tuning disks that increase the filter losses [2-15]. This is done to achieve low insertion loss (as fixed filters) during the tuning process and also to reduce the design complexity and fabrication cost.

5.2 Literature Review

The majority of the published papers on tunable filters are devoted to the tuning of the filter centre frequency [2-15], and there are few published studies on the tuning of the filter BW [16-19]. The BW tuning depends on tuning the value of the internal and external couplings ($M_{i,i+1}$ and Q_e) [1]. The tuning process of $M_{i,i+1}$ and Q_e is usually

implemented by using tuning elements, such as tuning disks or varactor diodes [17, 19]. The literature studies show that using the tuning elements with the tunable filters leads to degraded resonators Q_u and increases the filter insertion loss [5]. As a result, in the published work on the tunable filters, the insertion loss is the most important design parameter and a challenge.

The microstrip tunable filters are the most common type of tunable filters in the published literature [2-4]. These filters have high insertion loss because of the tuning elements (varactor diodes) and the microstrip material [2-4]. Due to the high insertion loss, the microstrip tunable filters are not suitable for most wireless systems, let alone wireless systems with stringent requirements [3]. In [16], a microstrip tunable filter has three combline-coupled resonators with capacitive coupling to input/output ports. This tunable filter used varactor diodes D1 to tune the filter centre frequency and the varactor diodes D2 to tune the filter BW, as shown Figure 5.1a. This filter gives a BW tuning range from 70 MHz to 100 MHz at 2.25 GHz, as shown in Figure 5.1b. The measured filter responses have very high insertion loss (5 dB) due to the use of the varactor diodes and the microstrip material. Note that this review shows only the BW tuning results because this chapter presents BW tunable filters.

More recently, some papers have been published on the tunable substrate-integrated coaxial cavity filters and substrate-integrated waveguide filters [5, 17]. Such tunable filters have an insertion loss lower than the microstrip tunable filters.

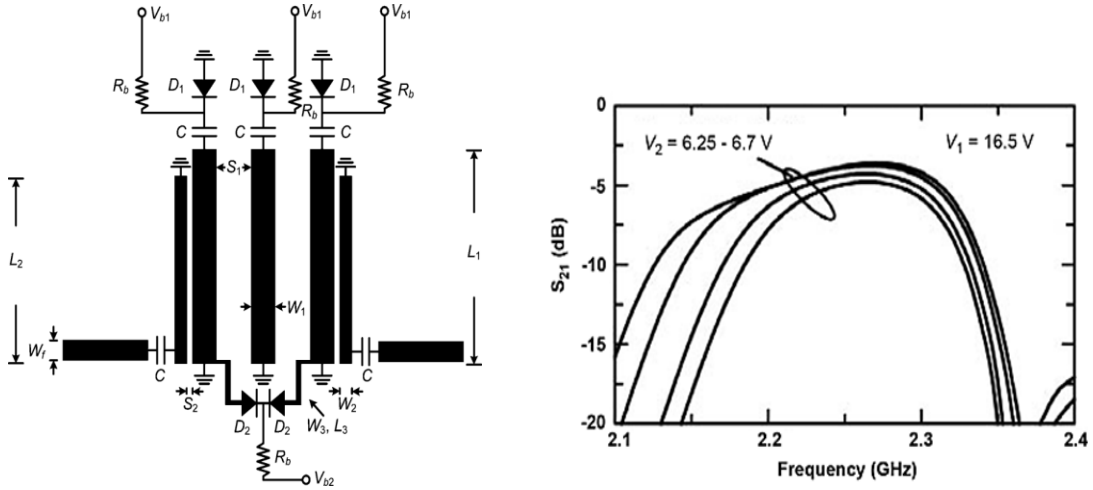

(a) (b)

Figure 5.1(a) 3rd order combline filter and (b) Measured S_{21} with bandwidth tuning at 2.25 [16]

In [18], a tunable substrate-integrated coaxial cavity filter has two coaxial resonators with dominant magnetic coupling, as shown in Figure 5.2a. A varactor diode C_{BW} is fixed between the two resonators from the top, where the most electric fields are allocated, as shown in Figure 5.2b. The overall coupling between the two coaxial resonators can be decreased by increasing the electric inter-resonator coupling through the varactor diode. As shown in Figure 5.2a the varactor diodes C_{Qe} are used for tuning the input/output coupling, while the rest of varactor diodes (C_{fo} with black colour) are fixed to tune the filter centre frequency. This tunable filter [18] has BW tuning range from 20 MHz to 100 MHz at 1.05 GHz, as shown in Figure 5.2c. The filter insertion loss increases with the smaller BWs. This is due to increasing the electric loss through the varactor diode C_{BW} when increasing the electric coupling.

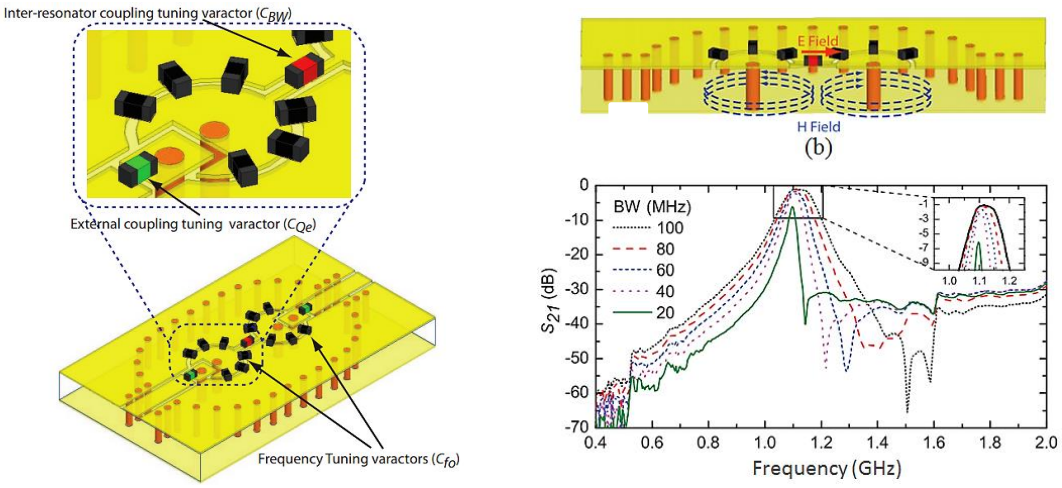

Figure 5.2 (a) Substrate-integrated coaxial-cavity filter (b) The electric and magnetic coupling between the 2 resonators from side view and (c) Measured S_{21} with bandwidth tuning at 1.05 GHz [18]

There are very little published papers on BW tunable filters using high-Q_u resonators such as dielectric resonator (DR) filters and waveguide filters [5]. The published studies on DR tunable filters are devoted to the centre frequency tuning [6]. Such filters are tuned to the centre frequency by adapting the capacitance of the DRs with tuning disks or varactor diodes [5, 6]. These DR tunable filters reported high insertion loss from 1 to 4 dB during the tuning process of centre frequency at S band [5]. In [6], a DR tunable filter has metal screws for tuning internal and external couplings, thereby tuning the filter BW. This filter also has tuning disks for each dielectric resonator to tune the filter centre frequency. The DR tunable filter [6] presents a centre frequency tuning range from to 1.93 GHz to 1.96 GHz and a BW tuning range from 5 MHz to 20 MHz with 1 dB insertion loss.

In [19], a waveguide tunable filter has non-resonant coupling resonators and tuning disks to tune the internal and external couplings, as shown in Figure 5.3a. The internal and external couplings of this waveguide filter are tuned by changing the length of the coupling resonators with the tuning disks. This filter [19] gives a frequency tuning range from 19.7 GHz to 20.2 GHz and BW tuning range from 36 MHz to 72 MHz at 20 GHz, as shown in Figure 5.3b. The insertion loss of this filter is relatively high (1.2 dB) because of the use of metal tuning disks. The waveguide filter [19] has a return loss better than 20 dB during the BW tuning process, which is achieved by using the tuning disks of the resonators (R1, R2, R3, and R4) to control the return loss.

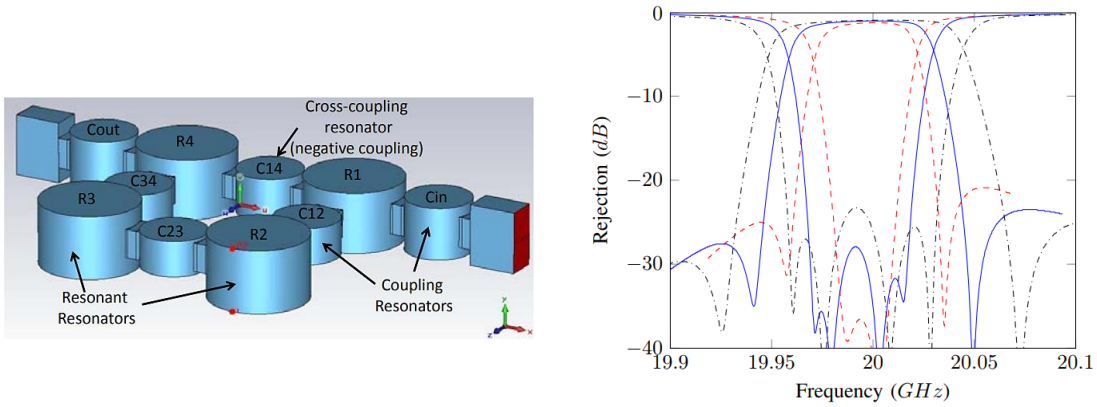

(a) (b)

Figure 5.3 (a) 4th order waveguide tunable filter and (b) measured results for BW tuning at 20 GHz [19]

In conclusion, the published papers on tunable microwave filters reported high insertion loss (S_{21}) during the tuning process as a result of using the tuning elements, such as tuning disks and varactor diodes. The filter tuning process also presents deterioration in the return loss, and this requires using additional tuning elements to control the filter return loss. The use of additional tuning elements usually leads to an increase of the

filter insertion loss, size, and the complexity of tuning process. However, the design of a tunable filter with low insertion loss and reasonable return loss is a change.

The published literature also shows that most DR tunable filters are for tuning only the centre frequency, and there are very little DR tunable filters for tuning both the centre frequency and BW [5, 6].

5.3 Tuning the Coupling Coefficient K_c

The EM field distributions of the Dielectric-SRR, as shown in Chapter 3, vary around the circumference due to the asymmetric structure, unlike ring, dielectric, and coaxial resonators which have a symmetric structure [20, 21]. This variation in EM field distributions is utilised to vary the coupling coefficient K_c between two adjacent Dielectric-SRRs by rotating these resonators.

Figure 5.4 shows a model used to extract K_c between the two Dielectric-SRRs labelled R1 and R2. The resonators and holders have the same specifications and dimensions as in Section 4.2. A Teflon rod of ε_r = 2.1 and diameter = 2 mm is fixed onto the Teflon holder of R1, as shown in Figure 5.4b. This rod is used to rotate the Dielectric-SRR manually in the real filter. This rod has a very small effect on the Q_u of the resonator because it has a very small loss tangent and low volume. The effect of Teflon material on the Q_u of the Dielectric-SRRs is given in Chapter 3.

K_c is tuned by rotating R1 with rotation angle θ_1 with three different wall widths W. These results are shown in Figure 5.5. Meanwhile, R2 is fixed in position, as shown in Figure 5.4a.

There are other parameters which have the same, or less, effect on the K_c tuning range compared to wall width W when R1 is rotated, such as the wall thickness and height and the separation distance between the resonators, but these have been fixed for this simulation.

Figure 5.5 shows that the K_c is lower when R1 is rotated clockwise (lower θ_1) and higher when R1 is rotated counter-clockwise (higher θ_1); θ_1 can have both positive and negative values. When rotating resonator R1 clockwise, the K_c values support a decrease the filter bandwidth, and, when rotating it counter-clockwise, the K_c values support an increase of the filter bandwidth.

The K_c tuning range is between 0.031 and 0.083 when W = 15 mm, as shown in Figure 5.5. This tuning range is able to achieve an FBW tuning range from 3% to 8% at 2.2 GHz for a 3rd order Chebyshev filter with passband ripple of 0.043 dB. The FBW tuning range is calculated by using equation (2-28) and the synthesised coupling matrix [m] of a 3rd order Chebyshev filter, as described in Chapter 2.

$$[m] = \begin{bmatrix} 0 & 1.0303 & 0 \\ 1.0303 & 0 & 1.0303 \\ 0 & 1.0303 & 0 \end{bmatrix}, \quad q_{e1} = q_{e2} = 0.9611 \tag{5-1}$$

$$FBW = \frac{M_{i,j}}{m_{i,j}} \tag{5-2}$$

The required external Q-factors for this calculated FBW tuning range can also be found by using equation (2-3). Table 5.1 shows the K_c tuning range when W=15 mm and the calculated tuning ranges of FBW and Q_e.

Table 5.1 θ_1 values with the corresponding K_c, FBW, and Q_e tuning ranges

θ_1	K_c	FBW	Q_e
-70°	0.031	0.03	32
-50°	0.04	0.038	25.3
-30°	0.05	0.048	20
-10°	0.063	0.061	15.7
10°	0.07	0.067	14.34
30°	0.077	0.074	13
50°	0.081	0.078	12.32
70°	0.083	0.08	12

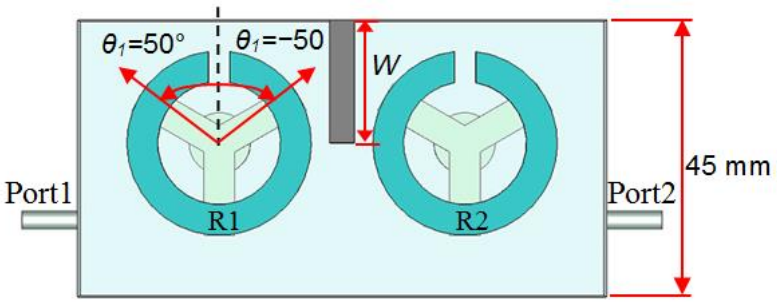

(a)

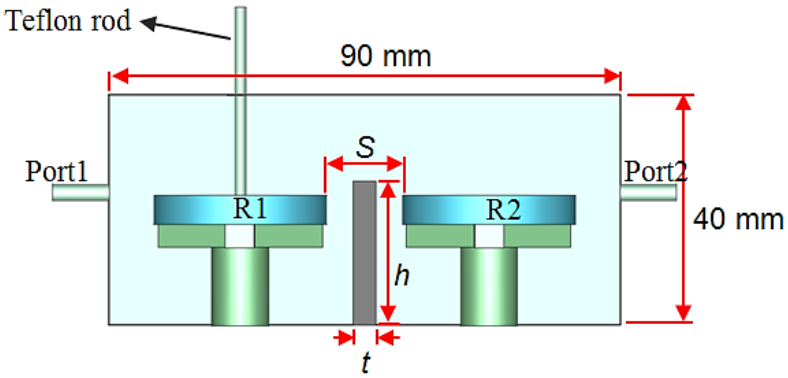

(b)

Figure 5.4 The model for extracting K_c, shows the angle θ_1 of R1 and the wall between R1 and R2 with width W, t=4 mm, and h=25 mm, (a) Top view and (b) Side view

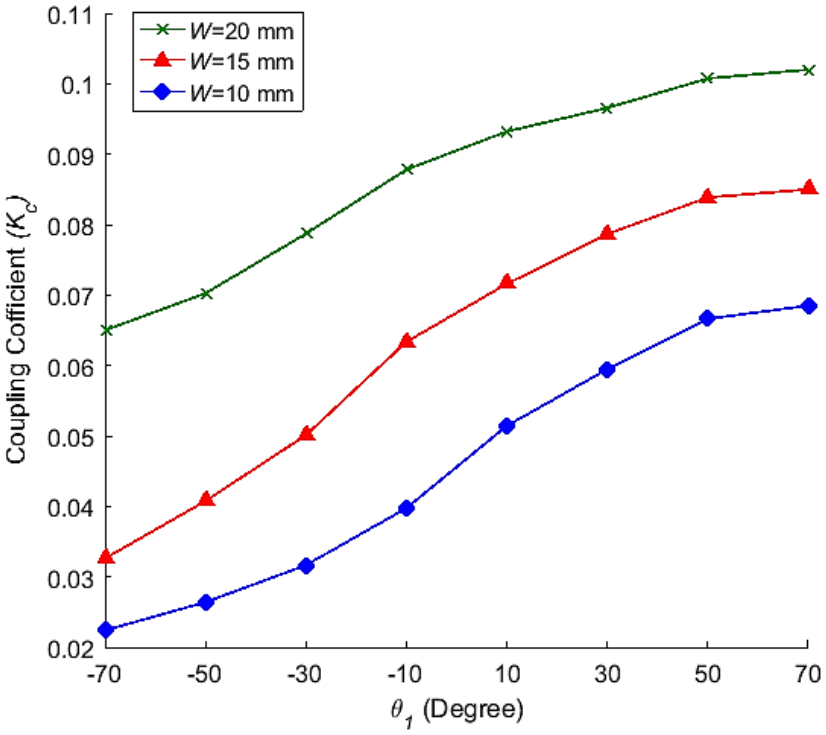

Figure 5.5 K_c against angle θ_1 of R1 and wall width W.

The above tuning of K_c is implemented based on rotating only one resonator (R1) and fixing the adjacent resonator (R2). This is in order to reduce the number of rotating elements, the design complexity, and time taken for tuning bandwidth.

When two adjacent resonators R1 and R2 are rotated together with the same rotation angles, θ_1 and θ_2, with R1 rotated clockwise and R2 counter-clockwise, as shown in Figure 5.6a, the K_c tuning range can also be extracted and is shown in Figure 5.6b. The rotation angles between −30° and −50° achieve electric coupling due to the resonators gaps being close to each other.

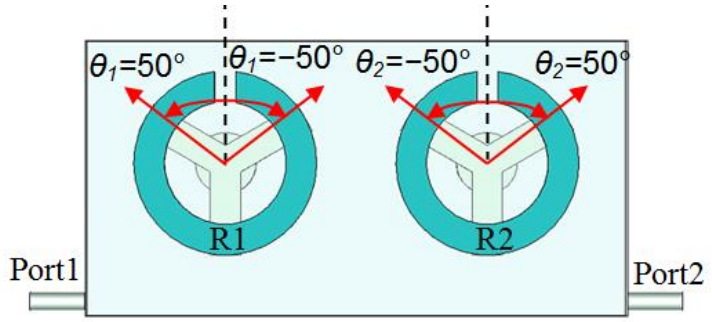

(a)

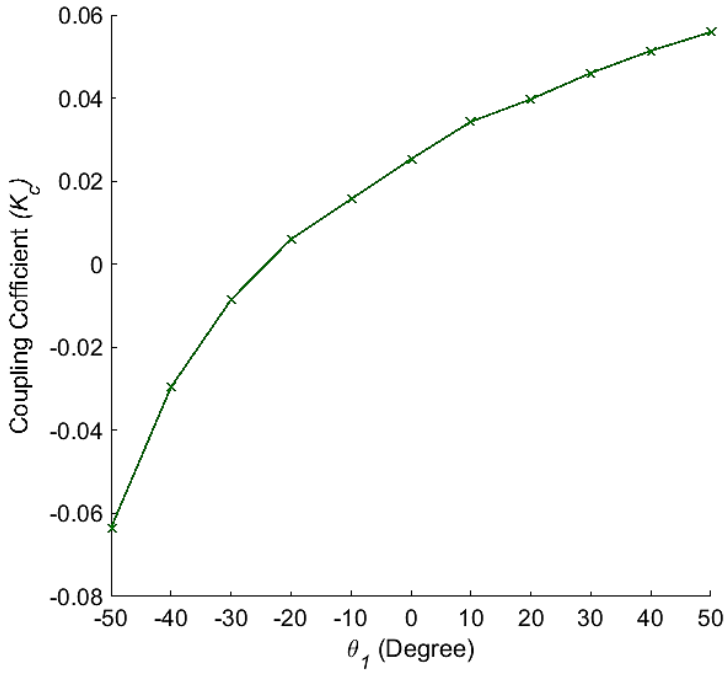

(b)

Figure 5.6 K_c for rotating two resonators. (a) The model from Top view and (b) K_c against rotation angles θ_1 and θ_2.

As shown in Figure 5.6b the K_c values have positive and negative values. This is because the K_c is the total of the magnetic fields coupling K_m and the electric fields coupling K_e between two adjacent resonators. These two couplings (K_m and K_e) are out

of phase with each other, so K_c can be defined as the magnetic fields coupling less the electric fields coupling, as given [22, 23]:

$$K_c = K_m - K_e \tag{5-3}$$

As a result, K_c can be obtained as a positive value when the magnetic coupling is stronger than the electric coupling and a negative value when the electric coupling is stronger than the magnetic coupling. Additionally, K_c can have zero value when the magnetic and electric couplings are equal.

5.4 Tuning Q_e by Feeding Probe Length

The Q_e values are extracted based on the method described in Section 4.3, and the Dielectric-SRRs and holders dimensions and specifications are the same as in Section 4.2. The Q_e is tuned by varying the length of the input coaxial feeding probe CL_1, as shown in Figure 5.7.

The acceptable Q_e values for the FBW tuning range (in Table 5.1) are extracted with the corresponding parameters CL_1 and θ_1, as given in Table 5.2. Figure 5.7b shows that this tuning method of Q_e presents a wide range of frequency shift due to the change in the length of the feeding probe CL_1, and this leads to decrease the FBW tuning range at 2.2 GHz. However, based on this tuning method, a tunable filter is modelled and simulated in Section 5.6.1, and another method of tuning Q_e without varying the feeding probe length is presented in the next section, with a filter using this method discussed in Section 5.6.2.

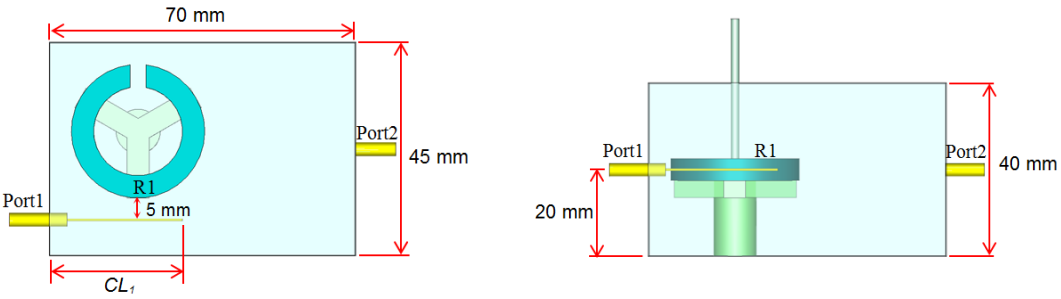

(Top view) (Side view)

(a)

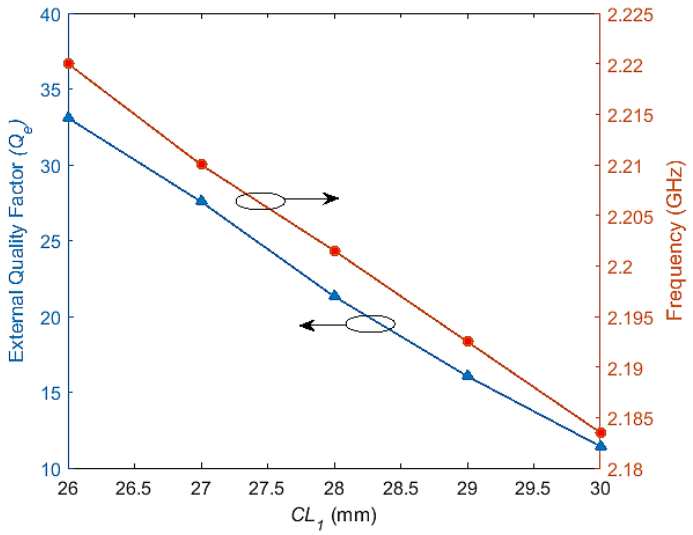

(b)

Figure 5.7 (a) Model for extracting Q_e and (b) Q_e and frequency shift against the length of feeding probe.

Table 5.2 θ_1 and CL_1 values with the corresponding Q_e tuning range.

θ_1	CL_1 (mm)	Q_e
-70°	24.3	32
-50°	25.7	25.3
-30°	26.9	20
-10°	27.5	15.7
10°	28.6	14.34
30°	29.1	13
50°	30.4	12.32
70°	32.6	12

5.5 Tuning Q_e by an Extra Dielectric-SRR

A new method and structure to tune Q_e is presented in this section. An extra Dielectric-SRR, RS, is added to the model for extracting Q_e in the previous section. This is shown in Figure 5.8. RS and R1 have the same dimensions and specifications as in Section 4.2. RS is strongly coupled to the input feeding probe and is essentially part of external source (Port 1). Therefore, the external coupling of Q_e in this model is between RS and R1. The method of Q_e extraction is explained in Section 4.3.

The Q_e is tuned against the rotation angle (θ_s) of RS with three different wall widths W, as shown in Figure 5.9. There are more parameter effects on the Q_e value, such as the distance between the feeding probe and the Dielectric-SRR, and this is described in more detail in Section 4.3.

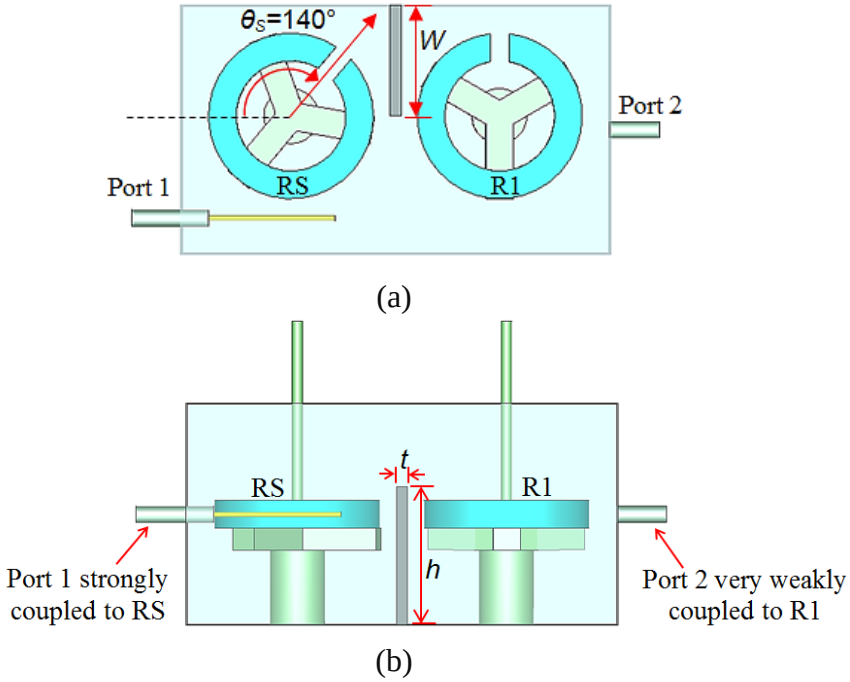

Figure 5.8 The model for extracting Q_e, (a) Top view and (b) Side view the wall height h = 25 mm and thickness t =2 mm

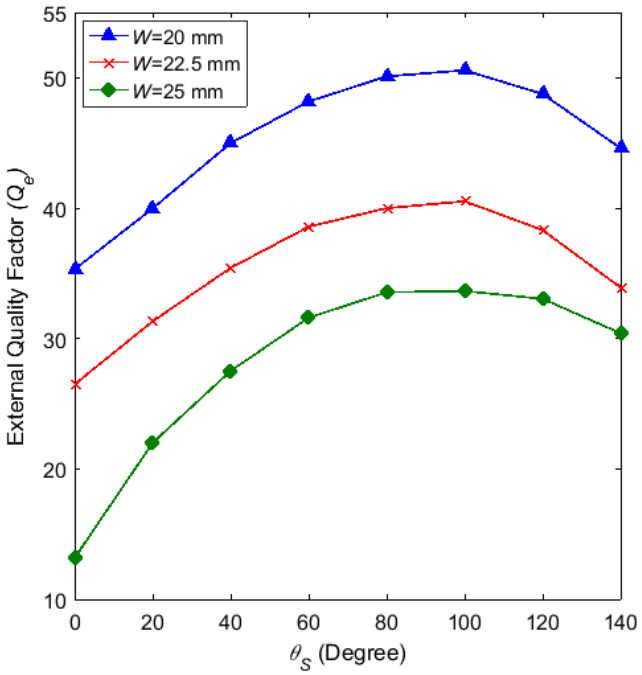

Figure 5.9 Q_e against θ_S and W

Figure 5.10 shows the simulated S_{21} response for the model given in Figure 5.8. The simulation results show resonance frequency close the desired centre frequency (2.2 GHz) of the tunable filter by about 330 MHz.

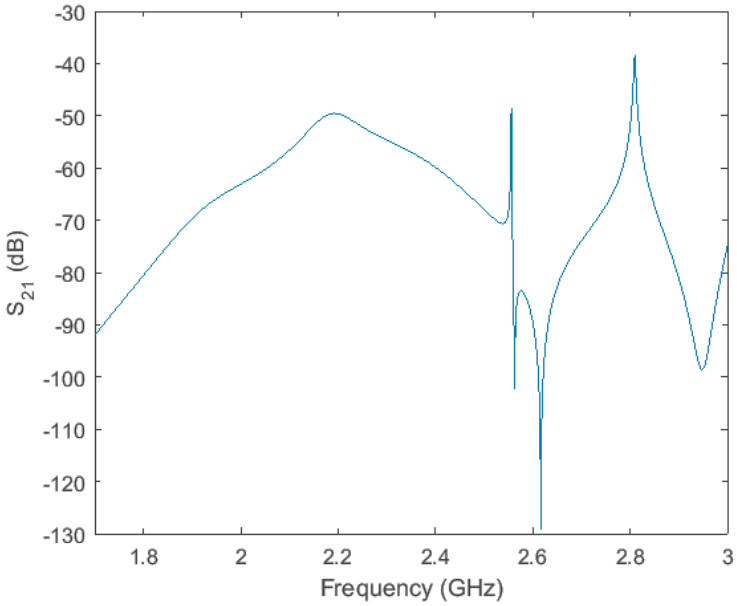

Figure 5.10 S_{21} results for the model in Figure 5.8

5.6 Design of 3rd Order Tunable Filter

In this section, a bandwidth tunable filter is designed based on the Dielectric-SRRs. This filter is a 3rd order Chebyshev filter with 20 dB return loss, and the filter coupling matrix $[m]$ is synthesised based on equation (2-28) as given

$$[m] = \begin{bmatrix} 0 & 1.0303 & 0 \\ 1.0303 & 0 & 1.0303 \\ 0 & 1.0303 & 0 \end{bmatrix}, \quad q_{e1} = q_{e2} = 0.9611. \tag{5-4}$$

Based on the filter coupling matrix, the filter topology is modelled as shown in Figure 5.11, and filter S-parameters are calculated as shown in Figure 5.12.

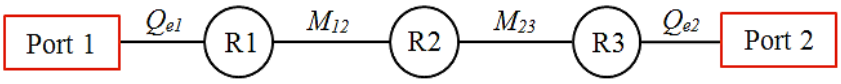

Figure 5.11 Topology of 3rd order passband filter

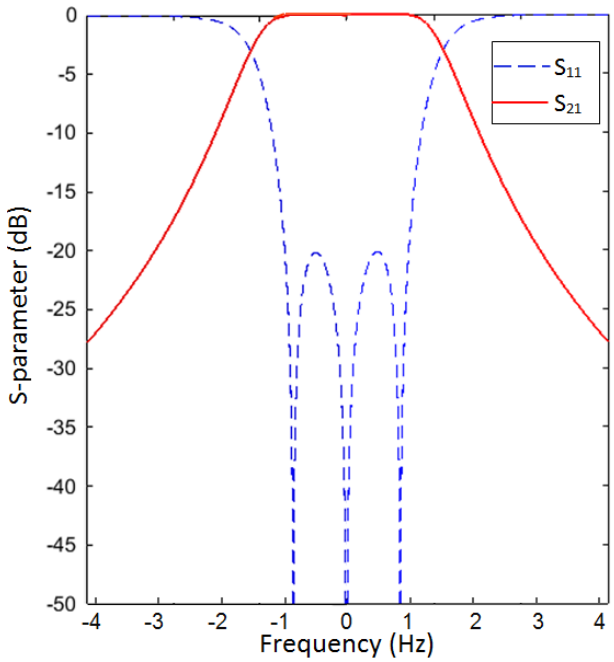

Figure 5.12 An S-parameter response for the 3rd order passband filter

In order to design a bandwidth tunable filter, it is necessary to consider both tuning the K_c value between the two resonators and tuning the Q_e between input/output ports and the first/last resonators. In this section, the tunable filters are implemented based on the K_c tuning method, as described in Section 5.3, and the two methods of tuning Q_e, as described in Sections 5.4 and 5.5.

The K_c tuning range from 0.031 to 0.083, as shown in Figure 5.5 is used for M_{12} and M_{23} of the 3rd order filter. M_{12} and M_{23} should have the same tuning range because the filter is symmetrical. As mentioned in Section 5.3, this coupling coefficient tuning range supports the tuning of the filter FBW from 3% to 8% at 2.2 GHz. For this FBW tuning range, the filter Q_{e1} and Q_{e2} are tuned from 12 to 33. This tuning range is obtained by using the two methods of tuning Q_e, as shown in Figures 5.7 and 5.9. Therefore, two filters are designed in the following two sections: the first used the method of moving the feeding probe, and the second used the method of adding an extra rotating Dielectric-SRR to tune Q_e.

5.6.1 The Tunable Filter Based on Moving Feeding Probe

5.6.1.1 Filter Configuration

Figure 5.13 shows the filter structure modelled by CST software and the physical dimensions obtained from the K_c and Q_e simulation results, as described in Chapter 4. The enclosure and walls are aluminium, and the Dielectric-SRRs and holders have dimensions and specifications as given in Section 4.2.

In the filter, the rotation angle θ_1 of R1 is always equal to the rotation angle θ_3 of R3, and the input and output feeding probe lengths CL_1 and CL_2 are always equal, as shown in Figure 5.13.

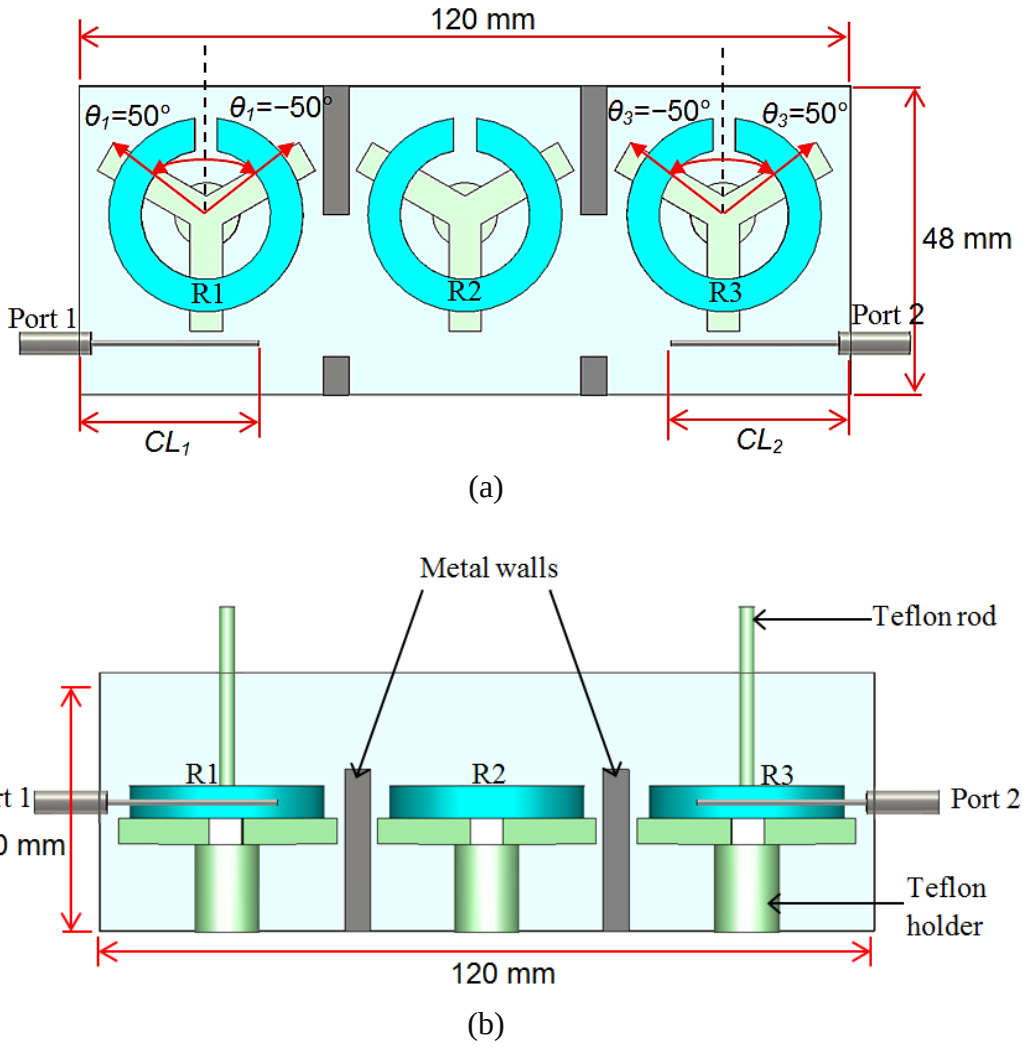

Figure 5.13 The structure of 3rd order passband filter modelled in CST, (a) Top view and (b) Side view

5.6.1.2 Passband Bandwidth Tuning

The above tunable filter model is simulated by CST software based on rotating the resonators and varying the length of the feeding probes. The coupling coefficients M_{12}

and M_{23} are tuned by rotating the resonators R1 and R3 with rotation angles θ_1 and θ_3, respectively, while the Q_{e1} and Q_{e2} are tuned independently by varying the length of feeding probes CL_1 and CL_2. During the tuning process, the rotation angle $\theta_1 = \theta_3$ and the length $CL_1 = CL_2$ to keep a symmetric configuration producing the same coupling values.

Figure 5.14 shows three simulated responses selected from the continuous tuning range. The passband insertion loss is from 0.1dB to 0.9dB, as shown in Figure 5.15, and most passband insertion loss is due to S_{11}. There is a transmission zero at about 1.9 GHz for each tuning response due to direct coupling between Port 1 and Port 2. The widest tuning range for filter 3dB FBW is from 6.8% to 8.4%. The FBW is determined at the 3 dB points due to the high return loss for the tuned responses. This deterioration in the return loss is because it is not possible for the filter structure to be optimised by CST software for the whole BW tuning range. Thus, a high return loss is expected from filters simulated with the initial dimensions as given in Chapter 4. The tunable filters in this chapter are simulated by using the parameter sweep option in the CST software. The parameter sweep option can run several simulations, one-by-one, for a range of parameter values. The values of the tuning parameters, like θ_1 and CL_1, can be determined as given in Sections 5.3 and 5.4. All combinations of these tuning parameters and their values can then be simulated by the CST parameter sweep. Following this, the best filter responses and their corresponding parameters values can be selected from the stored results in the CST software. Table 5.3 shows FBWs selected from the BW tuning range with corresponding parameters values.

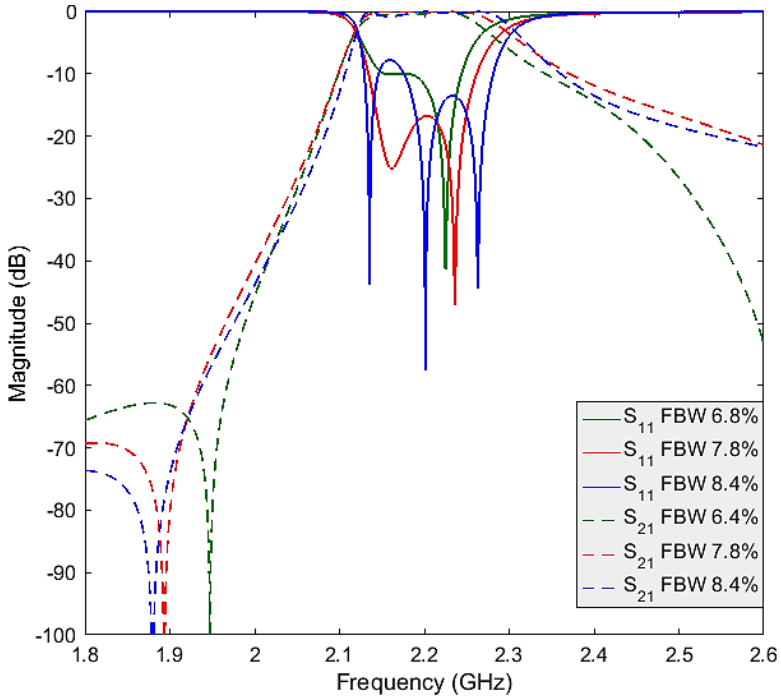

Figure 5.14 CST simulation responses of 3rd order tunable Dielectric-SRR filter

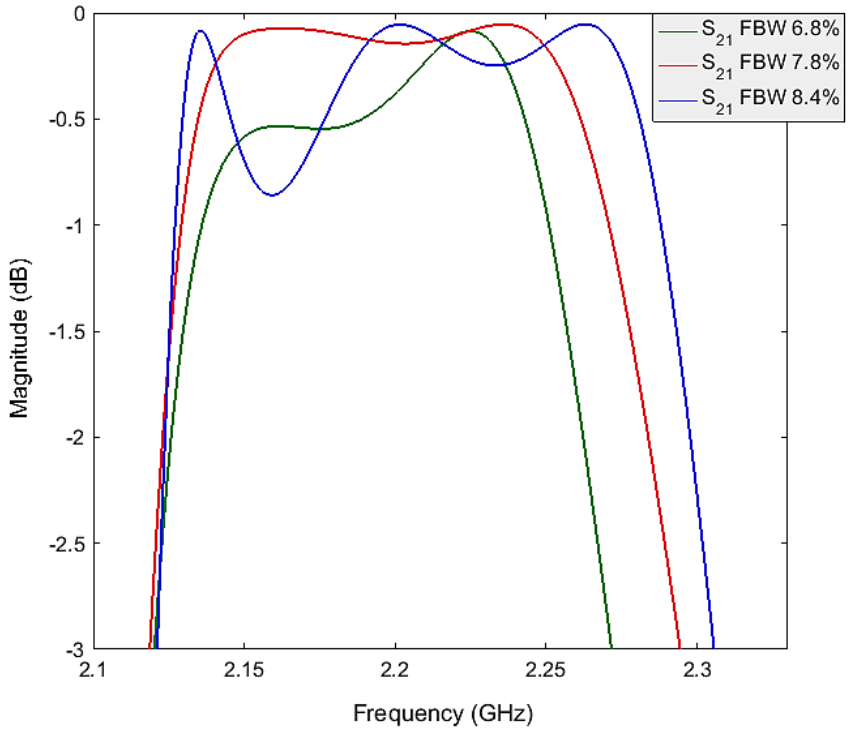

Figure 5.15 Passband insertion losses of the Dielectric-SRR tunable filter

Table 5.3 Five CST results for FBWs and corresponding parameters

3dB FBW	$\theta_1 = \theta_3$	$CL_1 = CL_2$ *(mm)*	Centre freq.(GHz)	Max. S_{11} (dB)
6.8%	−5°	29.6	2.194	-11
7.1%	5°	30.1	2.198	-15
7.6%	15°	30.8	2.206	-17
7.9%	25°	31.4	2.209	-12
8.4%	35°	31.9	2.212	-8

5.6.2 Design of 3rd Order Tunable Filter with Extra Resonators

5.6.2.1 Filter Configuration

The resonators, holders, and rods used in this filter design have the same material specifications and dimensions of the previous filter in Section 5.6.1. In this section, extra resonators, RS and RL, are added and utilised to tune Q_e, as shown in Figure 5.16. The filter has a symmetrical structure, and, during the rotation of resonators R1, R3, RS and RL, the rotation angles θ_S and θ_L as well as θ_S and θ_L are equal. This keeps the configuration and internal and external coupling values symmetrical.

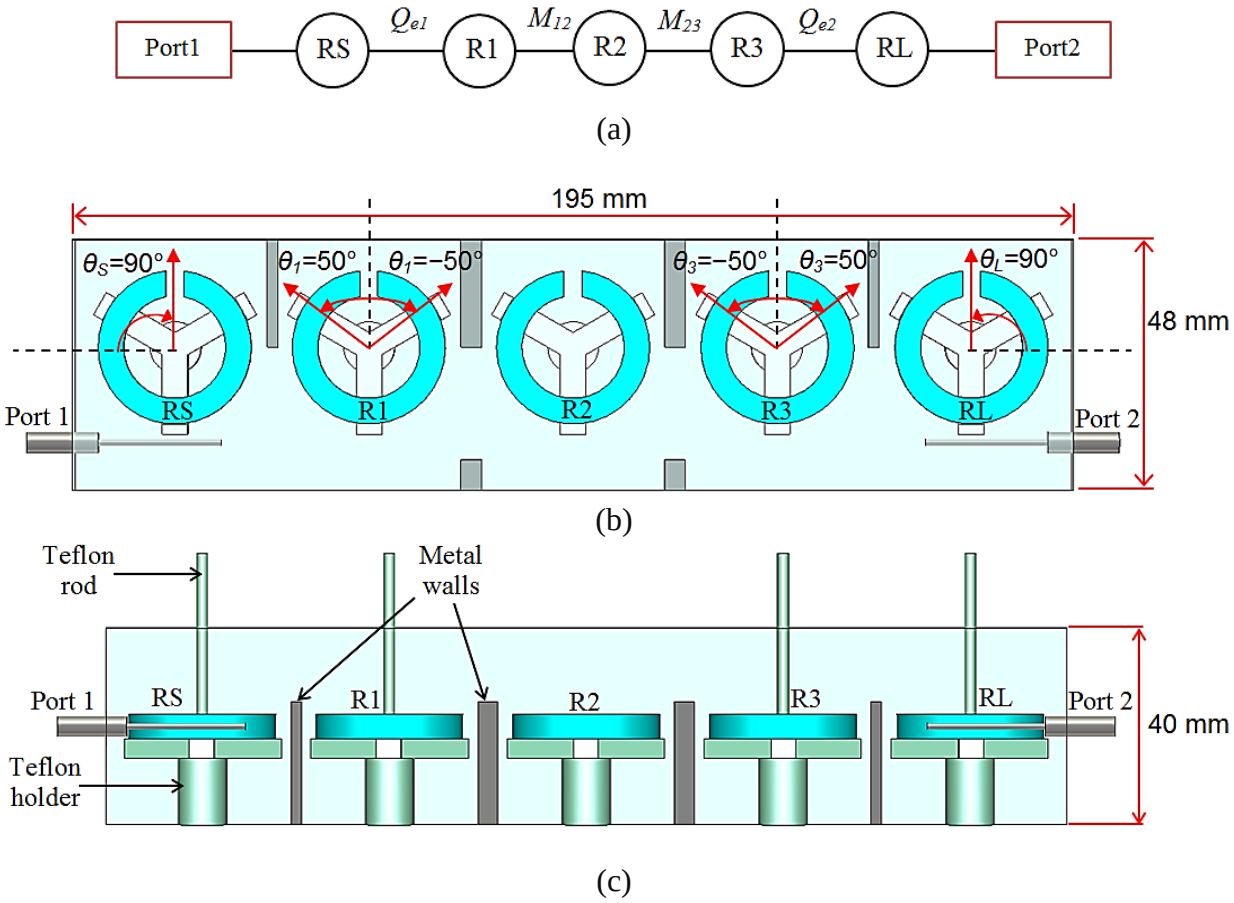

Figure 5.16 The model of 3rd order filter with two extra resonators. (a) Filter topology, (b) the model top view, and (c) side view

5.6.2.2 Passband Bandwidth Tuning

The tunable filter model in Figure 5.16 is simulated in CST software, and five responses are selected from the continuous tuning range, as shown in Figure 5.17. The passband insertion loss is between 0.1dB and 0.9dB. Most insertion loss is due to the return loss, as shown in Figure 5.18. The widest tuning range for the 3dB FBWs is from 4% to 7.8%. This range is more than twice the tuning range of the tunable filter in Section 5.6.1. There is a transmission zero at about 2.05 GHz for each tuned response due to direct coupling between ports 1 and 2. This cross-coupling is proofed by varying the

length L of the feeding probes. Figure 5.19 shows the transmission zero pushed up towards the filter passband when L increases. This is because the increasing of L leads to an increase in cross-coupling between ports 1 and 2.

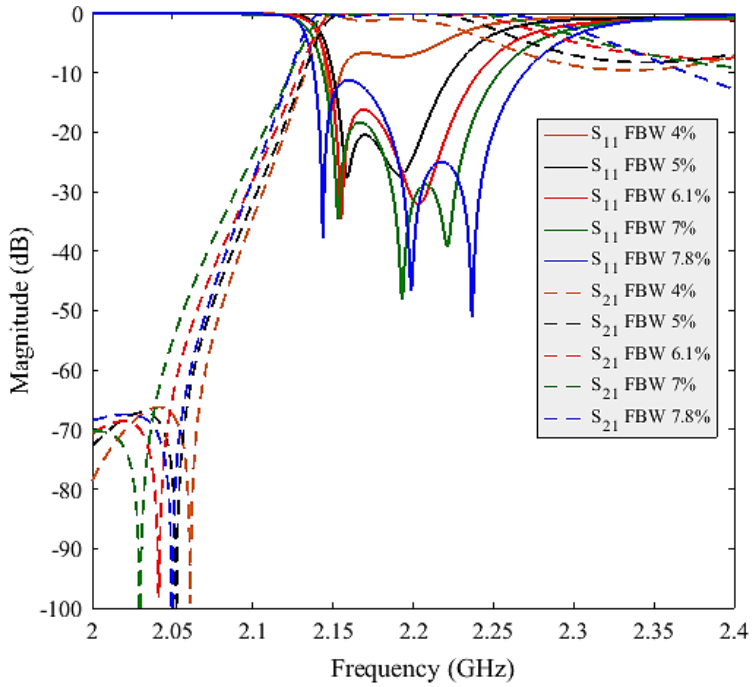

Figure 5.17 CST simulation results of 3rd order tunable filter with two extra resonators

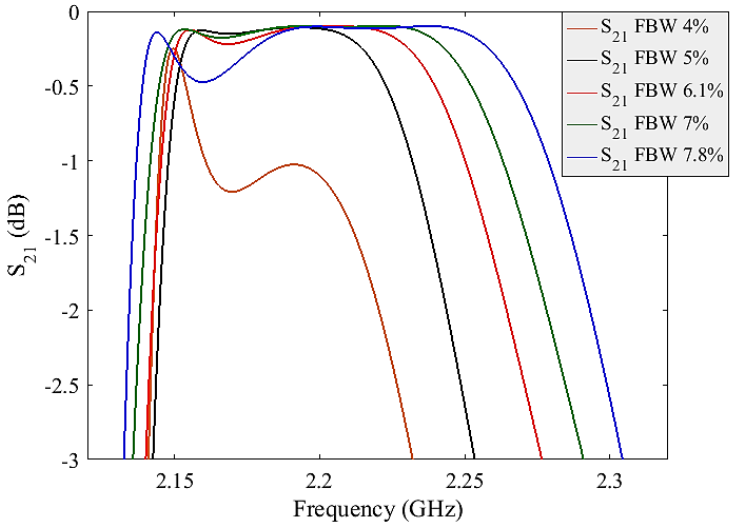

Figure 5.18 Passband insertion losses of the tunable filter responses

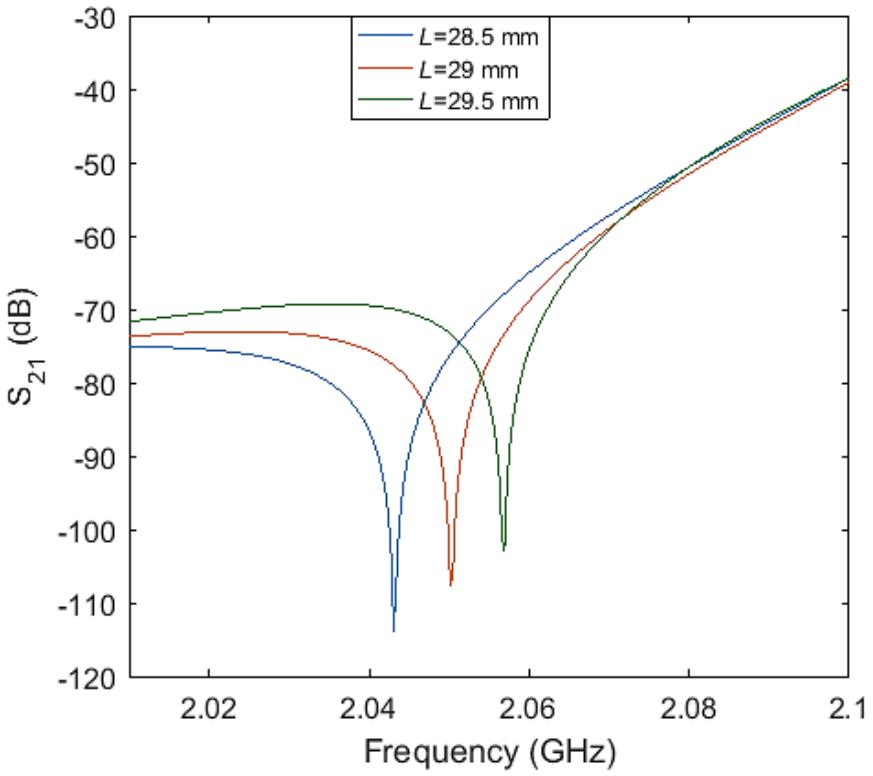

Figure 5.19 S_{21} results with three different probe lengths *L*

The upper stopbands of the filter responses are deteriorated due to a resonance frequency close to the filter passband by about 330 MHz, as shown in Figure 5.20. The electric fields of this resonance frequency are monitored by the CST software, as given in Figure 5.21. The monitored results show the resonance frequency is from the cavity surrounding the Dielectric-SRRs. This frequency peak can be moved up to the higher frequency by decreasing the cavity volume.

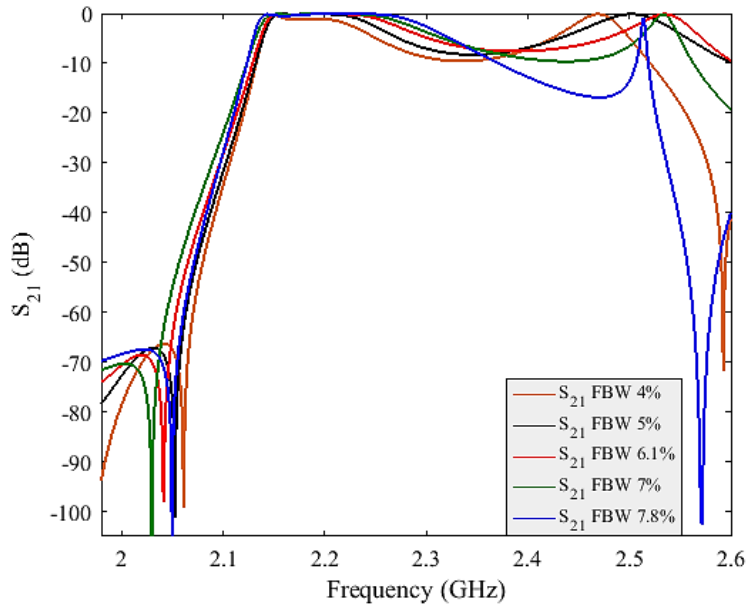

Figure 5.20 Wide-band frequency for the tunable filter responses

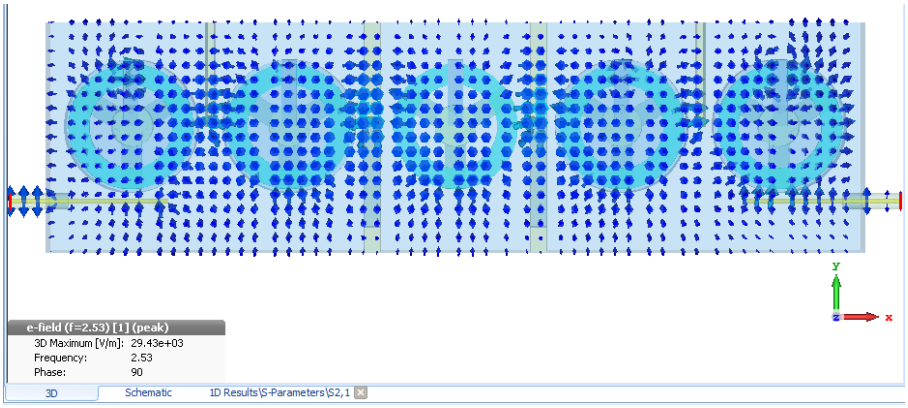

(Top view)

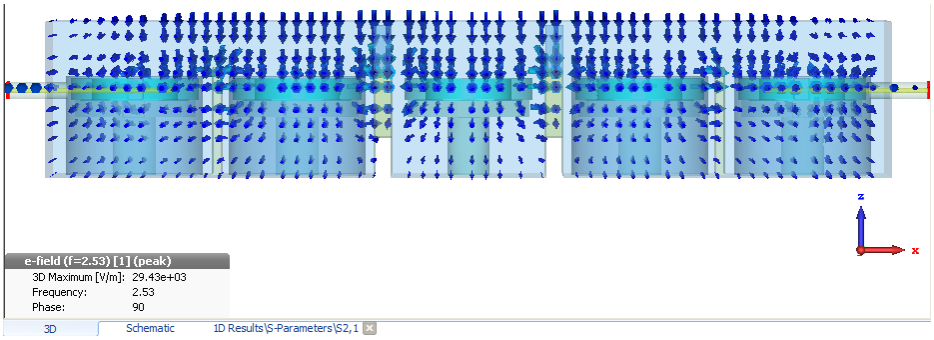

(Side view)

Figure 5.21 Monitored results of the electric fields at 2.53 GHz

Table 5.4 shows FBWs selected from the continuous tuning range with the corresponding parameters.

Table 5.4 CST results for FBWs and corresponding parameters

3dB FBWs	$\theta_1 = \theta_3$	$\theta_S = \theta_L$	Centre freq.(GHz)	Max. S_{11} (dB)
4%	-30°	86°	2.194	-16.7
4.4%	-20°	75°	2.197	-19.2
4.8%	-15°	67°	2.199	-24.3
5.1%	-5°	59°	2.203	-20.4
5.7%	5°	41°	2.207	-17.5
6.3 %	10°	34°	2.211	-18.4
6.8%	20°	23°	2.213	-25.8
7.1%	30°	14°	2.215	-20.2
7.8%	40°	7°	2.218	-15.6

5.7 5th and 3rd Order Tunable Filter

In this section, a filter with a 5th order Chebyshev response, 10% FBW at 2.3 GHz, and 5 Dielectric-SRRs is designed. The filter topology is as shown in Figure 5.22.

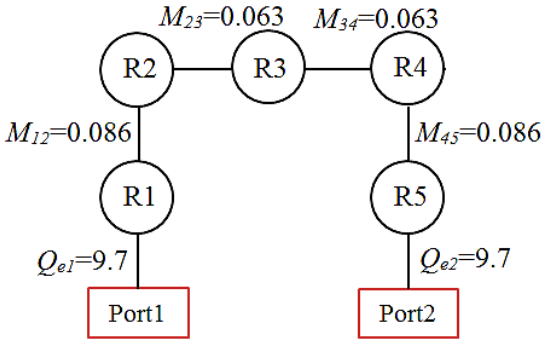

Figure 5.22 5th order filter topology

The internal and external couplings of this 5th order filter are tuned by rotating the Dielectric-SRRs to achieve another function. This function is 3rd order filter with

tunable BW the same as the tunable filter given in Section 5.6.2. Figure 5.23 shows the tunable filter topology with the second function of a 3rd order filter. The filter resonators R1, R2, R3, R4. and R5 (in Figure 5.22) of 5th order filter are identical to resonators RS, R1, R2, R3, and RL (in Figure 5.23) of a 3rd order filter.

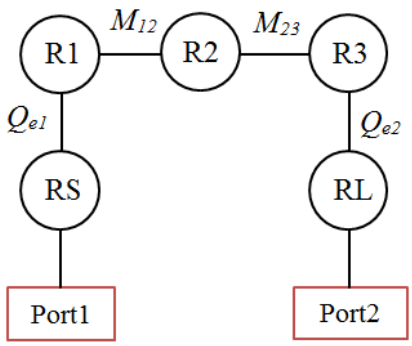

Figure 5.23 3rd order filter topology

The tunable filter in this section has two functions, the first function is a 5th order filter and the second function is a 3rd order filter. The filter in this section is designed to achieve a 5th order filter with fixed BW, similar to the filters presented in Chapter 4. This filter is also designed to act as a 3rd order filter with tunable bandwidth by rotating the first/last resonators to be very strongly coupled to the external ports, just as the tunable filter presented in Section 5.6.2. The BW of the 5th order filter is chosen to be higher than the BW tuning range of the 3rd order filter in order to increase the BW tuning range, as shown in the next section.

The Dielectric-SRRs and holders have dimensions and material specifications the same as those in Section 4.2. The enclosure considered is aluminium, and its overall dimensions are given in Figure 5.24.

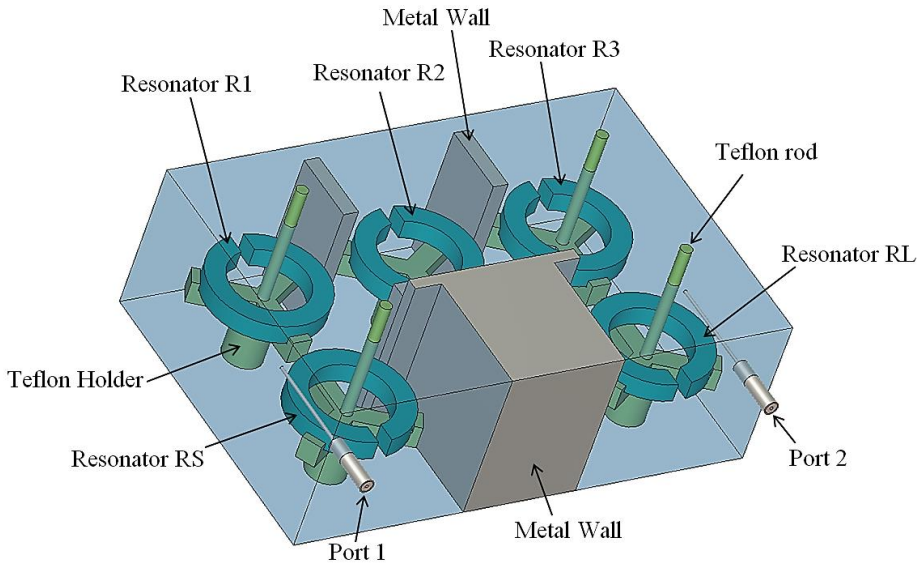

(a)

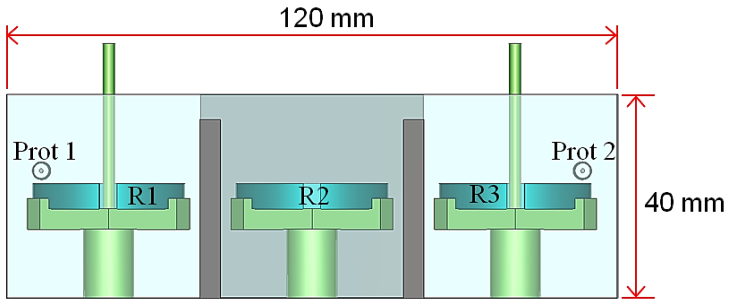

(b)

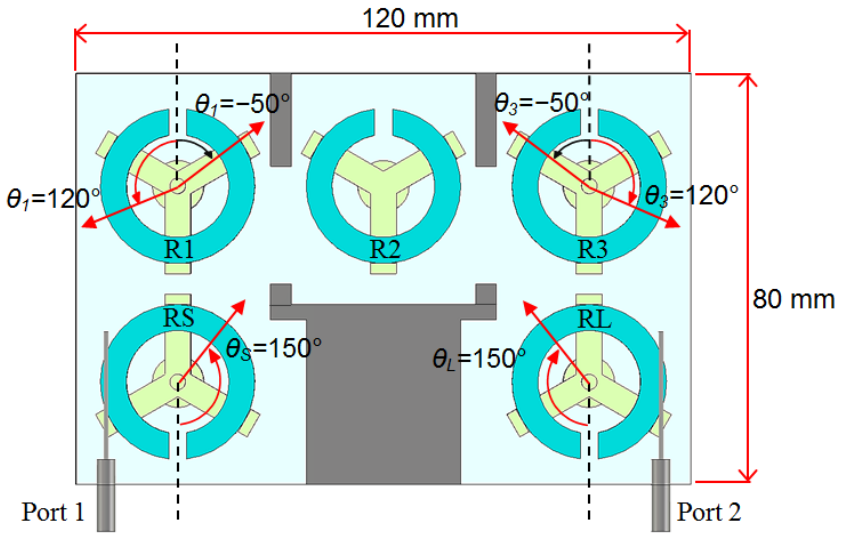

(c)

Figure 5.24 The filter structure modelled by CST. (a) 3-D model, (b) front view, and (c) top view

5.7.1 CST Simulation

The tunable filter model described in the previous section is simulated by CST software. The filter resonators R1, R3, RS, and RL are rotated to tune the filter bandwidth whilst the rotation angles are maintained $\theta_1 = \theta_3$ and $\theta_S = \theta_L$. This is to maintain a symmetrical configuration and coupling values.

The simulation results presented 11.6% 3 dB FBW at 2.3GHz for the 5th order filter and 3 dB FBW tuning range from 6% to 10.6% for the 3rd order responses, as shown in Figure 5.25. The simulated tunable filter achieved two functions by rotating the Dielectric-SRRs. The first function is a 5th order filter, and the second function is a 3rd order filter with tunable BW and two extra resonators at the input/output ports. The 3rd order filter has responses with high return loss and less than three reflection poles because it is not possible for the CST optimiser to be used for the entire BW tuning range. The only response of the 5th order filter is optimised by the CST software. Table 5.5 shows FBW values and the corresponding parameters when the filter achieves both functions the 5th and 3rd order filters.

Figure 5.26 shows the passband insertion loss from 0.2 dB to 1 dB. This loss is due to the metal cavity, dielectric material, input/output connectors, and the high return loss. S_{21} is low due to the use of high Q_u resonators without adding any tuning elements, such as screws, disks, or varactor diodes. Figure 5.27 shows resonance at 2.8 GHz due to the 2nd mode of the Dielectric-SRR. There is a transmission zero at about 2.1 GHz for each tuning response due to the direct coupling between ports 1 and 2.

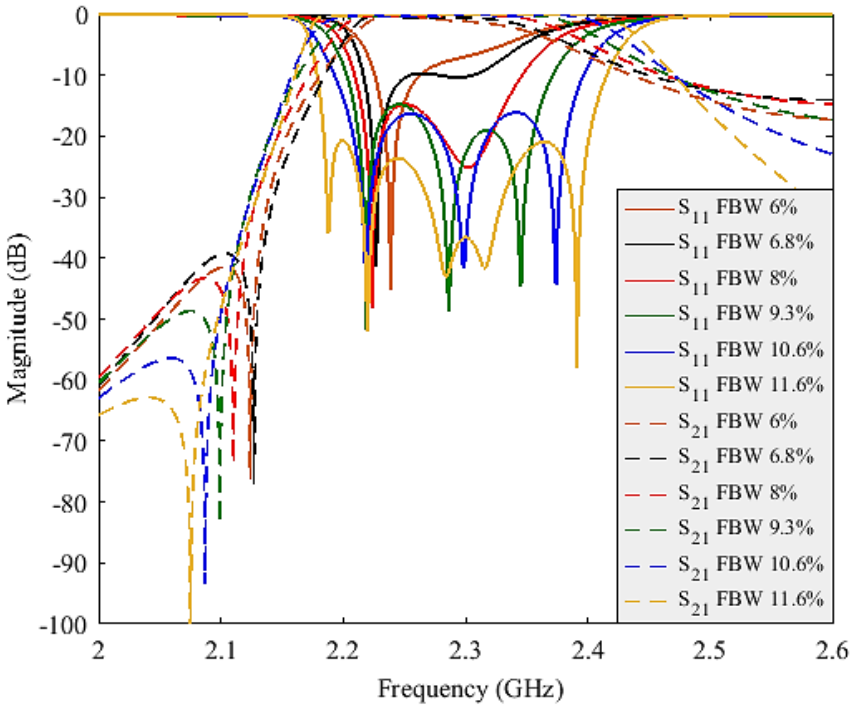

Figure 5.25 CST results for the 5th order filter with FBW of 11.6% and the 3rd order tunable filter with FBW tuning range from 6% to 10.6%

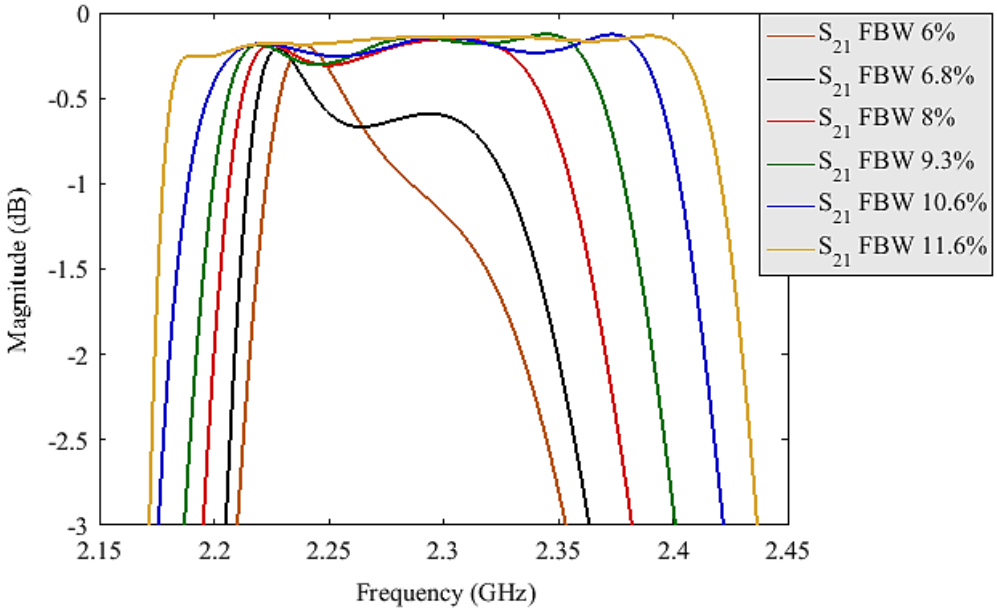

Figure 5.26 The CST results of Passband insertion loss

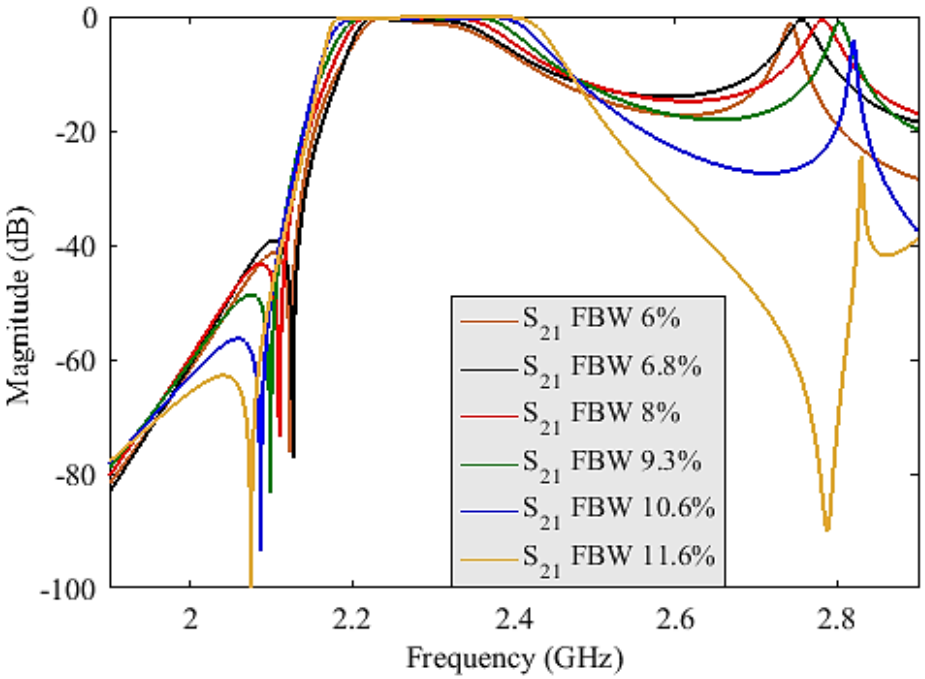

Figure 5.27 The simulated filter passband response and resonance at 2.5 GHz

Table 5.5 CST results for FBWs and corresponding parameters

Filter Order	3dB FBWs	$\theta_1 = \theta_3$	$\theta_s = \theta_L$	Centre Freq. (GHz)	Max. S_{11} (dB)
3rd Order Responses	6%	20°	11°	2.287	-7
	6.4%	30°	19°	2.289	-14.9
	6.8%	40°	26°	2.290	-10
	7.5 %	50°	32°	2.293	-16.2
	8 %	70°	45°	2.294	-15.1
	9.3%	60°	57°	2.295	-15
	10%	70°	63°	2.296	-15.7
	10.6%	80°	76°	2.297	-16.8
5th Order Response	11.6%	102°	112°	2.3	-20.6

5.7.2 Fabrication and Measurements

The fabricated tunable filter without lid is shown in Figure 5.28. The Dielectric-SRRs are rotated manually, and the angles of rotation are determined by markers on the lid and pointers in the Teflon rods, as shown in Figure 5.29. The pointers are rotated with rods and are used to point out the rotation angles of resonators.

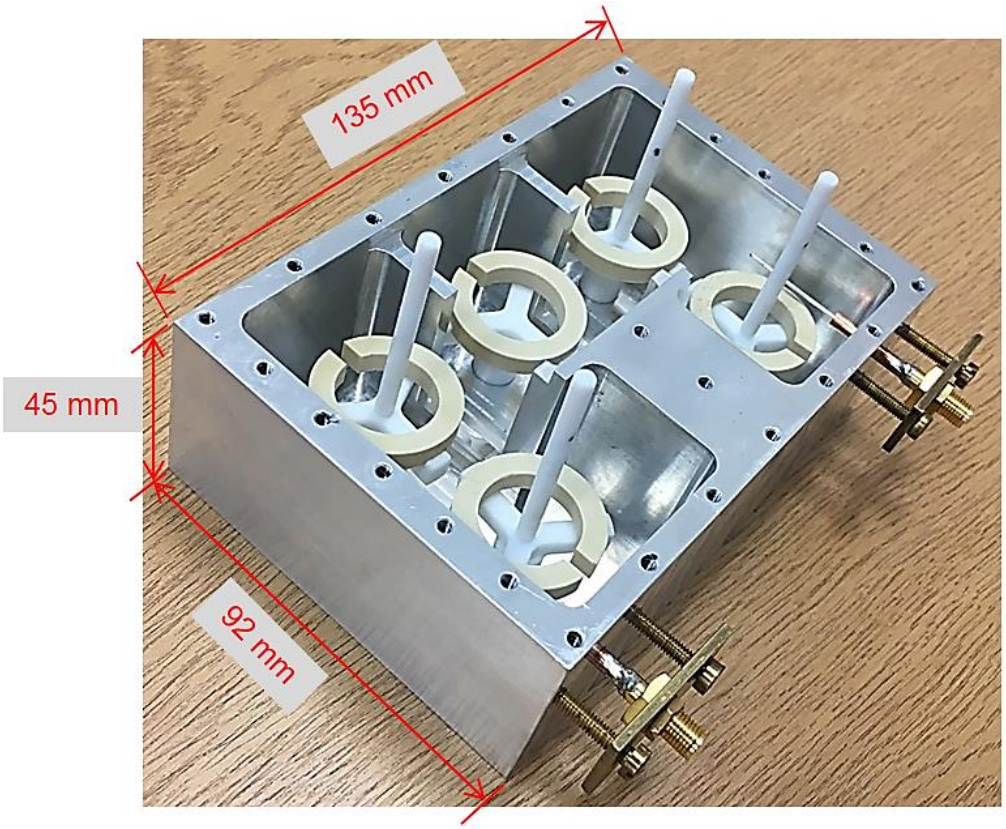

Figure 5.28 The fabricated 5th order filter and 3rd order tunable filter without lid

The measured results, shown in Figure 5.30, are 13.2% 3dB FBW at 2.3 GHz for the 5th order filter and FBW tuning range from 7.6% to 12.3%, for the 3rd order filter. Figure 5.31 shows that the mid-band insertion loss is between 2dB and 0.3dB.

The measured tuning range is close to the simulation results. However, the FBWs values are much higher than the simulation results. This difference occurred due to in measurement as the Dielectric-SRRs are rotated by hand, and it is too difficult to keep the rotation angles $\theta_1=\theta_3$ and $\theta_S=\theta_L$ manually. The measured insertion loss has good agreement with the simulation results. Table 5.6 shows measured FBW of the 5th order response and FBWs selected from the continuous tuning range of the 3rd order responses with the corresponding parameters.

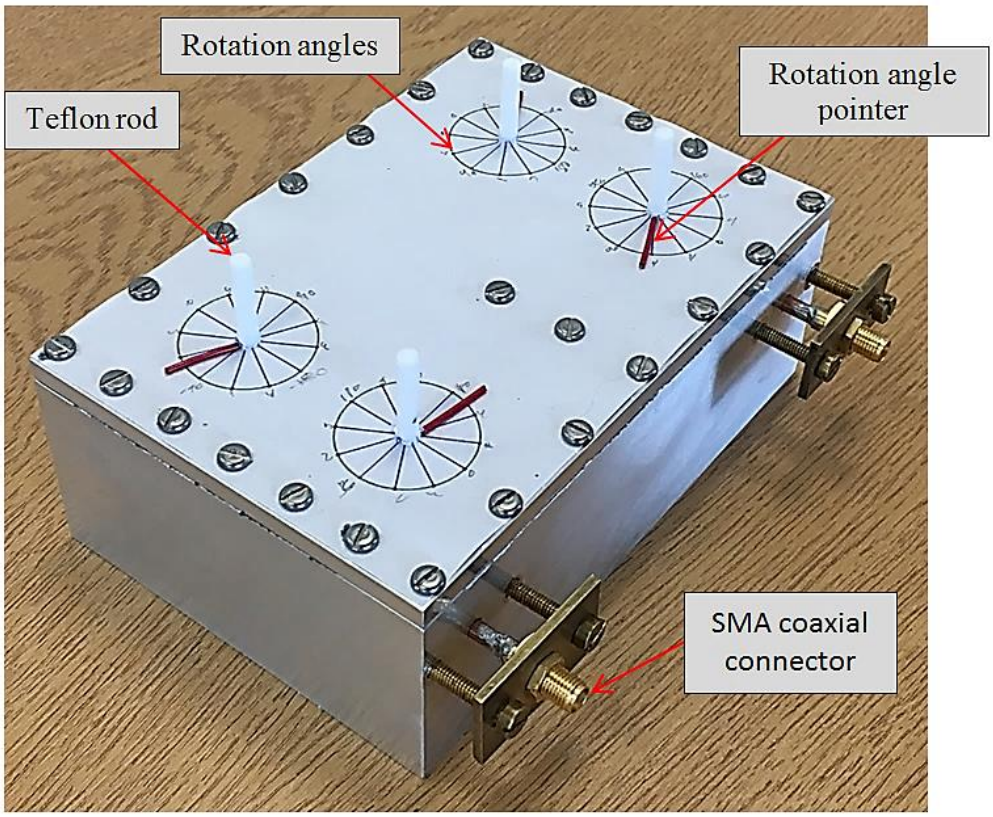

Figure 5.29 Fabricated filter (with lid)

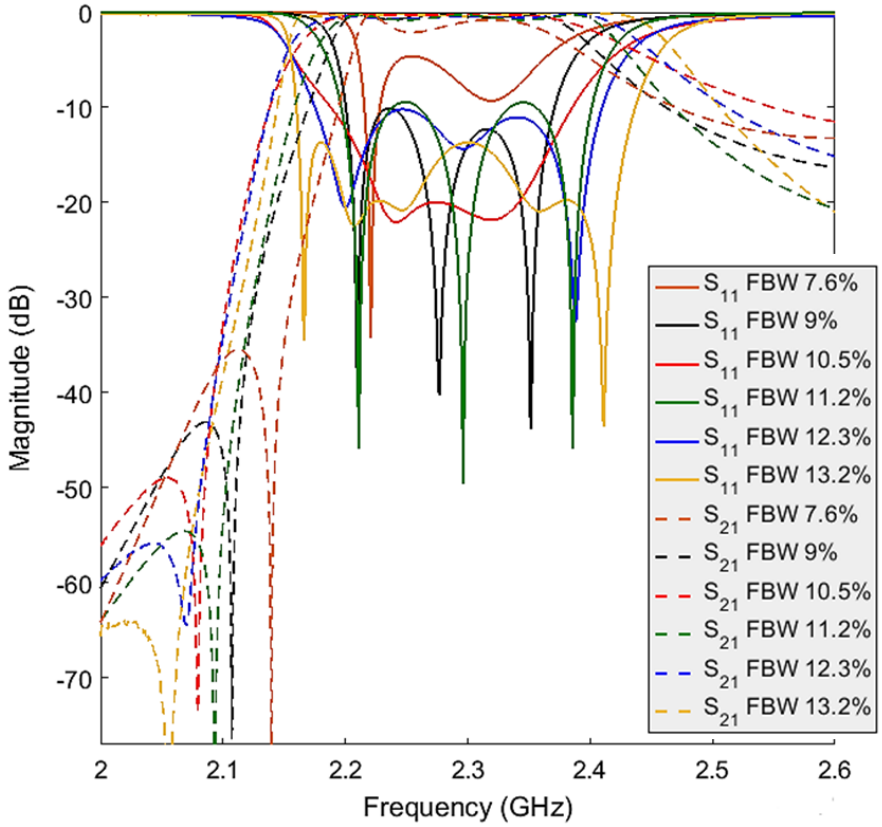

Figure 5.30 The measured results for the 5th order filter with FBW of 13.2% and the 3rd order tunable filter with FBW tuning range from 7.6% to 12.3%

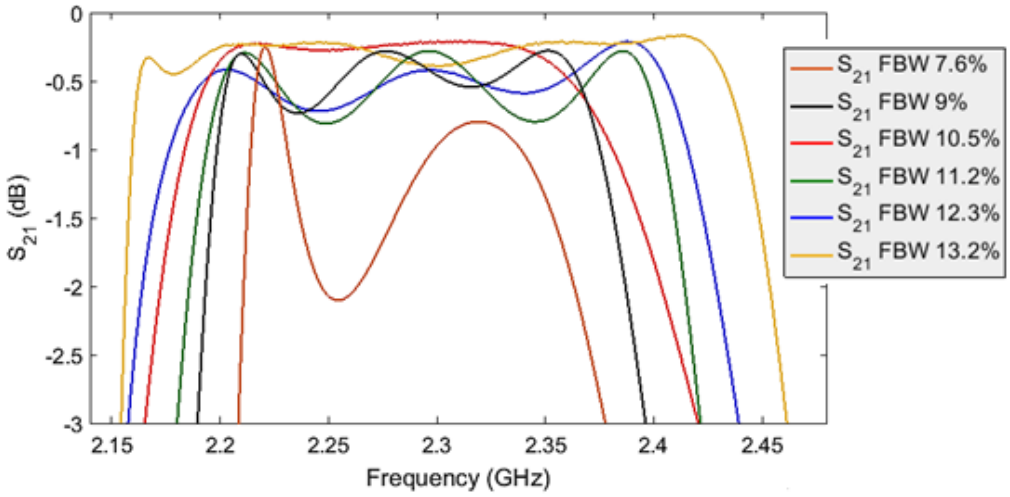

Figure 5.31 The measured results of passband insertion loss

Table 5.6 The measured results for FBWs and corresponding parameters

Filter order	3dB FBWs	$\theta_1 = \theta_3$	$\theta_s = \theta_L$	Centre Freq. (GHz)	Max. S_{11} (dB)
3rd Order Tunable Filter	7.6%	5°	8°	2.294	-4.5
	8%	15°	17°	2.290	-13.9
	9%	25°	25°	2.293	-9.8
	9.7 %	40°	38°	2.296	-13.4
	10.5%	55°	43°	2.301	-19.8
	11.2%	60°	50°	2.294	-9.2
	11.8%	75°	61°	2.297	-15.3
	12.3%	90°	78°	2.299	-10.4
5th Order Filter	13.2%	114°	108°	2.3	-14.1

The FBW tuning range, as given in Table 5.6, is limited by the maximum tuning range of K_c and Q_e. As a result, increasing the BW tunability requires increasing the tuning ranges of the internal and external couplings. The tunable filter, in general, has a high return loss, as given in Figures 5.25 and 5.30, which is a result of the CST optimiser not being able to be used for the entire BW tuning range. This shortcoming of high return loss can be controlled by using tuning screws, but this leads to an increase in the time and the complexity of the BW tuning process.

As given in Figure 5.25, the tuned responses of the filter have a spurious response close to filter centre frequency by about 500 MHz. This resonance frequency is the first higher order of the Dielectric-SRR and led to deterioration of the filter stopband performance. This poor performance of the filter stopband can be improved by using Dielectric-SRRs and Metal-SRRs in the tunable filter. This is because the separation between the fundamental mode and first higher order mode for the Metal-SRRs is about 1600 MHz [24]. Also, the tunable filter can be designed by using only Metal-SRRs to achieve much better spurious performance, but this leads to increased filter insertion loss due to the Metal-SRRs Q_u being three times lower than the Dielectric-SRRs Q_u, as given in Chapter 3.

The measured insertion loss of the tunable filter based on Dielectric-SRRs is varied between 0.3 dB to 0.8 dB, as shown in Figure 5.31. The insertion loss being higher than 0.3 dB is mostly due to the high return loss, so better insertion loss can be achieved by correcting the high return loss. However, this tunable filter still has relatively low insertion loss due to using the high Q_u resonators and tuning the BW without using tuning elements, such as tuning disks and varactor diodes. In general, the drawbacks of this tunable filter are a high return loss with the most tuned BWs, poor spurious performance, and the slow speed of the mechanical tuning.

5.8 Summery

This chapter presented a new type of tunable filter designed based on the Dielectric-SRRs. This filter was utilised to tune the filter bandwidth by rotating the Dielectric-SRRs and without adding tuning elements, such as disks or varactor diodes.

Three different designs are presented for this type of bandwidth tunable filter. The 1st and 2nd designs are only simulated, but the 3rd filter design is simulated and measured. The first tunable filter was a 3rd order Chebyshev filter and was designed to tune the response bandwidth by rotating the Dielectric-SRRs and varying the length of external feeding probes. This filter has achieved an FBW tuning range from 6.8% to 8.4% at 2.2 GHz. It possesses a limited tuning range due to the frequency shift when varying the length of external feeding probes.

The second filter was a 3rd order Chebyshev filter and was designed with two extra Dielectric-SRRs (RS and RL) to tune the external coupling (Q_e) instead of varying the length of feeding probes. By this tuning method, the filter achieved a higher FBW tuning range from 4% to 7.8% at 2.2 GHz.

The third design was a 5th order Chebyshev filter and designed with 5 Dielectric-SRRs, By rotating these resonators, this filter achieved 3rd order responses with tunable bandwidth, just as the second filter design. The filter bandwidth of the 5th order response was chosen to be higher than the bandwidth tuning range of 3rd order responses in order to increase the filter bandwidth tuning range. In simulation, this tunable filter achieved an FBW from 6% to 11.6% at 2.3 GHz and, in measurement, achieved an FBW from 7.6% to 13.2% at 2.3 GHz. The differences between simulation and measurement results were due to the Dielectric-SRRs being rotated by hand. As a result, it is too difficult to keep a symmetric configuration producing the same coupling values manually.

References:

[1] J.-S. G. Hong and M. J. Lancaster, *Microstrip Filters for RF/Microwave Applications*. New York, NY, USA: Wiley, 2011.

[2] R. Gomez-Garcia, M. A. Sanchez-Soriano, K. W. Tam and Q. Xue, "Flexible Filters: Reconfigurable-Bandwidth Bandpass Planar Filters with Ultralarge Tuning Ratio," *IEEE Microw. Mag.*, vol. 15, no. 5, pp. 43-54, July-Aug. 2014.

[3] P. W. Wong and I. Hunter, "Electronically Tunable Filters," *IEEE Microw. Mag.*, vol. 10, no. 6, pp. 46-54, Oct. 2009.

[4] C. Lugo, and J. Papapolymerou, "Single switch reconfigurable bandpass filter with variable bandwidth using a dual-mode triangular patch resonator," *IEEE MTT-S Int. Microw. Symp. Dig*., 2005, pp. 779–782.

[5] R. R. Mansour, F. Huang, S. Fouladi, W. D. Yan and M. Nasr, "High-Q Tunable Filters: Challenges and Potential," *IEEE Microw. Mag.*, vol. 15, no. 5, pp. 70-82, July-Aug. 2014.

[6] S. B. Cohn, "Microwave Bandpass Filters Containing High-Q Dielectric Resonators," *IEEE Trans. Microw. Theory and Tech.*, vol. 16, no. 4, pp. 218-227, Apr 1968.

[7] S. Fouladi, F. Huang, W. D. Yan and R. R. Mansour, "High-Q Narrowband Tunable Combline Bandpass Filters Using MEMS Capacitor Banks and Piezomotors," *IEEE Trans. Microw. Theory and Tech.*, vol. 61, no. 1, pp. 393-402, Jan. 2013.

[8] R. V. Snyder, "A wide-band tunable filter technique based on double-diplexing and low-Q tuning elements," *IEEE MTT-S Int. Microw. Symp. Dig*., June 2000, vol. 3, pp. 1759–1762.

[9] B. Yassini, M. Yu and B. Keats, "A Ka-Band Fully Tunable Cavity Filter," *IEEE Trans. Microw. Theory and Tech.*, vol. 60, no. 12, pp. 4002-4012, Dec. 2012.

[10] B. Yassini, M. Yu, D. Smith and S. Kellett, "A Ku-Band High-Q Tunable Filter with Stable Tuning Response," *IEEE Trans. Microw. Theory and Tech.*, vol. 57, no. 12, pp. 2948-2957, Dec. 2009.

[11] S. Kurudere and V. B. Erturk, "Novel Microstrip Fed Mechanically Tunable Combline Cavity Filter," *IEEE Microw. and Wireless Compon. Lett.*, vol. 23, no. 11, pp. 578-580, Nov. 2013.

[12] P. W. Wong and I. C. Hunter, "A New Class of Low-Loss High-Linearity Electronically Reconfigurable Microwave Filter," *IEEE Trans. Microw. Theory and Tech.*, vol. 56, no. 8, pp. 1945-1953, Aug. 2008.

[13] A. I. Abunjaileh and I. C. Hunter, "Tunable Bandpass and Bandstop Filters Based on Dual-Band Combline Structures," *IEEE Trans. Microw. Theory and Tech.*, vol. 58, no. 12, pp. 3710-3719, Dec. 2010.

[14] G. M. Rebeiz, K. Entesari, I. C. Reines, *et al*, “Tuning in to RF MEMS,” *IEEE Microw. Mag*., vol. 10, no. 5, pp. 55–72, Oct. 2009.

[15] X. G. Wang, Y. H. Cho and S. W. Yun, "A Tunable Combline Bandpass Filter Loaded With Series Resonator," *IEEE Trans. Microw. Theory and Tech.*, vol. 60, no. 6, pp. 1569-1576, June 2012.

[16] Y. C. Chiou and G. M. Rebeiz, "A Quasi Elliptic Function 1.75–2.25 GHz 3-Pole Bandpass Filter With Bandwidth Control," *IEEE Trans. Microw. Theory and Tech.*, vol. 60, no. 2, pp. 244-249, Feb. 2012.

[17] A. Anand and X. Liu, "Reconfigurable Planar Capacitive Coupling in Substrate-Integrated Coaxial-Cavity Filters," *IEEE Trans. Microw. Theory and Tech.*, vol. 64, no. 8, pp. 2548-2560, Aug. 2016.

[18] A. Anand and X. Liu, “Substrate-integrated coaxial-cavity filter with tunable center frequency and reconfigurable bandwidth,” in *Proc. IEEE 15th Annu. Wireless Microw. Technol. Conf. (WAMICON)*, Jun. 2014, pp. 1–4

[19] C. Arnod, J. Parlebas and T. Zwick, "Center frequency and bandwidth tunable waveguide bandpass filter with transmission zeros," in *proc. Eur. Microw. Inter. Circuits Conf.*, 2015, pp. 1220-1223

[20] C. Wang and K. A. Zaki, "Dielectric resonators and filters," *IEEE Microw. Mag.*, vol. 8, no. 5, pp. 115-127, Oct. 2007.

[21] C. Wang, K. A. Zaki, A. E. Atia and T. G. Dolan, "Dielectric combline resonators and filters," *IEEE Trans. Microw. Theory and Tech.*, vol. 46, no. 12, pp. 2501-2506, Dec 1998.

[22] J. B. Thomas, “Cross-coupling in coaxial cavity filters-a tutorial overview,” *IEEE Trans. Microw. Theory Tech*., vol. 51, no. 10, pp. 1368–1376, Apr. 2003.

[23] D. M. Pozar, *Microwave Engineering*. 4th ed. Hoboken, NJ, USA: Wiley, 2012.

[24] A. S. Noori, X. Shang, C. Guo, T. J. Jackson, P. A. Smith and M. J. Lancaster, “Microwave filters based on novel dielectric split-ring resonators with high unloaded quality factors,” *IET Microw., Antennas & Propag.*, vol. 12, no. 8, pp. 1389-1394, July, 2018.

Chapter 6 Conclusion

6.1 Conclusion

The novelties presented in this thesis can be grouped into two categories: (i) Dielectric-SRRs with high Q_u; (ii) tunable and non-tunable filters with low insertion loss combined with the use of Dielectric-SRRs.

A new type of microwave resonator with high Q_u, called Dielectric-SRR, is presented in Chapter 3. This new resonator is made from high constant dielectric with a shape similar to the conventional Metal-SRR. The new Dielectric-SRR achieved EM field distributions similar to the EM distributions of the conventional Metal-SRR. The advantage of these EM field distributions is that most electric fields are stored outside the Dielectric-SRR which leads to the reduction of electric loss due to the loss tangent while most electric fields with conventional DRs are stored inside the dielectric material. The shortcoming with the EM field distributions of Dialectic-SRR is an increased electric loss within the resonator holder. This problem is solved by using a new holder with Y configuration instead of the conventional cylindrical holder. The Q_u of Dielectric-SRR is increased by 50% with the holder of Y configuration as a result of the Teflon material of this holder being eliminated from the resonator gap where the most electric fields are stored.

The Dielectric-SRRs have Q_u three times higher than the Metal-SRR and two times higher than the conventional CDR. While the separation between the fundamental mode

and the first higher order mode for the Dielectric-SRR is about 820 MHz, the CDR is about 600 MHz and the Metal-SRR is about 1600 MHz.

The Dielectric-SRR is compared to the conventional Metal-SRR Q_u because both resonators have a similar shape and EM fields distributions. It is also compared to the conventional CDR because both resonators have the same dielectric material.

The EM field distributions of the Dielectric-SRRs, on the other hand, are useful to tune the coupling coefficients between two adjacent Dielectric-SRRs by rotating these resonators. Therefore, these new Dielectric-SRRs are utilised to design a new BW tunable filter, as discussed in Chapter 5. The adjacent Dielectric-SRRs of this filter are rotated to tune the internal and external couplings, thereby tuning the filter BW. This tunable filter achieved FBW tuning range from 6% to 11.6% at 2.3 GHz in the simulations and from 7.6% to 13.2% at 2.3 GHz in the measurements. This difference between the simulations and measurements is due to the Dielectric-SRRs are rotated by hand. As a result, it is too difficult to keep a symmetric configuration maintaining the same rotation angles as simulations manually. Several ideas are suggested in the next section of the future work for increasing the filter BW tuning range as well as for rotating the filter resonators more accurately in the measurements.

On the other hand the tunable filter by rotating the Dielectric-SRRs had a high return loss in most tuned BWs. This shortcoming can be solved by using tuning screws to adjust the degradation in the return loss, but this leads to the consumption of more time for the BW tuning and a slight increase in the insertion loss.

The tunable filters usually use tuning elements to tune the filter centre frequency and BW. The most common tuning elements in the published papers are the varactor diodes and the tuning disks [1, 2]. Table 6.1 shows the performance of the tunable filter by rotating the Dielectric-SRRs and tunable filters using varactor diodes and tuning disks, as given in Chapter 5.

Table 6.1 Performance for different types of tunable filters

Filter Type	Number of Resonators	Tuning Method	BW Tuning Range (MHz)	f_o Tuning Range (GHz)	Passband S_{21} (dB)	Ref.
Microstrip Filter	3	Varactor Diodes	70-100 at 2.25 GHz	1.75-2.25	5	[14]
Substrate Filter	2	Varactor Diodes	20-100 at 1.13 GHz	0.55-1.13	1.1-6	[15]
DR Filter	7	Tuning Disks	5-20 at 1.95 GHz	1.93-1.96	1	[2]
Waveguide Filter	4	Tuning Disks	36-72 at 20 GHz	19.7-20.2	1.2	[16]
Dielectric-SRR Filter	5	Rotating Resonators	174-300 at 2.3 GHz	––	0.6	This thesis, Chapter 5

As shown in Table 6.1, the insertion loss is relatively high for the tunable filters using varactor diodes and tuning disks. While the tunable filter with Dielectric-SRRs has an insertion loss relatively low. This is because the filter BW is tuned only by rotating the filter resonators and without using the lossy tuning elements, such as varactor diodes and tuning disks. The drawback with the tuning method by rotating the filter resonators is the slow speed of the mechanical tuning compared to the fast tuning speed by using varactor diodes. However, BW tuning by rotating only the filter resonators without using tuners like diodes/disks can maintain the Q_u of resonators and, thereby, lower the insertion loss for the tunable filter.

Besides the tunable filter, a new class of non-tunable filter with two different configurations are presented in Chapter 4. These two filters are designed based on the new Dielectric-SRRs. The first filter is a 3rd order Chebyshev filter, and the second is a 4th order filter with two symmetric transmission zeros. The technique of synthesising an $n \times n$ coupling matrix for bandpass filters, as presented in Chapter 2, is utilised to determine the design parameters ($M_{i,i+1}$ and Q_{en}) and the S-parameters of the filters. Both filters achieved a low insertion loss of about 0.3 dB and a return loss greater than 20 dB. The measurements of both filters show a small frequency shift of about 12 MHz and a BW larger than that in simulations by 12 MHz for the 3rd order filter and 20 MHz for 4th order filter. Tuning screws are not used to correct this small frequency shift because the measured filters, in general, have acceptable performance (S_{11}=20 dB and S_{21}=0.3 dB). The insertion loss of these Dielectric-SRR filters (0.3 dB) is much lower than the insertion loss of the Metal-SRR filters (1dB) [3] and similar or slightly lower than the insertion loss of the conventional DR filters [4].

6.2 Future Work

The conventional Metal-SRRs are commonly used in the microwave sensors [5-10], by using the new high Q_u Dielectric-SRRs instead of the conventional Metal-SRRs sensors can be designed with improved performance. The Dielectric-SRRs also can be utilised to design microwave devices such as diplexers, multiplexers, and antenna [11-13].

The tunable filter as presented in Chapter 5 can employ tuning elements to tune the filter centre frequency in addition the BW tuning, but this way present more loss from tuners. The BW tuning method of rotating resonators as presented in this thesis can be

implemented by using another type of resonators in order to increase the BW tuning range, for example using squared-shaped or elliptical-shaped ring resonators. On the other hand, the filter BW can be tuned more accurately by a setup with electric stepper motors to rotate the Dielectric-SRRs; also this can tune the filter automatically by using programmed microprocessor with the electric motors. Moreover by using programmable electric motors the design of tunable filters with complex motion of the resonators in order to increase the filters flexibility. For example moving the Dielectric-SRR up and down as well as rotating the resonators as show in Figure 6.1a, or rotate the Dielectric-SRR with 2 rotation angles as shown in Figure 6.1b.

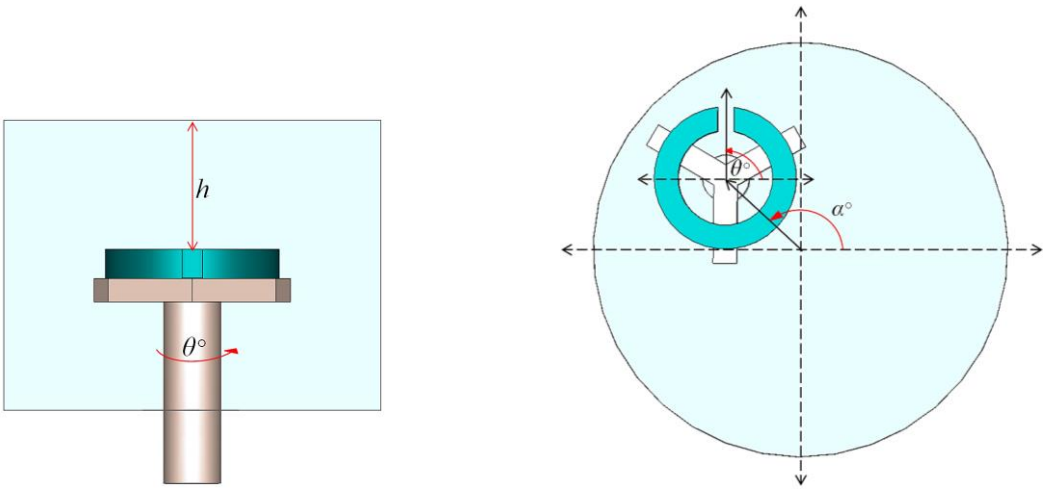

(a) (b)

Figure 6.1 Two Models show the directions of moving the Dielectric-SRR inside cylindrical cavity (a) moving the resonator with 2 directions h and $\theta°$, and (b) rotating the resonator with 2 angles $\theta°$ and $\alpha°$

Reference

[1] R. R. Mansour, F. Huang, S. Fouladi, W. D. Yan and M. Nasr, "High-Q Tunable Filters: Challenges and Potential," *IEEE Microw. Mag.*, vol. 15, no. 5, pp. 70-82, July-Aug. 2014.

[2] R. R. Mansour, "High-Q tunable dielectric resonator filters," *IEEE Microw. Mag.*, vol. 10, no. 6, pp. 84-98, Oct. 2009.

[3] R. F. Mostafavi, D. Mirshekar-Syahkal and Y. C. M. Lim, "Small filters based on slotted cylindrical-ring resonators," *IEEE Trans. Microw. Theory and Tech.*, vol. 49, no. 12, pp. 2369-2375, Dec. 2001.

[4] C. Wang and K. A. Zaki, "Dielectric resonators and filters," *IEEE Microw. Mag.*, vol. 8, no. 5, pp. 115-127, Oct. 2007.

[5] H. Choi, J. Naylon. S. Luzio, *et al*, “Design and In Vitro Interference Test of Microwave Noninvasive Blood Glucose Monitoring Sensor," *IEEE Trans. Microw. Theory and Tech.*, vol. 63, no. 10, pp. 3016-3025, Oct. 2015.

[6] D. J. Rowe, S. al-Malki, A. A. Abduljabar, A. Porch, D. A. Barrow and C. J. Allender, "Improved Split-Ring Resonator for Microfluidic Sensing," *IEEE Trans. Microw. Theory and Tech.*, vol. 62, no. 3, pp. 689-699, Mar. 2014.

[7] A. Masood, O. Castell, D. Barrow, and A. Porch, ”Split ring resonator technique for compositional analysis of solvents in microcapillary systems,” in *Proc. Int. Conf. MicroTAS*, San Diego, USA, Oct. 2008, pp.1636-1638.

[8] M. Violetti, M. Pellaton, C. Affolderbach, *et al*., "The Microloop-Gap Resonator: A Novel Miniaturized Microwave Cavity for Double-Resonance Rubidium Atomic Clocks," *IEEE Sensors Journal*, vol. 14, no. 9, pp. 3193-3200, Sept. 2014.

[9] Y. Sakamoto, H. Hirata and M. Ono, "Design of a multicoupled loop-gap resonator used for pulsed electron paramagnetic resonance measurements," *IEEE Trans. Microw. Theory and Tech.*, vol. 43, no. 8, pp. 1840-1847, Aug. 1995.

[10] J. S. Bobowski, “Using split-ring resonators to measure the electromagnetic properties of materials: An experiment for senior physics undergraduates,” *Amer. J. Phys.*, vol. 81, no. 12, pp. 899–906, Dec. 2013.

[11] Z. C. Zhang, Q. Chu, S. Wong, *et al*., "Triple-Mode Dielectric-Loaded Cylindrical Cavity Diplexer Using Novel Packaging Technique for LTE Base-Station Applications," *IEEE Trans. Compon, Packag., Manuf. Technol.*, vol. 6, no. 3, pp. 383-389, Mar. 2016.

[12] V. Singh, K. S. Parikh, S. Singh and R. B. Bavaria, "DR OMUX for Satellite Communications: A Complete Step-by-Step Design Procedure for the C-Band Dielectric Resonator Output Multiplexer," *IEEE Microw. Mag.*, vol. 14, no. 6, pp. 104-118, Sept.-Oct. 2013.

[13] R. Tian, V. Plicanic, B. K. Lau and Z. Ying, "A Compact Six-Port Dielectric Resonator Antenna Array: MIMO Channel Measurements and Performance Analysis," *IEEE Trans. Antennas and Propag.*, vol. 58, no. 4, pp. 1369-1379, April 2010.

[14] Y. C. Chiou and G. M. Rebeiz, "A Quasi Elliptic Function 1.75–2.25 GHz 3-Pole Bandpass Filter With Bandwidth Control," *IEEE Trans. Microw. Theory and Tech.*, vol. 60, no. 2, pp. 244-249, Feb. 2012.

[15] A. Anand and X. Liu, "Substrate-integrated coaxial-cavity filter with tunable center frequency and reconfigurable bandwidth," in *Proc. IEEE 15th Annu. Wireless Microw. Technol. Conf. (WAMICON)*, Jun. 2014, pp. 1–4

[16] C. Arnod, J. Parlebas and T. Zwick, "Center frequency and bandwidth tunable waveguide bandpass filter with transmission zeros," in *proc. Eur. Microw. Inter. Circuits Conf.*, 2015, pp. 1220-1223

Appendix I Publication

A. Noori, X. Shang, C. Guo, T. Jackson, P. Smith, M. J. Lancaster, “Microwave Filters Based on Novel Dielectric Split Ring Resonators with High Unloaded Quality Factors” IET Microwaves, Antennas & Propagation.

This research paper accepted on 16/2/2018

Microwave Filters Based on Novel Dielectric Split Ring Resonators with High Unloaded Quality Factors

Ahmed S. Noori*, Xiaobang Shang, Cheng Guo, Timothy J. Jackson, Paul A. Smith, Michael J. Lancaster

School of Electrical, Electronic and Systems Engineering, University of Birmingham, Edgbaston, Birmingham B15 2TT, UK

Abstract: Here we present a new type of split ring resonator constructed from high dielectric constant material. Compared to conventional metal split ring resonators, such resonators have significantly higher unloaded quality factor (Q_u). A new class of microwave filter is presented using the dielectric split ring resonator. Two examples of different filter configurations are investigated, and the measured results show excellent performance. Good agreement between measurements and simulations has been achieved.

1. Introduction

Filters formed of resonators with high unloaded quality factor (Q_u) are in demand for applications with stringent requirements on insertion loss, this includes satellite systems and wireless base stations [1-4] as well as many others. Dielectric Resonators (DRs) are a popular choice for such applications [1-8]. Another common high Q_u resonator is the metal or less common dielectric combline resonator, the latter has a Q_u as high as DRs (≈10,000 at S band and ε_r=36) [1, 9]. The electromagnetic field distributions and filter configuration for this dielectric combline is approximately the same as the conventional metal combline resonator provided the dielectric constant is high [9-12].

Another type of resonator is the metal Split Ring Resonator (SRR) with Q_u of about 4000 at S band manufactured with copper material [13-15]. This resonator is a hollow cylindrical ring with a longitudinal gap as shown in Fig 1. Cavity filters based on Metal-SRR are rarely reported [13, 14], but the Metal-SRRs used more with the microwave sensors [16-21].

This paper investigates a SRR but with the metal replaced by a high permittivity dielectric. Such Dielectric-SRRs have similar electromagnetic field distributions as the Metal-SRR, but importantly they have a higher Q_u if made of a low loss dielectric material. The higher Q_u is due to the removal of the conduction current on the surface of the Metal-SSR where most of the losses conventionally occur. Because these ohmic losses are removed, the main contribution to the loss in the Dielectric-SRR is loss tangent of the dielectric material forming the resonator [9, 22].

The Q_u of the Dielectric-SRR can be even higher than the Q_u of DRs with the same ε_r and loss tangent. This is because with DRs most of the energy is stored inside the DR [1, 22] which presents losses due to the loss tangent of dielectric material. In the case of Dielectric-SRR most of the energy is stored outside the dielectric material which reduces the effect of the loss tangent.

This paper looks at filters where the Dielectric-SSRs are all in the same plane, alternatives have been investigated for Metal-SRRs where they are placed on top of each other in a cylindrical housing [13, 14]. The advantage of a planer configuration is it can easily achieve only electric or magnetic coupling between two adjacent resonators. Here full wave analysis software (CST [23]) and the methodology of coupled resonator circuits [24], have been used to design new class of filter with examples of two high Q_u filters based on the novel Dielectric-SRRs.

Fig. 1. *Metal Split Ring Resonator (Metal-SRR)*

2. The Dielectric-SRR

The Dielectric-SRR and Metal-SRR have been modelled with the same dimensions as shown in Fig 2*a*. Each is mounted on Teflon holder and in a copper enclosure, as shown in Fig 2*b*. The fundamental mode field distributions have been simulated using an Eigenmode solver, and the results are shown in Fig 3. As expected most electric field is in the gap and the magnetic field peaks at the opposite side of the loop in both metal and dielectric SSRs. The fields are not high inside the dielectric material of the Dielectric-SRR.

The dielectric and metal SSR have also been made, and the measurements together with the simulation results and are summarized in Table 1 which include details of the loss tangent for the high dielectric constant materials. It can be seen in Table 1 that the Dielectric-SRR has a Q_u around 3 times higher than that of Metal-SRR in exactly the same configuration. Note the Metal-SSR has a slightly lower frequency then the Dielectric-SSR. However, simulations show that if the Metal-SSR is reduced in size to give the same frequency as the Dielectric-SSR (2.3 GHz) then the Q_u changes to 6200 still almost three times lower than the Dielectric-SSR.

The Q_u of the Dielectric-SRR shown in Fig 2 is now compared with Q_u of the disk/cylindrical Dielectric Resonator (DR) at fundamental resonance frequency of 2.3 GHz with same ε_r and loss tangent. The DR model is shown in Fig 4, with the ratio of $W/2R$ = 0.4 to achieve the best Q_u for the fundamental mode [1]. It is mounted on a Teflon holder and in a copper enclosure of 30 mm diameter and 50 mm height. Table 2 shows the CST Eigenmode simulation results for comparison between the now named Dielectric-SRR1 and the DR1.

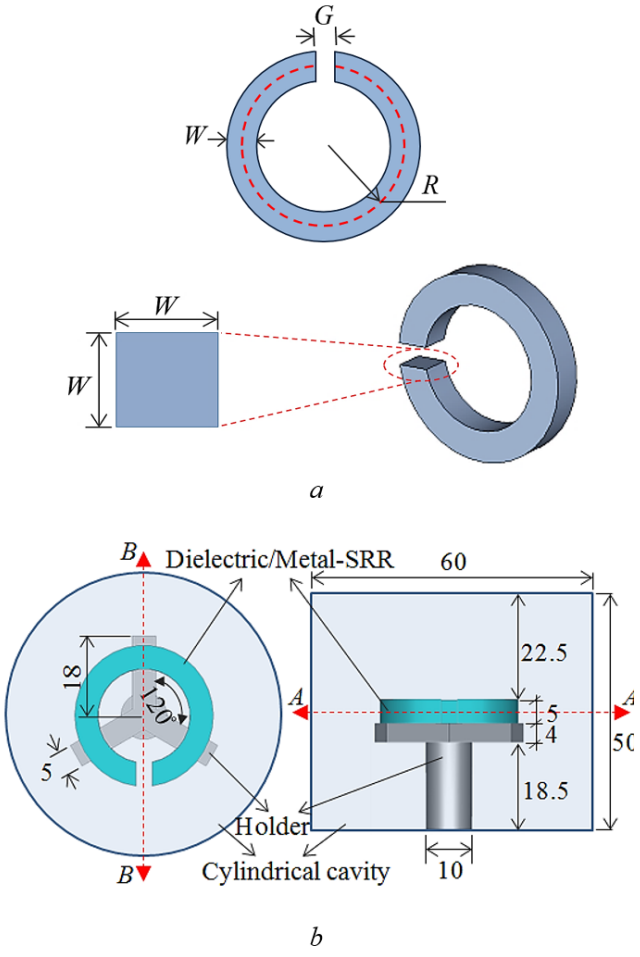

Fig. 2. *Configuration and dimensions in (mm), (a) Dielectric/Metal-SRR: G=3.5, R=12.5, and W=5, and (b) Single resonator inside metal enclosure and mounted on PTFE holder.*

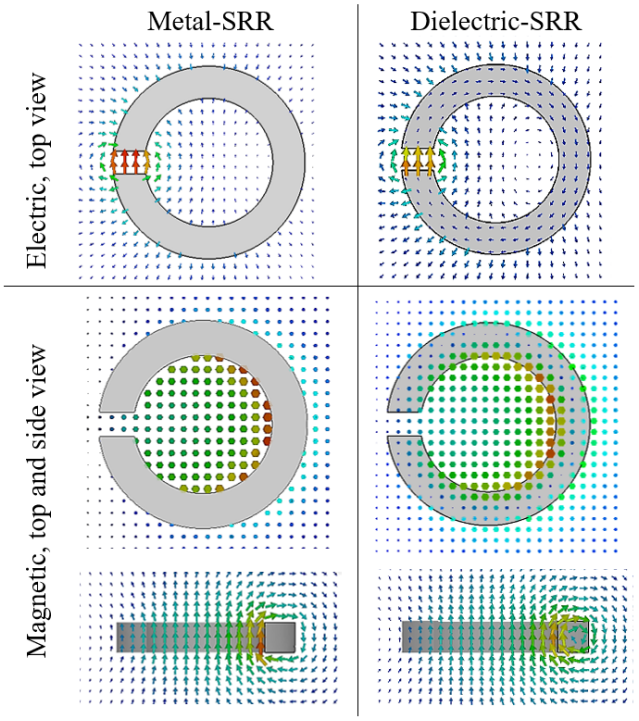

Fig. 3. *EM field distributions for Dielectric-SRR of ε_r=97 and Metal-SRR. Section AA for top view and BB for side view, see Fig. 2b*

Table 1 Q_u comparison for Dielectric-SRR and Metal-SRR. Both resonators have same dimensions as in Fig. 2

	Dielectric-SRR Titania, ε_r = 97 Tan δ = 7.2×10^{-5} at (2.3GHz)		Metal-SRR Copper σ=5.813×10^7	
	Simulated	Meas.	Simulated	Meas.
f (GHz)	2.3	2.29	1.66	1.68
Q_c cavity	122,510		124,010	
Q_c resonator			7,176	
Q_d holder	315,080		108,810	
Q_d resonator	24,502			
Q_u	19,176	17,021	6,732	4,630

Q_c: Conductive quality factor, Q_d: Dielectric quality factor

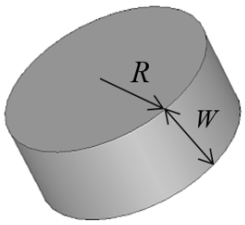

Fig. 4. *Configuration of Disk dielectric resonator DR. R is the radius and W is the height of DR*

Table 2 Eiegenmode CST simulation results for comparison between Dielectric-SRR1 and DR1.

	Titania, ε_r=97 tan δ=7.2×10^{-5} @ 2.3GHz	
	Dielectric-SRR1	DR1
Resonator size (mm)	G=3.5, R=12.5, W=5	R=7.5, W=6
f	2.3 GHz	2.3 GHz
Q_c	122,510	112,890
Q_d	22,734	14,030
Q_u	19,176	12,478

The comparison in Table 2 shows that for this particular configuration the Q_u of the Dielectric-SRR1 is 50% higher than the Q_u of DR1, but the radius of the Dielectric-SRR1 about twice that of the radius of DR1. It is the high Q_u which is of interest here and the fact that they are slightly larger than DR is of less importance.

There are other advantages of the SRR not used in the filters in this paper, this includes the ability to produce tuneable coupling by just rotation of the resonators [25] and the electromagnetic field distributions are very useful for the microwave sensors [16-21].

The dielectric constant (ε_r) of the material making the SSRs and DRs influences the amount of stored energy inside resonators. For instance, dielectric material of ε_r=97 stores more energy inside the resonator than the case when ε_r=36 [1, 6]. For this reason, the comparison between Dielectric-SRR1 and DR1 has been repeated with the same enclosure and both resonators having the commonly used ε_r of 36. This is shown in Table 3. The Eigenmode CST simulation results in Table 3 have revealed the Dielectric-SRR2 has a Q_u higher than DR2 by 30%. This percentage increase is less than the percentage increase from the comparison in Table 2, but is still significant. Again The Dielectric-SRR2 has radius about twice the radius of DR2.

Table 3 Eiegenmode CST simulation results for comparison between Dielectric-SRR2 and DR2.

	ε_r=36, tan δ=1×10^{-4} @ 4.5 GHz Material series 8300 from Trans-Tech Manufacture [1].	
	Dielectric-SRR2	DR2
Resonator size (mm)	G=1, R=12.5, W=5	R=6, W=5
f	4.5 GHz	4.5 GHz
Q_c	61,696	116,810
Q_d	15,748	10,228
Q_u	12,546	9,404

The Dielectric-SSR configuration in Fig. 2 has been used to find the effects of dimensions on the fundamental mode frequency with the results shown in Fig 5. These were all simulated with ε_r=97. The gap of Dielectric-SRR can be considered to represent a capacitor and loop represents inductor in the resonator equivalent circuit. Increasing the gap (G) (when the radius (R) and cross section (W) are fixed) decreases the capacitance leading to an increase in the resonance frequency in Fig 5*a*. The resonance frequency decreases when R increases due to an increase in the inductance loop length Fig 5*b*. The cross section (kept square in this case) has more effect on the resonance frequency than G and R because increasing W will increase the capacitor surface area, leading to decrease of the resonance frequency as shown in Fig 5*b*.

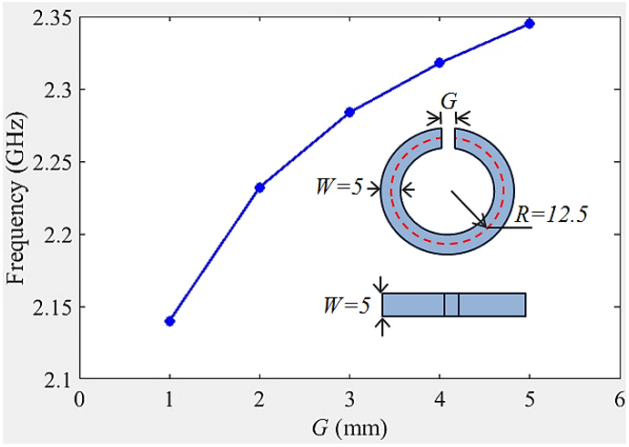

a

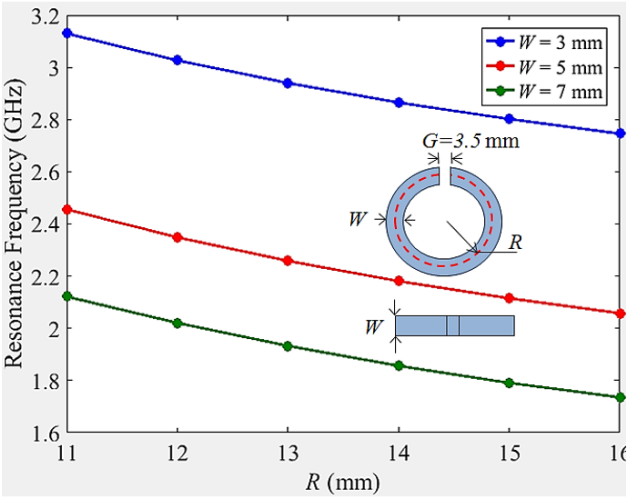

b

Fig. 5. *Fundamental resonance frequency f against Dielectric-SRR dimensions, (a) f against G, (b) f against R and W*

The effects of Dielectric-SRR dimensions, with ε_r = 97 and loss tangent of 7.2 × 10^{-5}, on the Q_u at the fundamental mode of 2.3 GHz are shown in Fig 6. The same

model shown in Fig 2 is used in the Eigenmode simulation. The metal enclosure radius is kept to twice the Dielectric-SRR radius (*R)* even when varying the *R* to decrease the enclosure effect on Q_u. The conductive quality factors due to the walls, Q_c, for all results in Fig. 6 are from 122,700 to 124,500, showing the walls have a minimal effect on the total Q_u. Here *W* is varied with three different *G* values; with *R* tuned to fix the fundamental mode at 2.3 GHz. *W* has significant effect on Q_u due to increased gap area of the Dielectric-SRR and the overall volume of resonator.

The mode separation between the fundamental mode of 2.3 GHz, and the first higher order mode against Dielectric-SRR dimensions, are shown in Fig 7. The simulation results show the best mode separation can be achieved when *W* is from about 5 to 6 mm depending upon the value of *G*.

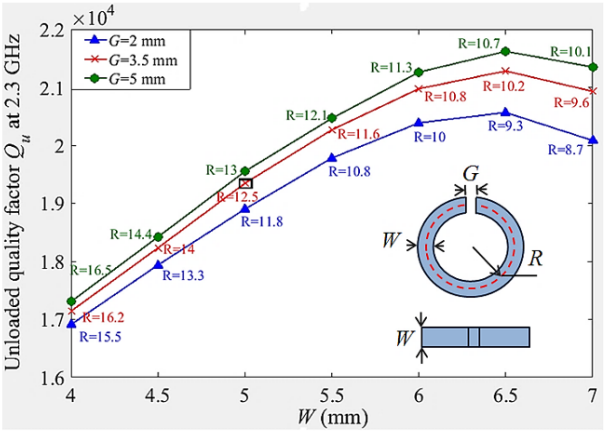

Fig. 6*. Q_u against Dielectric-SRR dimensions. The point inside a square indicates to Dielectric-SRR dimensions (G=3.5mm, R=12.5mm and W=5mm) has chosen in this paper*

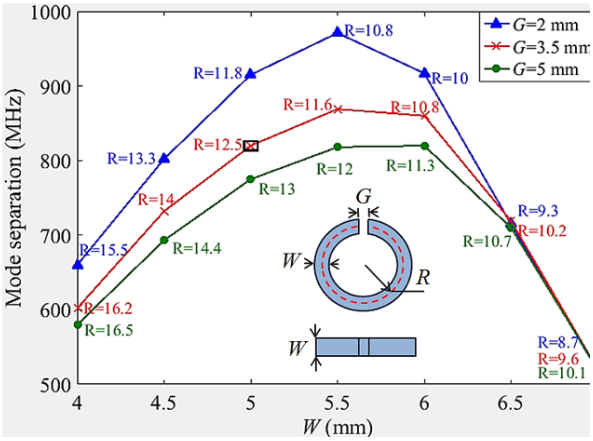

Fig. 7*. Mode separation against Dielectric-SRR dimensions. The point inside a square indicates the Dielectric-SRR dimensions (G=3.5, R=12.5 and W=5) chosen as an example in this paper*

3. Filter design

In order to design filters using the coupled resonator approach [24] we need to consider both the coupling to an external input/output transmission line and the coupling between two resonators. This is done in the following two sections followed by the full filter design.

3.1. Coupling between resonators

The Dielectric-SRRs (ε_r=97) with dimensions as shown in Fig 2*a* and holder with ε_r=2.1 with dimensions as shown in Fig 2*b* have been chosen for the filter design. Firstly, we need to extract the coupling coefficients between two adjacent Dielectric-SRRs. The published work about Metal-SRR filters considered only a coaxial configuration [13, 14]. In this paper, novel Dielectric-SRRs with a planer configuration has been examined. This introduces more flexibility in the design and can easily achieve electric coupling as well as magnetic and mixed coupling.

The coupling coefficients (K_c) are extracted by CST software for configuration when the angle θ_1 of the first resonator and angle θ_2 of the second resonator are 90°, as shown in Fig. 8*a*. On the dimensional scales shown, the K_c values are small and nearly independent of the distance *S* between resonators. This is due to both electric and magnetic couplings providing partial cancelation and the coupling can be increased by having a metal wall between Dielectric-SRRs. This is only from one side as shown by the insert in Fig. 8*b*. The K_c for configuration in Fig. 8*b* can be controlled by varying the metal wall dimensions between Dielectric-SRRs as well as the distance *S*.

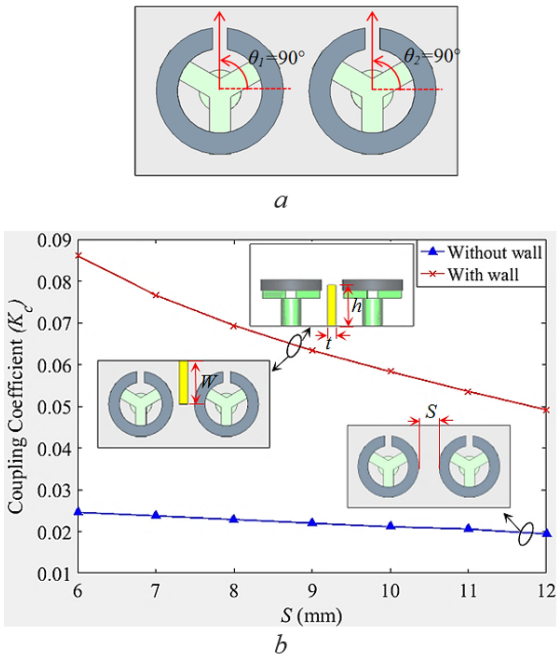

Fig. 8*. Two Dielectric-SRRs inside metal enclosure, (a) Top view with angle θ_1 and θ_2=90°, (b) K_c against distance S with and without wall. Wall dimensions: W=20mm, h=20mm, and t=4mm*

Alternatively, significant, usable values for K_c can be obtained, without the metal wall, by changing the Dielectric-SRRs angles (θ_1 and θ_2) and varying distance S as shown in Fig 9. A further configuration is shown in Fig 10, when the gaps of two adjacent Dielectric-SRRs face each other with a wall coming down from the top of the cavity housing in this case. This configuration can easily achieve electric coupling with the negative K_c values as given in Fig. 10. It should be noted there are many more possibilities for coupling the resonators, for example as a function of the rotation angle θ. However, only the coupling used in the filters have been discussed here.

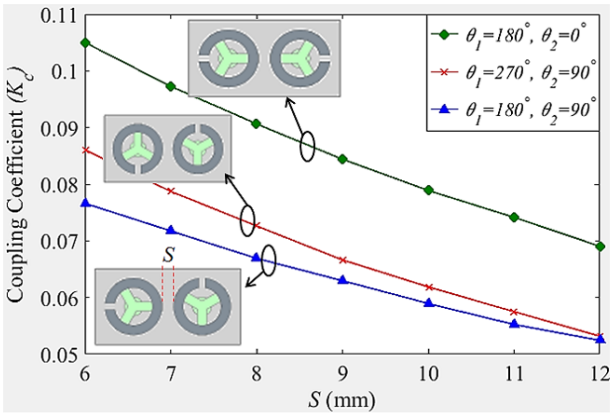

Fig. 9. *K_c of two Dielectric-SRRs against distance S for different angles*

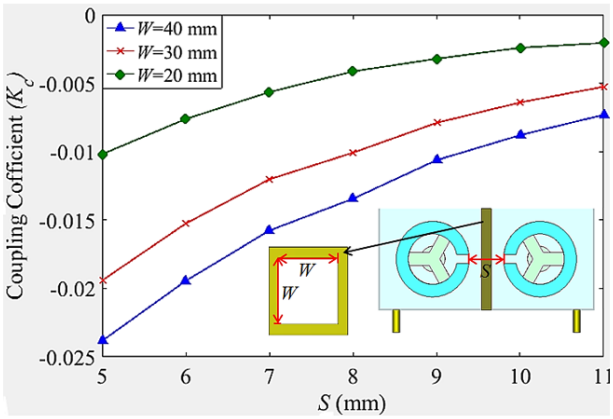

Fig. 10. *Electric K_c of two Dielectric-SRRs against distance S and aperture W*

3.2. Extraction of external quality factor

The coupling to the input and output, as defined though the external quality factor Q_e, for the Dielectric-SRRs is extracted based on method described in [24]. This coupling is achieved through a probe as shown in Fig 11*a*. The model configuration and CST simulation results for Q_e against two different probe lengths (L) and heights (H) for probe moving from the centre of Dielectric-SRR towards right are shown in Fig 11*b*.

In addition, the Q_e is extracted when moving feeding probe from Dielectric-SRR centre towards the left where the gap is located. This is shown in Fig 11*c*. There are many other possibilities of coupling to the resonator, such as the rotation angle of the resonator or the probe vertical position, but we limit the discussion to this particular structure which has been found suitable for the filters described below.

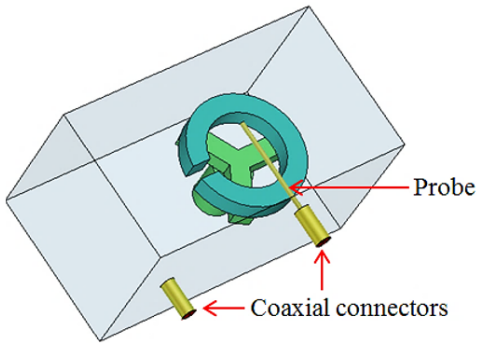

a

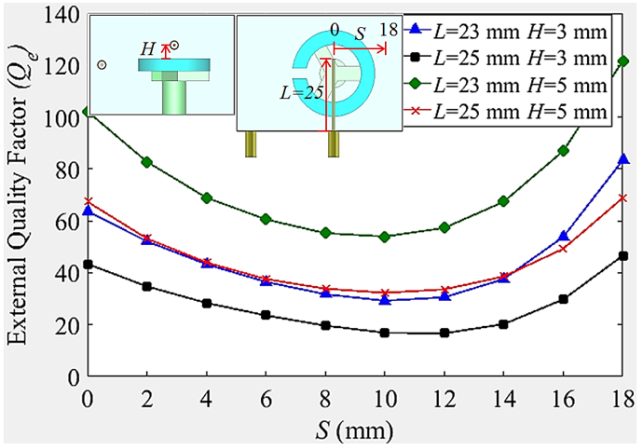

b

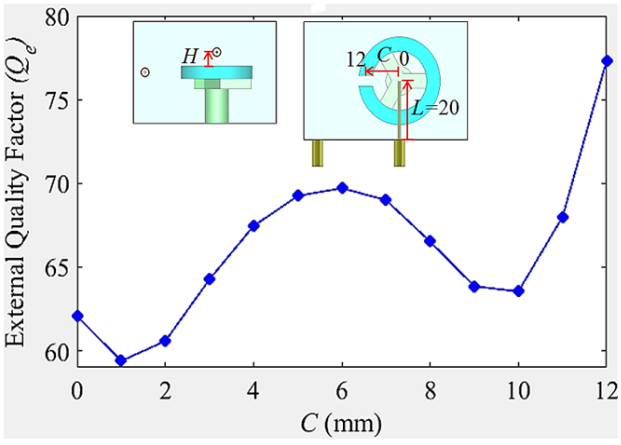

c

Fig. 11. *Simulation model and results of Q_e, (a)Single Dielectric-SRR inside metal enclosure, (b)Q_e of probe has moved from resonator centre to its loop, with different lengths (L) and heights (H), (c) Q_e of probe has moved from resonator centre to its gap with H=1mm*

3.3. Third order filter

This filter is designed to have a Chebyshev response, with a centre frequency of 2.2 GHz, fractional bandwidth (FBW) of 5% and return loss of 20 dB. The non-zero coupling coefficients of filter are calculated to be $M_{12} = M_{23} = 0.05$, and the external quality factor are $Q_{e1} = Q_{e2} = 17$ [24]. Fig 12 shows the filter configuration as well as overall dimensions and the fabricated filter. Detailed dimensions of the resonators and holders can be found in Fig 2.

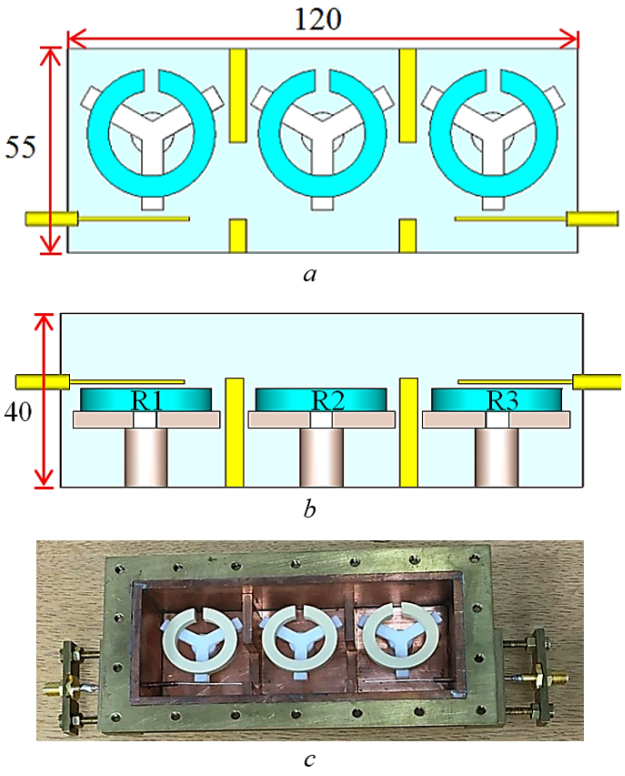

Fig. 12. *Third order Dielectric-SRR filter configuration, (a) Top view, (b) Side view. R1, 2, and 3 indicates to resonators, and (c) Fabricated filter with lid removed. Unit: millimetre.*

The simulation and measurement results are shown in Fig 13a. The S_{21} response is not symmetrical; this is due to the appearance of a transmission zero. Simulation has shown this zero is attributed to the unwanted cross coupling between the input and output coaxial cables. Such a transmission can be moved in frequency or suppressed by a more complex use of walls. However, this study is not part of this work. There is a small frequency shift in measured response, and this is due to small errors in fabrication. Note that there has been no tuning of the filter. Tuning screws are able to correct this small frequency shift, however the agreement is good and therefore we have not done the tuning. Results without tuning demonstrate more about the accurate construction and design than do tuned results.

The return loss is greater than 20 dB which is an excellent result. The measured insertion loss is about 0.3 dB higher than simulated. From this measured insertion loss, the effective unloaded Q of resonators can be calculated as 11,125 [24]. This can be compared with 19,176 in Table 2. So both the insertion loss and Q_u tell us that are additional unexpected losses. This can be attributed to (i) potential small errors in the assumed material parameters such as the loss tangent, (ii) the losses in the 3 cm semi-rigid cables connecting to the devices, (iii) losses in SMA connectors (iv) manufacturing problems, particularly with the cables and earth connection to the outer cavity (v) the small effect of the return loss on the insertion loss. Some of these errors are small, some are difficult to quantify but the expectation is that the additional loss is a combination.

The S_{21} responses across a wider band are shown in Fig 13b, the first higher spurious response occurs at 2.85 GHz, and is at a similar frequency to simulation results of the single Dielectric-SRR and comparable with the spurious performance of DR filters [1].

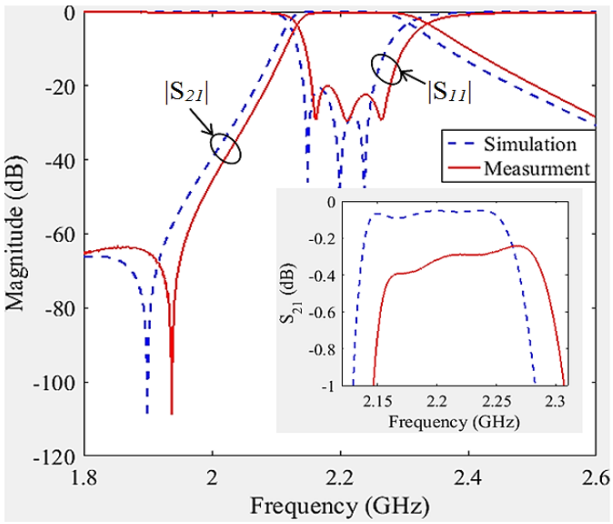

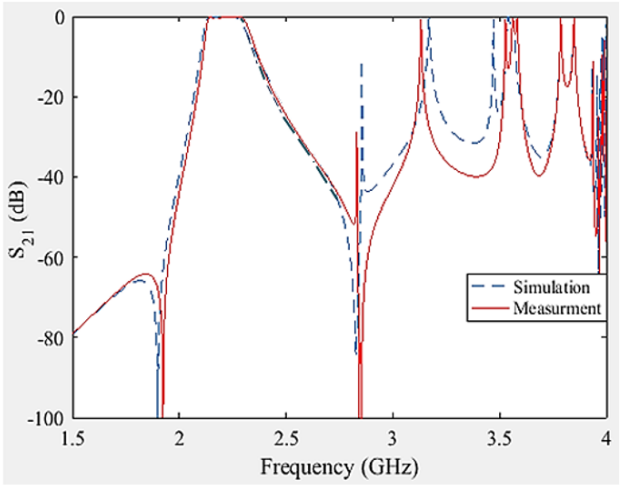

Fig. 13. *The measured and simulated responses of the 3rd order Dielectric-SRR filter, (a) Close to the center frequency and (b) Wider band showing the spurious response*

3.4. Fourth order filter with symmetric transmission zeros

This filter is designed to have a centre frequency of 2.3 GHz, fractional bandwidth (FBW) of 4%, and return loss of 20 dB. A cross coupling is added between resonators R1 and R4 to provide a pair of transmission zeros at the frequencies of 2.227 GHz and 2.374 GHz. The non-zero coupling coefficients are calculated as [24] $M_{12} = M_{24} = 0.033$, $M_{23} = 0.032$ and $M_{14} = -0.01$, and the external quality factor are $Q_{e1} = Q_{e2} = 24$. The configuration and filter dimensions as well as the fabricated filter are shown in Fig. 14, the dimensions of resonator and holder as given in the previous section in Fig. 2. Note that between resonators R1 and R4 there is the negative electric coupling required to generate the transmission zeros as discussed previously and shown in Fig 14.

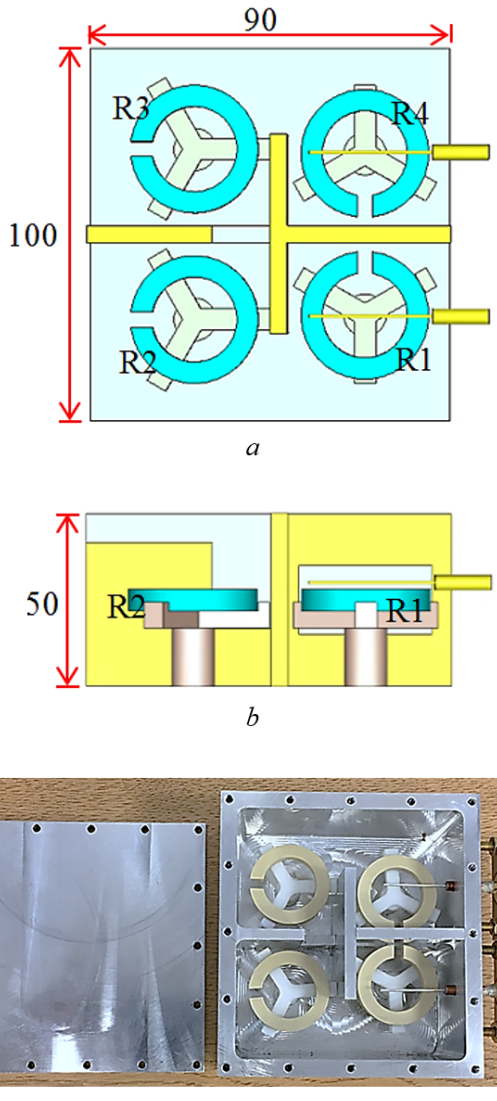

Fig. 14. *Fourth order Dielectric-SRR filter configuration. (a) Top view, (b) Side view, R1, 2, and 3 indicates to resonators, and (c) Fabricated filter. Unit: millimeter*

The simulation and measurement results are shown in Fig 15. Again this filter has an excellent return loss of greater than 20 dB with a minimum insertion loss of only about 0.3 dB. The untuned filter has a small frequency shift which also moves the position of the transmission zeros slightly.

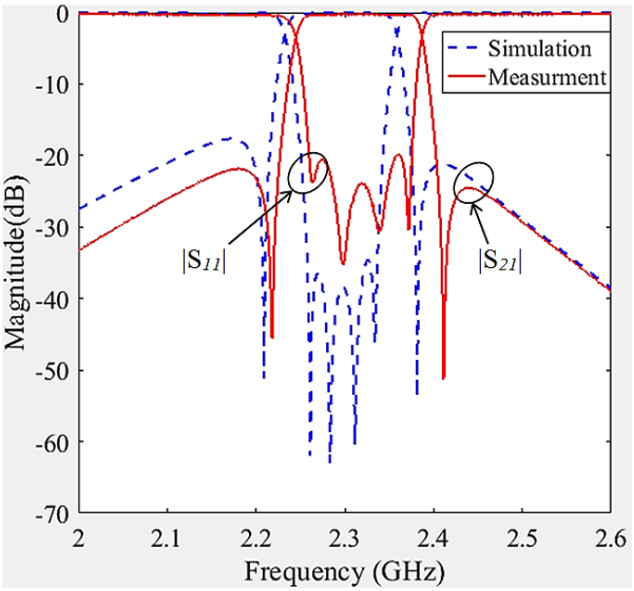

Fig. 15. *Measurement and simulation results of the Fourth order Dielectric-SRR filter.*

4. Conclusion

A new high Q_u resonator has been described; it uses a high dielectric constant material to implement a Dielectric-SRR, rather than the conventional Metal-SRR. The novel Dielectric-SRR has higher Q_u than both the Metal-SRR and the conventional disk Dielectric Resonator. The effect of Dielectric-SRR dimensions on the Q_u and mode separation has been described.

For filter design the internal and external couplings for Dielectric-SRRs have been extracted and studied. A new class of microwave filter have been presented with 3rd and 4th order examples based on the novel Dielectric-SRRs and the method of a coupled resonator circuits. The measurement results of both filters have very good agreement with the simulation results and a very low insertion loss, of about 0.3 dB, has been achieved.

5. Acknowledgements

Ahmed S. Noori would like to thank the Iraqi Ministry of Higher Education and Scientific Research and Wasit University for financing his PhD study at the University of Birmingham. The work has been partly funded by the UK Engineering and Physical Science Research Council.

6. References

[1] Wang, C., Zaki, K.A.: 'Dielectric resonators and filters', IEEE Microwave Magazine, 2007, 10, vol. 8, no. 5, pp. 115-127

[2] Mansour R.R.:'Filter technologies for wireless base stations' IEEE Microwave Magazine, 2004, 3, vol. 5, no. 1, pp. 68-74

[3] Cameron, R.J.:'Advanced coupling matrix synthesis techniques for microwave filters', IEEE Microwave Theory and Techniques, Transactions, 2003, vol. 51, pp. 1-10

[4] Zhang, D.-D., Zhou, L., Wu, L.-S., *et al.*:'Novel bandpass filters by using cavity-loaded dielectric resonators in a substrate integrated waveguide', IEEE Transactions on Microwave Theory and Techniques, 2014, 5, vol. 62, no. 5, pp 1173–1182

[5] Penaranda-Foix, F.L., Janezic, M.D., Catala-Civera, J.M., *et al.*:'Full-Wave Analysis of Dielectric-Loaded Cylindrical Waveguides and Cavities Using a New Four-Port Ring Network', IEEE Transactions on Microwave Theory and Techniques, 2012, 9, vol. 60, no. 9, pp 2730-2740

[6] Mansour, R.R., Huang, F., Fouladi, S., *et al.*:'High-Q Tunable Filters: Challenges and Potential," in IEEE Microwave Magazine, 2014, 8, vol. 15, no. 5, pp. 70-82

[7] Chu, Q.X., Ouyang, X., Wang, H., *et al.*:'$TE_{01\delta}$-Mode Dielectric-Resonator Filters with Controllable Transmission Zeros', IEEE Transactions on Microwave Theory and Techniques, 2013, 3, vol. 61, no. 3, pp. 1086-1094

[8] Fiedziuszko, S.J., Hunter, I.C., Itoh, T., *et al.*: 'Dielectric materials, devices, and circuits', IEEE Transactions on Microwave Theory and Techniques, 2002, 3, vol. 50, no. 3, pp. 706-720

[9] Wang C., Zaki, K.A., Atia, A.E., *et al.*: 'Dielectric Combline Resonators and Filters', IEEE Transactions on Microwave Theory and Techniques, 1998, vol. 46, pp. 2501-2506

[10] Mansour, R.R.:'High-Q tunable dielectric resonator filters', IEEE Microwave Magazine, 2009, 10, vol. 10, no. 6, pp. 84-98

[11] Zhan,Y., Chen, J.X., Qin, W., *et al.*:Spurious-Free Differential Bandpass Filter Using Hybrid Dielectric and Coaxial Resonators', IEEE Microwave and Wireless Components Letters, 2016, 8, vol. 26, no. 8, pp. 574-576

[12] Kajtez, D., Guillon, P.:'Dielectric Resonators' (Noble, 2nd edn, 1998)

[13] Mehdizadeh, M., Ishi, T.K., Hyde, J.S., *et al.*:'Loop-gap resonator: A lumped mode microwave resonant structure' IEEE Trans. Microwave Theory Tech., 1983, 12, vol. MTT- 31, pp. 1059–1063

[14] Mostafavi, R.F., Mirshekar-Syahkal, D., LIM, Y.C.:'Small filters based on slotted cylindrical-ring resonators', IEEE Transactions on Microwave Theory and Techniques, 2001, Vol 49, pp 2369 - 2375

[15] Salehi, H., Mansour, R.R., Dokas, V.:'Lumped-element conductor-loaded cavity resonators', IEEE MTT-S International Microwave Symposium Digest, 2002, *vol.* 3, pp 1601-1604

[16] Bobowski J.S.:'Using split-ring resonators to measure the electromagnetic properties of materials: An experiment for senior physics undergraduates', Amer. J. Phys., 2013, Dec., vol. 81, no. 12, pp. 899–906

[17] Choi H., Naylon J., Luzio S., *et al.*:'Design and In Vitro Interference Test of Microwave Noninvasive Blood Glucose Monitoring Sensor', IEEE Trans. Microwave Theory & Tech., 2015, Oct., vol. 63, no. 10, pp. 3016-3024

[18] Rowe D.J., Al-Malki, S., Abduljabar, A.A., *et al.*: 'Improved split-ring resonator for microfluidic sensing', IEEE Trans. Microw. Theory Techn., 2014, Mar., vol. 62, no. 3, pp. 689–699

[19] Masood A., Castell O., Barrow D.A., *et al.*:'Split ring resonator technique for compositional analysis of solvents in microcapillary systems', Proc. Int. Conf. MicroTAS, San Diego, USA, 2008, Oct., pp.1636-1638

[20] Violetti M., Pellaton M., Merli F., *et al*:.'The microloop-gap resonator: A novel miniaturized microwave cavity for double-resonance rubidium atomic clocks," IEEE J. Sensors, 2014, Sep., vol. 14, no. 9, pp. 3193–3200

[21] Sakamoto Y., Hirata H., Ono M.:'Design of a multicoupled loop-gap resonator used for pulsed electron paramagnetic resonance measurements', IEEE Trans. Microwave Theory Tech., 1995, Aug., vol. MTT-43, pp. 1840-1847

[22] Pozar, D.:'Microwave Engineering' (John Wiley & Sons, Inc., 4th edn, 2012)

[23] CST Computer Simulation Technology AG., USA, (Jul. 2015). [Online]. Available: www.cst.com.

[24] Hong, J.-S., Lancaster, M.J.:'Microstrip Filters for RF/Microwave Applications' (John Wiley & Sons, Inc., 2001)

[25] Sun H., Wen G., Huang Y., et al.:'Tunable band notch filters by manipulating couplings of split ring resonators', Appl. Opt., 2013, Vol. 52, pp. 7517-7522